# REPORT 1360

## CONTENTS


| | Page |
|---|---|
| SUMMARY | 547 |
| ACKNOWLEDGMENTS | 547 |
| INTRODUCTION | 547 |
| Dependence of Turbulent Flame Speed on Disturbances Originating in Shear Regions | 547 |
| Effect of Combustor Oscillations in Increasing Rate of Flame Propagation | 548 |
| SYMBOLS | 548 |
| THEORY: STABILITY OF FLOW FOR A FLAME IN A DUCT | 549 |
| Introduction | 549 |
| Steady-State Flow Field of a Flame Anchored in a Duct | 549 |
| Stability Problem | 549 |
| Interpreting Results of Stability Analysis | 551 |
| Stability Analysis | 551 |
| Steady-State Solution | 551 |
| First-Order Disturbance Problem | 552 |
| Boundary Conditions | 552 |
| Solution of the Boundary-Value Problem | 553 |
| Results | 555 |
| Construction of Stability Map | 557 |
| Phase Velocity | 557 |
| Disturbance Growth | 558 |
| Disturbance Velocity Distribution in $y$-Direction | 560 |
| Relation of Theoretical Results to Measurable Quantities | 561 |
| Effect of Flameholder | 563 |
| Summary of Theoretical Results | 565 |
| EXPERIMENT: EXAMINATION OF DISTURBANCE GROWTH IN A V-FLAME | 565 |
| Introduction | 565 |
| Apparatus | 566 |
| Burner Test Section | 566 |
| Auxiliary Equipment | 567 |
| Properties of System | 568 |
| Calibration of Disturbance Amplitude With Speaker Input | 570 |
| Ratio of Turbulent to Laminar Flame Speed Determined by Photomultiplier Probe | 571 |
| Results | 572 |
| Examination of Method | 572 |
| Comparison of Flame Speed with Flame Appearance | 573 |
| Distribution of Local $V_T/V_L$ Values with Respect to Various Frequencies | 575 |
| Disturbance-Displacement Growth | 576 |
| Disturbance Phase Velocities | 576 |
| Effect of Test-Section Depth | 578 |
| Effect of Amplitude | 579 |
| Effect of Flameholder Size | 579 |
| Effect of Velocity | 579 |
| Symmetric Disturbances | 581 |
| DISCUSSION | 581 |
| SUMMARY OF RESULTS | 588 |
| Theory | 588 |
| Experiment | 588 |
| CONCLUDING REMARKS | 588 |
| APPENDIX—AXISYMMETRIC DISTURBANCES IN AXISYMMETRIC FLOW WITH DENSITY JUMPS | 589 |
| Disturbance Equation | 589 |
| Boundary Conditions | 589 |
| Boundary-Value Problem | 590 |
| REFERENCES | 591 |

# REPORT 1360

## GROWTH OF DISTURBANCES IN A FLAME-GENERATED SHEAR REGION [1]

By Perry L. Blackshear, Jr.


### SUMMARY

*The growth of transverse velocity disturbances in the shear region caused by a flame in a duct was examined theoretically and experimentally. In the theoretical stability analysis, a flow field arising from a flame in a duct was analyzed. The flow was neutrally stable to symmetric disturbances and unstable to antisymmetric ones. As a disturbance of given frequency moves downstream from the flameholder, a most-amplified frequency is found that is equal to flow velocity divided by duct width. Disturbances at frequencies greater or less than this are less amplified. The amount that an incoming disturbance is amplified depends on the flame slope. For the most-amplified frequency, the ratio of terminal to initial transverse disturbance velocity is equal to* $(1.1)^{1/slope}$*, where the slope is roughly turbulent flame speed divided by flow velocity. This ratio of terminal to initial transverse disturbance velocity depends on inlet velocity and flame speed only in the stated manner and is essentially independent of density ratio.*

*The critical wavelength separating disturbances that grow from those that do not grow varies as a constant times flame width. The constant is 2½ for flames that are narrow compared with duct width and becomes infinite as the flame reaches the wall. The flow is unstable to disturbances having wavelengths greater than critical. Thus, short-wavelength (i. e., high-frequency) disturbances achieve their terminal amplifications near the flameholder, while long-wavelength disturbances achieve theirs farther downstream. The most-amplified disturbance achieves its terminal amplification when the flame fills 0.60 of the duct. The results are related to measurable quantities in the form of (1) flame-front displacement, (2) phase velocity, and (3) to a first approximation, the effect of disturbance frequency on flame-propagation velocity.*

*In the experimental part of the program disturbances of various frequencies were imposed on a flame stabilized in a duct, and the effects were measured by shadow photography and photomultiplier-probe surveys. Efforts to verify elements of the theory are encouraging but not conclusive. Reasonable agreement is achieved in the comparison of flame-front displacement and phase velocity. In the measurements of the effect of frequency of disturbance on flame speed, there appeared to be a most-effective frequency, which was twice the most amplified frequency given by theory. There is no direct evidence of transition due to the amplified disturbances. The flow was turbulent in all cases owing to transition in the flameholder boundary layer, either on the flameholder or near the point of separation. There was some evidence of an increased small-scale turbulence in the flame when long-wavelength disturbances were present. In other words, the large-amplitude, long-wavelength disturbances cause a sort of transition in the already turbulent flow and amplify the smaller-scale disturbances.*



### ACKNOWLEDGMENTS

The information presented herein was originally submitted as a thesis in partial fulfillment of the requirements for the degree of Doctor of Philosophy, Case Institute of Technology, Cleveland, Ohio, June 1956. The project represented a cooperative effort wherein the experimental work was carried out at the Lewis laboratory with Professor Harold G. Elrod of the Case Institute of Technology acting as the author's faculty advisor. The author is also indebted to Professors Ray. E. Bolz and Gustav Kuerti for discussions and suggestions that were of great help in the successful completion of this investigation.


### INTRODUCTION

The stability of the flow field arising from an anchored flame in a duct is of interest for two reasons: (1) Experimental investigations have shown that the turbulent flame speeds attained in a flame anchored in a duct depend more on the turbulence originating in the shear regions generated by the flameholder and flame than on the turbulence in the incident gas stream; and (2) some transverse modes of burner resonance encountered have been accompanied by an increase in the rate of flame propagation.

#### DEPENDENCE OF TURBULENT FLAME SPEED ON DISTURBANCES ORIGINATING IN SHEAR REGIONS

The problem of describing the flow field that arises when a flame is anchored in a duct was first posed and solved by Scurlock (ref. 1). One result of this work was the relation between the fraction of mixture burned and the local flame width. Scurlock used this result to measure turbulent flame speeds in an experiment originally designed to give the effect of inlet turbulence on flame speeds. He found that turbulence associated with two regions of shear flow masked, to a great extent, the effect of imposed stream turbulence. These

[1] Supersedes NACA Technical Note 3830 by Perry L. Blackshear, Jr., 1956.

two regions are the near wake of the flameholder and the shear region associated with the fully developed flame in a duct. The latter shear region is caused by the pressure gradient acting on gases of different densities. Scurlock calculated the velocity profile in this region.

In flow past cylinders without flames, eddies are encountered. Scurlock found that the flame seated on a cylindrical flameholder prevented eddies from shedding from the flameholder over the range of Reynolds numbers investigated (up to approximately 15,000). Haddock (ref. 2) and Zukoski and Marble (ref. 3), in investigating the mechanism of flames seating on cylindrical rods, found that the boundary layer separating from either side of the rod underwent transition from laminar to turbulent flow. The transition point approached the point of separation at a Reynolds number of about $10^4$. References 2 and 3 show that transition in the flameholder boundary layer is one mechanism for producing turbulence in the shear region near the flameholder.

The role played by the second shear region cited by Scurlock as a source of turbulence has not been directly investigated. After obtaining experimental results similar to those of Scurlock, several investigators [e. g., refs. 4 (Wohl) and 5] concluded that turbulence is generated in this region. The arguments leading to this conclusion are briefly indicated in the following discussion.

Theories of turbulent flame propagation have been postulated for two types of turbulence: (1) turbulence with a scale that is small compared with laminar flame-front thickness, and (2) turbulence with a scale that is large compared with laminar flame-front thickness (refs. 6 to 8). Experiments conducted in the absence of shear regions yielded flame speeds in good agreement with values predicted by the large-scale-turbulence theory (refs. 9 to 12). Experiments conducted in the presence of shear regions (refs. 4, 5, and 8) gave flame speeds higher than those predicted by theory. The interpretation of this difference is the subject of a current controversy (refs. 4, 5, 8, 13, and 14). It is generally agreed that, when an existing shear region is of the type associated with an anchored flame in a duct, the higher flame speed is due in part to turbulence amplified by or originating in this shear region.

Rayleigh (ref. 15) observed that some jets and diffusion flames are sensitive to certain imposed transverse disturbances. From an inviscid stability analysis, he found a _/_ velocity profile unstable to antisymmetric disturbances but neutrally stable to symmetric wavy disturbances. This result agreed with his observations on sensitive flames and jets. Some of the limitations of Rayleigh's work are considered in the theoretical section of this report. The analytical method used by Rayleigh is applied in the present examination of the instability of flame-zone flow to imposed disturbances.

## EFFECT OF COMBUSTOR OSCILLATIONS IN INCREASING RATE OF FLAME PROPAGATION

A great variety of combustion-chamber resonances have been observed in jet-engine combustors (refs. 16 to 19). These resonances most often involve some mode of acoustic oscillation in the combustion chamber. Reference 16 discusses modes that involve longitudinal gas and flame motion and reports a deterioration in combustor performance when these oscillations occur. Reference 17 discusses a type of resonance identified as a transverse mode of oscillation in the combustion chamber. Accompanying this type of oscillation was an apparent increase in combustion efficiency (ref. 17) and in the rate of flame spreading (ref. 18). This type of oscillation, with an acoustic wavelength controlled by duct dimensions, could possibly excite a wavy disturbance that would subsequently be amplified by the flame-generated shear region.

Unfortunately, these transverse modes (called screech) also cause the destruction of the burner walls when the screech becomes severe enough (ref. 18). Reference 19 shows pictures of the flame near the flameholder when a combustor was resonating in a transverse mode. A strong interaction was apparent in the form of flame wrinkles forming at the flameholder and growing in amplitude as they moved downstream. It seems apparent that at least one of the ways the transverse oscillation increases the rate of flame spreading is by wrinkling and hence extending the interface between the burned and unburned gases.

If the oscillation that disturbs the flame at the flameholder is supplied locally (by some suitable exciting mechanism) and not by the sometimes destructive combustor resonance, some of the benefits of screech can be realized without its penalties. The gains in flame speed should be greatest for those frequencies of excitation that are amplified by the flame. It is hoped that, by examining the sensitivity of a flame in a duct to imposed disturbances, an excitation frequency may be found that gives the optimum increase in flame speed.

This report is divided into three parts—theory, experiment, and discussion. Separate introductions are given for the first two parts describing the purpose of each. The discussion weighs the results of the other parts and includes some extrapolations.

## SYMBOLS

| | |
|---|---|
| $A, B, C, D$ | constants of integration |
| $b$ | width of shear region in Rayleigh's problem |
| $b'$ | width of plateau in _/‾_ velocity profile |
| $c$ | complex phase velocity, ft/sec |
| $d$ | flameholder width |
| $E$ | voltage |
| $F$ | fraction burned |
| $f$ | frequency, cps |
| $G$ | gain; $v'=v'_o G^{1/K_2}$ |
| $G'$ | gain; $v'=v'_o (G')^{1/K_1}$ |
| $h$ | flame-front displacement from mean, ft |
| $h_1$ | duct half-width, ft |
| $h_2$ | flame half-width, ft |
| $K_1$ | constant, $dF/[d(x/h_1)]$ |
| $K_2$ | constant, $dh_2/dx$, for an assumed flame-spreading mechanism |
| $\mathscr{K}$ | proportionality factor |
| $k$ | constant |
| $L$ | Eulerian scale of turbulence, ft |
| $l$ | length, ft |
| $l_F$ | length of flame measured from wake, ft |
| $l_w$ | length of flameholder wake, ft |

| | |
|---|---|
| $P$ | mean pressure, lb/sq ft |
| $p$ | pressure, lb/sq ft |
| $p'$ | perturbation pressure, lb/sq ft |
| $Re$ | Reynolds number |
| $S$ | flame surface area |
| $t$ | time, sec |
| $U$ | flow velocity in $x$-direction, ft/sec |
| $U_1$ | flow velocity in $x$-direction in cold gas, ft/sec |
| $U^*$ | flow velocity in $x$-direction at apex of hot-gas velocity profile, ft/sec |
| $u'$ | disturbance velocity in $x$-direction, ft/sec |
| $V$ | flame speed, ft/sec |
| $v'$ | disturbance velocity in $y$-direction, ft/sec |
| $x$ | coordinate in direction of duct axis, ft |
| $y$ | coordinate perpendicular to duct axis, ft |
| $\alpha$ | wave number of disturbance, $ft^{-1}$ |
| $\alpha_o$ | wave number of disturbance based on initial velocity and frequency, $f2\pi/U_o$ |
| $\alpha_s$ | wave number for neutral stability based on inviscid analysis, $ft^{-1}$ |
| $\beta$ | hot-gas velocity gradient, $(U^*-U_1)/h_2$, $sec^{-1}$ |
| $\gamma_y$ | $e^{-\alpha y}$ |
| $\gamma_1$ | $e^{-\alpha h_1}$ |
| $\gamma_2$ | $e^{-\alpha h_2}$ |
| $\zeta$ | $\frac{\gamma_2^2+\gamma_1^2}{\gamma_2^2-\gamma_1^2}$ |
| $\lambda$ | wavelength, ft |
| $\lambda_s$ | $2\pi/\alpha_s$, ft |
| $\xi$ | $\frac{1+\gamma_2^2}{1-\gamma_2^2}$ |
| $\rho$ | density, lb-sec$^2$/ft$^4$ |
| $\rho_1$ | density of cold gas, lb-sec$^2$/ft$^4$ |
| $\rho_2$ | density of hot gas, lb-sec$^2$/ft$^4$ |
| $\rho'$ | perturbation density, lb-sec$^2$/ft$^4$ |
| $\varphi(y)$ | $y$-distribution of disturbance amplitude, ft$^2$/sec |
| Subscripts: | |
| $cr$ | critical |
| $d$ | disturbed |
| $f$ | frequency |
| $i$ | imaginary part |
| $L$ | laminar |
| $max$ | maximum |
| $o$ | initial; plane of flameholder |
| $pg$ | measured from flame photographs |
| $pm$ | measured by photomultiplier |
| $r$ | real part |
| $T$ | turbulent |
| $t$ | total |
| $u$ | undisturbed |

## THEORY: STABILITY OF FLOW FOR A FLAME IN A DUCT

### INTRODUCTION

#### STEADY-STATE FLOW FIELD OF A FLAME ANCHORED IN A DUCT

The problem of describing the flow field that exists when a flame is anchored in a duct was first posed and solved by Scurlock in 1948 (ref. 1). Subsequently, Tsien (ref. 20) and others (ref. 21) elaborated on the problem. The following table summarizes Scurlock's and Tsien's assumptions and results as they pertain to the present work:

| Scurlock | Common | Tsien |
|---|---|---|
| **Assumptions** | | |
| (1) Fluid is incompressible. | (1) Fluid is steady-state, two-dimensional, inviscid, non-heat-conducting, non-turbulent. | (1) Two cases are treated, compressible and incompressible. In the incompressible, Scurlock's assumption (2) holds; in the compressible, density is allowed to vary in the direction of flow. |
| (2) Density jumps from $\rho_1$ to $\rho_2$ across the flame front and is constant in each region. | (2) Velocity, density, and pressure are uniform at combustor inlet. (3) Static pressure is uniform at any cross section. (4) The flameholder is of negligible size and spans the combustor. (5) The flame front is of negligible thickness. (6) The chamber is of constant width. | (2) Density ratio is constant across flame front at any station. (3) The velocity profile is composed of four straight-line segments. |
| **Results** | | |
| (1) Velocity profile as a function of flame width: ∩ slightly concave to incoming gas). (2) Momentum pressure drop as a function of flame width (i. e., of fraction burned). | (1) Fraction burned as a function of flame width. (2) Cold-gas velocity as a function of flame width. | (1) Peak hot-gas velocity as a function of flame width. (2) Limiting inlet velocity beyond which complete combustion cannot occur as a function of density ratio (for compressible case). |

A stability analysis is made herein of a parallel flow having a velocity profile approximating the one found by Scurlock by means of straight-line segments and a density distribution as taken by Scurlock (i. e., constant $\rho_1/\rho_2$).

#### STABILITY PROBLEM

The study of the origins of turbulent motion has received considerable attention in the past, particularly with respect to turbulence occurring in boundary layers. One way of treating the problem is to assume the existence of infinitesimal wavy disturbances in the flowing stream and to seek the conditions under which these disturbances are amplified (refs. 22 and 23). In the application of this method to the study of the stability of the laminar boundary layer, a major objective is to determine a minimum Reynolds number below which all disturbances decay and to determine the effect of velocity profile on this minimum Reynolds number.

The amplification of wavy disturbances supposedly leads to the transition to turbulence under certain circumstances. The desirability of maintaining laminar flow on airfoils makes an understanding of transition an important practical problem. In 1941, Schubauer and Skramstad conducted an experiment in which the disturbances introduced into a laminar boundary layer were carefully controlled (ref. 24). They found a relation between the wave numbers of amplified, neutral, and damped disturbances and the Reynolds number that confirmed the predictions of the infinitesimal wavy disturbance theory in almost every important respect.

The practical value of learning about the stability of a flow field created by a flame in a duct is in furnishing information that will enable combustor designers to encourage the growth of disturbances in this region, because turbulence generally aids flame spreading. The information needed is (1) a range of Reynolds numbers over which the flow is unstable and (2) the kind of disturbance that possesses the greatest rate of amplification within this range. In the following qualitative discussion most flames of practical interest appear to be in a Reynolds number range where amplified disturbances always exist and where the wavelengths of disturbances that will be amplified may be obtained when viscosity is neglected.

If the disturbance varies as $v'=\varphi(y)e^{i\alpha(x-ct)}$, where the wave number $\alpha$ is real and the phase velocity $c$ is generally complex, then the stability of boundary-layer flows (or of flows with symmetric profiles in a two-dimensional channel) can be illustrated by a graph of values for $\alpha$ for neutral stability (i. e., where the imaginary part of $c$ vanishes) against Reynolds number $Re$ (ref. 22).

A profile without a point of inflection would possess the following plot of $\alpha$ against $Re$ for $c_i=0$:

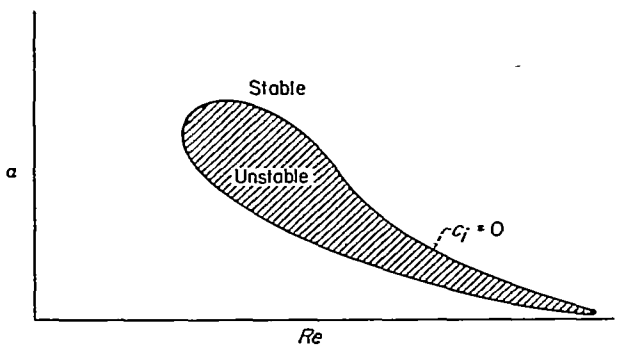


Sketch (a)

This curve is called the neutral envelope for the profile in question. Inside the envelope, disturbances are amplified ($c_i>0$); outside, disturbances are damped ($c_i<0$). Proceeding to the right from the minimum Reynolds number attained by the $c_i=0$ curve are two branches of the curve $c_i=0$ As $Re$ becomes indefinitely great, both curves asymptotically approach $\alpha=0$.

For the profile with a point of inflection, a similar relation $\alpha(c,Re)$ is obtained:

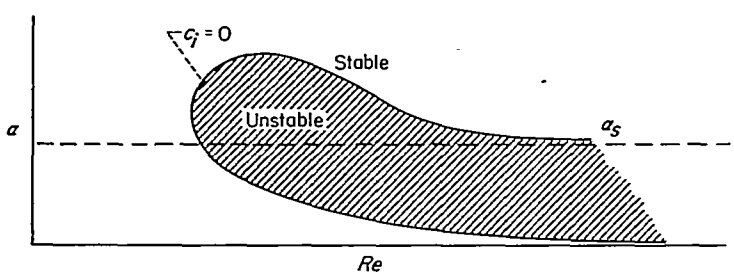


Sketch (b)

The significant difference between this plot for a profile with an inflection point and sketch (a) for a profile without an inflection point is that the asymptotic values of the two branches approach different limits for large values of $Re$. The upper branch approaches $\alpha=\alpha_s$, the wave number for neutral stability obtained by neglecting viscosity, and the lower branch approaches $\alpha=0$. The Reynolds number range over which the flow with an inflection point is unstable extends to indefinitely large Reynolds numbers. The flow generated by a flame in a duct has, in effect, an inflection point.

It is desirable either by example or direct calculation to determine the order of magnitude of the Reynolds number range over which the neutral $\alpha$ departs from $\alpha_s$; that is, where viscosity has a dominating influence. In two examples in the literature, Pretsch (ref. 25) and Lessen (ref. 26) examined a flow with a flex for stability. In both instances the minimum Reynolds number for $c_i=0$ was of the order of 10; the maximum $Re$, where $\alpha$ for $c_i=0$ differed from $\alpha_s$ calculated from inviscid theory by more than 2 percent, was of the order of $10^3$. The profile of reference 25 is for a boundary layer with pressure rise; that of reference 26 is for the free boundary layer between streams of differing velocities.

If these values are taken to suggest the order of Reynolds number where the stability of a profile with a flex is sensitive to the effects of viscosity, some idea of flame-zone sizes can be estimated for the range of velocities encountered in jet engines (i. e., 50 to 500 ft/sec). For example, at 50 feet per second, the range of flame width where viscous forces are important is 1/3000 to 1/30 inch. At 500 feet per second, the range is 1/30,000 to 1/300 inch. Most of the flame zones of practical interest are much wider than these dimensions and may be considered well within the range of Reynolds numbers where disturbances are amplified and where viscosity effects are small. Therefore, the following inviscid stability analysis may give meaningful information on the value of the wave numbers $\alpha$ where amplification can occur.

Lin (ref. 22) and Heisenberg (ref. 27) have criticized the use of broken-line profiles because there is a separate solution for $c$ for each corner of the profile. These objections might be met by the following observations:

(1) The steady-state flow field solved by Scurlock possesses corners (places where the velocity gradient jumps) and can be very closely approximated by straight-line segments without introducing new corners into the profile. The jumps in velocity gradient that occur at the corners result from the assumption that the flame front is of negligible thickness compared with the width of the flame zone.

(2) The following results show that the flame zone is unstable to disturbances having wavelengths 2.5 times the flame-zone width and greater. Thus, any rounding of the corners over a distance that is small compared with the flame-zone width should not affect the results; to the long-wavelength disturbances that are amplified, the corners will still appear sharp.

In order to examine the effect of corners in a velocity profile, three profiles of a similar shape are shown in the following sketch:

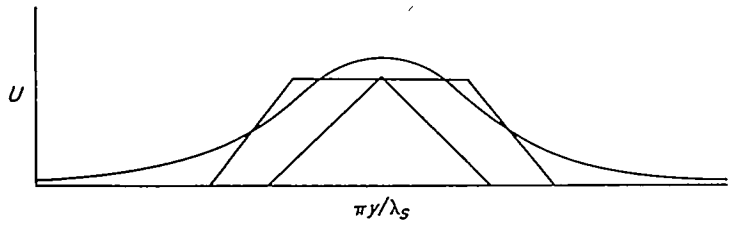


Sketch (c)

Each of these profiles has been examined for instability, and a wavelength for neutral stability has been computed. The scale of the abscissa is chosen so that the value of the neutral wavelength is the same for the three profiles. The two broken-line profiles are from Rayleigh (ref. 15); the continuous profile, from Savic (ref. 28). These solutions correspond to the antisymmetric disturbance. The flow in each case is inviscid.

A similar comparison can be made between the velocity profile $U=1+\sin[(2\pi y/l)-(\pi/2)]$ treated briefly by Lin (ref. 22) and a corresponding broken-line approximation. Lin's result yields $\alpha_s l=\pi\sqrt{3}$ for the sine profile. Equation (37) in the following analysis was used to obtain the dimensions of a profile having the same $\alpha_s l$. The following two profiles are given for flow between parallel walls, $v'$ vanishing at the walls:

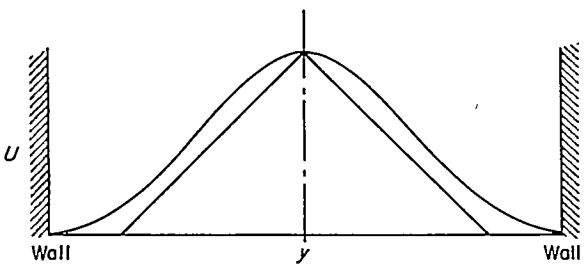


Sketch (d)

Since the widths of the profiles composed of broken-line segments are so nearly equal to those with continuous velocity gradients (having identical neutral wave numbers), it is believed that the broken-line profile used herein does not involve the introduction of extraneous solutions.

### INTERPRETING RESULTS OF STABILITY ANALYSIS

The stability analysis gives an amplification rate $\alpha c_i$ and a phase velocity $c_r$ for disturbances as functions of the wave number $\alpha$ and the fraction of duct occupied by flame $h_2/h_1$ for any one station along the axis of the duct. From this information a stability map is constructed, consisting of a plot of contours of constant $\alpha c_i$ on a grid of $\alpha h_1$ against $h_2/h_1$. This is a generalized map, with no assumption regarding the rate of change of flame width with distance. Lines of constant frequency are shown on the stability map calculated from the phase velocity $c_r$. From the map and an assumption of the nature of flame-spreading rates, the total amplification of a disturbance of given frequency is calculated.

Some aspects of this information are reduced to measurable quantities that can subsequently be compared with experimental results. These quantities include

(1) Qualitative dependence of turbulent flame-spreading rate on disturbance frequency
(2) Relation between critical wave number and flame width
(3) Qualitative behavior of amplified disturbances as affected by the steady-state condition (velocity, fuel-air ratio)

One section of the analysis deals with the effect of a flameholder of finite size on the steady-state profile and hence on the stability analysis.

## STABILITY ANALYSIS

### STEADY-STATE SOLUTION

The equations for incompressible flow derived by Tsien (ref. 20) relating $U_1$, $U_o$, $U^*$, $\rho_1/\rho_2$, $h_2/h_1$, and $F$ are listed first; these relations are based on the assumption that the velocity profile can be approximated by straight-line segments:

Apex velocity:

$$\frac{U^*}{U_o}=\sqrt{1+\frac{\rho_1}{\rho_2}\left[\left(\frac{U_1}{U_o}\right)^2-1\right]} \tag{1}$$

Hot-gas velocity distribution:

$$\frac{U}{U_o}=\sqrt{1+\frac{\rho_1}{\rho_2}\left[\left(\frac{U_1}{U_o}\right)^2-1\right]}-\left\{\sqrt{1+\frac{\rho_1}{\rho_2}\left[\left(\frac{U_1}{U_o}\right)^2-1\right]}-\frac{U_1}{U_o}\right\}\frac{y}{h_2} \tag{2}$$

Flame width:

$$\frac{h_2}{h_1}=\frac{\frac{U_1}{U_o}-1}{\left(1-\frac{1}{2}\frac{\rho_2}{\rho_1}\right)\frac{U_1}{U_o}-\frac{1}{2}\frac{\rho_2}{\rho_1}\sqrt{1+\frac{\rho_1}{\rho_2}\left[\left(\frac{U_1}{U_o}\right)^2-1\right]}} \tag{3}$$

Fraction burned:

$$F=1-\frac{U_1}{U_o}\left(1-\frac{h_2}{h_1}\right) \tag{4}$$

The hot-gas distribution (eq. (2)) and the relation between $h_2/h_1$ and $U_1/U_o$ (eq. (3)) are used in interpreting the results of the stability analysis. In the analysis the hot-gas velocity distribution (eq. (2)) is represented by

$$U=U_1+(h_2-y)\beta \qquad (y>0)$$

$$U=U_1+(h_2+y)\beta \qquad (y<0)$$

where

$$\beta=\frac{U^*-U_1}{h_2}$$

Tsien's analysis says nothing about the distribution of $h_2/h_1$ with distance $x$. This must come from further assumptions

regarding flame slope, flame speed, or rate of change of $F$ with $x$. For the present it is sufficient to say that the rate of change of $h_2/h_1$ with $x$ is small; that is,

$$\frac{\partial(h_2/h_1)}{\partial x}\lambda \ll \frac{h_2}{h_1}$$

where $\lambda$ is the wavelength of a disturbance of interest.

The stability of the profile assumed by Tsien, which closely approximates that calculated by Scurlock, is treated as a parallel-flow problem.

### FIRST-ORDER DISTURBANCE PROBLEM

Two excellent summary papers are available on the stability of parallel flows (refs. 22 and 23). No attempt to review the field is made herein. The method employed here dates back to some of Rayleigh's early work (ref. 15) with very slight modification. The development of the disturbance equation that follows is from reference 29.

The flow is assumed parallel, inviscid, incompressible, plane, and non-heat-conducting. Gravity is neglected. The equations of motion are

$$\frac{\partial p}{\partial x}=-\rho\left(\frac{\partial u}{\partial t}+u\frac{\partial u}{\partial x}+v\frac{\partial u}{\partial y}\right) \tag{5}$$

$$\frac{\partial p}{\partial y}=-\rho\left(\frac{\partial v}{\partial t}+u\frac{\partial v}{\partial x}+v\frac{\partial v}{\partial y}\right) \tag{6}$$

The fluid is assumed incompressible (but the density is allowed to vary with $y$), so that

$$\frac{\partial \rho}{\partial t}+u\frac{\partial \rho}{\partial x}+v\frac{\partial \rho}{\partial y}=0 \tag{7}$$

and the equation of continuity is

$$\frac{\partial u}{\partial x}+\frac{\partial v}{\partial y}=0 \tag{8}$$

Let

$$\left.\begin{aligned} u&=U(y)+u'(x,y,t)\\ v&=v'(x,y,t)\\ p&=P+p'(x,y,t)\\ \rho&=\bar{\rho}(y)+\rho'(x,y,t)\end{aligned}\right\} \tag{9}$$

where primed quantities are of first order of smallness. Assume $u'$, $v'$, $p'$, and $\rho'$ to vary with $x$ and $t$ as $e^{i\alpha(x-ct)}$, where $\alpha$ is real and $c$, in general, is complex.

By substituting equation (9) in equations (5) to (8) and retaining terms of the first order, equations (5) to (8) become

$$\bar{\rho}\left[i\alpha(U-c)u'+\frac{dU}{dy}v'\right]=-i\alpha p' \tag{10}$$

$$\bar{\rho}[i\alpha(U-c)v']=-\frac{\partial p'}{\partial y} \tag{11}$$

$$i\alpha(U-c)\rho'+v'\frac{d\bar{\rho}}{dy}=0 \tag{12}$$

$$\frac{\partial v'}{\partial y}+i\alpha u'=0 \tag{13}$$

Eliminating $p'$, $\rho'$, and $u'$ from equations (10) to (13) yields an equation for $v'$:

$$(U-c)\left(\frac{\partial^2 v'}{\partial y}-\alpha^2 v'\right)-v'\frac{\partial^2 U}{\partial y^2}+\frac{1}{\bar{\rho}}\frac{d\bar{\rho}}{dy}\left[(U-c)\frac{\partial v'}{\partial y}-v'\frac{\partial U}{\partial y}\right]=0 \tag{14}$$

It is apparent that, though equations (7) and (12) are useful in defining the type of incompressible flow field assumed, they are not required to obtain the disturbance equation (14) unless it becomes necessary to specify $\rho'$.

Defining

$$v'=-i\alpha\varphi(y)e^{i\alpha(x-ct)}$$

equation (14) becomes

$$(U-c)\left(\frac{d^2\varphi}{dy^2}-\alpha^2\varphi\right)-\varphi\frac{d^2U}{dy^2}+\frac{1}{\bar{\rho}}\frac{d\bar{\rho}}{dy}\left[(U-c)\frac{d\varphi}{dy}-\varphi\frac{dU}{dy}\right]=0 \tag{15}$$

In regions where $\bar{\rho}$ and $dU/dy$ are constant, equation (15) reduces to

$$\frac{d^2\varphi}{dy^2}-\alpha^2\varphi=0 \tag{16}$$

with the solution

$$\varphi=A_1e^{\alpha y}+A_2e^{-\alpha y} \tag{17}$$

The disturbance velocities given by definition and equation (13) are the real parts of

$$\left.\begin{aligned} u'&=(A_1\alpha e^{\alpha y}-A_2\alpha e^{-\alpha y})e^{i\alpha(x-ct)}\\ v'&=-i\alpha(A_1e^{\alpha y}+A_2e^{-\alpha y})e^{i\alpha(x-ct)}\end{aligned}\right\} \tag{18}$$

### BOUNDARY CONDITIONS

The geometry of the flow field is shown in figure 1. Equation (16) and the solutions (eqs. (18)) apply to each of the regions 1 to 4 considered separately. The establishment of the boundary-value problem consists in assigning suitable

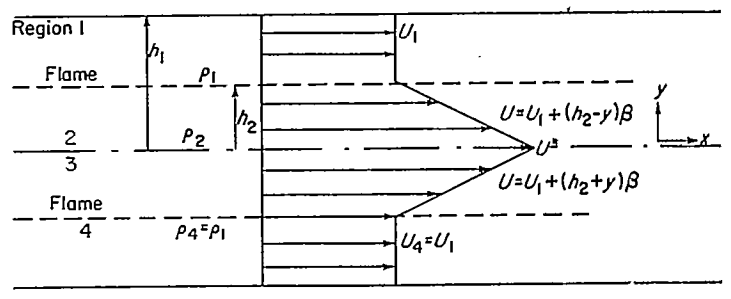


FIGURE 1.—Geometry of flow field.

boundary conditions at the walls and at the boundaries of regions 1 to 4. These boundary conditions are:

(1) $v'$ vanishes at $y=\pm h_1$.

(2) $v'$ is continuous at interfaces.

(3) $p'$ is continuous at interfaces (or, equivalently, the complete eq. (14) integrated across each interface is satisfied).

Let the equation of the interface at $y=h_m$ be

$$y=h_m+h(x,t) \tag{19}$$

(In the following derivation the subscripts $m$ and $n$ represent conditions evaluated in a region $m$ or $n$.) Then, to the first order of approximation, at the interface,

$$v'=\frac{\partial h}{\partial t}+U\frac{\partial h}{\partial x} \tag{20}$$

where $U$ is the mean velocity at the interface. In order for the pressure to be continuous at the interface, it is necessary that

$$\frac{\mathrm{d}p_m}{\mathrm{d}x_1}=\frac{\mathrm{d}p_n}{\mathrm{d}x_1}$$

where $x_1$ is along the interface, or equivalently in the $x,y$-system,

$$\frac{\partial p_m}{\partial x}+\frac{\partial p_m}{\partial y}\frac{\partial h}{\partial x}=\frac{\partial p_n}{\partial x}+\frac{\partial p_n}{\partial y}\frac{\partial h}{\partial x} \tag{21}$$

where at the interface

$$\frac{\partial y}{\partial x}=\frac{\partial h}{\partial x}$$

From the equation of motion,

$$\frac{\partial p}{\partial x}=-\rho\left(\frac{\partial u}{\partial t}+u\frac{\partial u}{\partial x}+v\frac{\partial u}{\partial y}\right) \tag{5}$$

$$\frac{\partial p}{\partial y}=-\rho\left(\frac{\partial v}{\partial t}+u\frac{\partial v}{\partial x}+v\frac{\partial v}{\partial y}\right) \tag{6}$$

where

$$\left.\begin{aligned} u&=U+u'\\ v&=v'\\ p&=P+p'\end{aligned}\right\} \tag{9}$$

By retaining terms of zero- and first-order approximations,

$$\left.\begin{aligned} \frac{\partial p}{\partial x}=\frac{\partial p'}{\partial x}&=-\rho\left(\frac{\partial u'}{\partial t}+U\frac{\partial u'}{\partial x}+v'\frac{\mathrm{d}U}{\mathrm{d}y}\right)\\ \frac{\partial p}{\partial y}=\frac{\partial p'}{\partial y}&=-\rho\left(\frac{\partial v'}{\partial t}+U\frac{\partial v}{\partial x}\right)\end{aligned}\right\} \tag{22}$$

or $\partial p/\partial x$ and $\partial p/\partial y$ are first-order terms. But, from equation (20), it is clear that $\partial h/\partial x$ is of the first order so that the products $(\partial p/\partial y)(\partial h/\partial x)$ are of the second order, and equation (21) becomes

$$\frac{\partial p_m}{\partial x}=\frac{\partial p_n}{\partial x} \tag{23}$$

or

$$\rho_m\left(\frac{\partial u'_m}{\partial t}+U_m\frac{\partial u'_m}{\partial x}+v_m\frac{\partial U_m}{\partial y}\right)=\rho_n\left[\frac{\partial u'_n}{\partial t}+U_n\frac{\partial u'_n}{\partial x}+v'_n\frac{\partial U_n}{\partial y}\right] \tag{24}$$

at the interface between the regions $m$ and $n$. Equation (24) results from a necessary condition for the pressure to be continuous at surfaces where either $\bar{\rho}$ or $\mathrm{d}U/\mathrm{d}y$ jumps.

In order to show that this condition is equivalent to requiring that the integrated equation (14) be satisfied at the interface, equation (14) is written

$$\frac{\partial}{\partial y}\left\{\bar{\rho}\left[(U-c)\frac{\partial v'}{\partial y}-v'\frac{\partial U}{\partial y}\right]\right\}-\bar{\rho}(U-c)\alpha^2v'=0 \tag{25}$$

Integrating equation (25) across the interface gives

$$\bar{\rho}_m\left[(U_m-c)\frac{\partial v'_m}{\partial y}-v'_m\frac{\partial U_m}{\partial y}\right]=\bar{\rho}_n\left[(U_n-c)\frac{\partial v'_n}{\partial y}-v'_n\frac{\partial U_n}{\partial y}\right]$$

which, with the insertion of the continuity equation, becomes

$$\bar{\rho}_m\left[(U_m-c)\frac{\partial u'_m}{\partial x}+v'_m\frac{\partial U_m}{\partial y}\right]=\bar{\rho}_n\left[(U_n-c)\frac{\partial u_n}{\partial x}+v'_n\frac{\partial U_n}{\partial y}\right] \tag{26}$$

But $u'$ varies as $e^{i\alpha(x-ct)}$, so that equation (26) can be recognized as another way of writing equation (24).

The boundary conditions can be written

$$v'_1=0 \quad \text{at} \quad y=h_1 \tag{27a}$$

$$v'_1=v'_2 \quad \text{at} \quad y=h_2 \tag{27b}$$

$$\frac{\partial p'_1}{\partial x}=\frac{\partial p'_2}{\partial x} \quad \text{at} \quad y=h_2 \tag{27c}$$

$$v'_2=v'_3 \quad \text{at} \quad y=0 \tag{27d}$$

$$\frac{\partial p'_2}{\partial x}=\frac{\partial p'_3}{\partial x} \quad \text{at} \quad y=0 \tag{27e}$$

$$v'_3=v'_4 \quad \text{at} \quad y=-h_2 \tag{27f}$$

$$\frac{\partial p'_3}{\partial x}=\frac{\partial p'_4}{\partial x} \quad \text{at} \quad y=-h_2 \tag{27g}$$

$$v'_4=0 \quad \text{at} \quad y=-h_1 \tag{27h}$$

where the subscripts 1 to 4 denote flow regions (fig. 1).

## SOLUTION OF THE BOUNDARY-VALUE PROBLEM

The solutions of equation (16) for regions 1 to 4 (fig. 1) are written as follows:

$$\left.\begin{aligned} &\text{Region 1:} \quad \varphi_1=A_1e^{\alpha y}+A_2e^{-\alpha y}\\ &\text{Region 2:} \quad \varphi_2=B_1e^{\alpha y}+B_2e^{-\alpha y}\\ &\text{Region 3:} \quad \varphi_3=C_1e^{\alpha y}+C_2e^{-\alpha y}\\ &\text{Region 4:} \quad \varphi_4=D_1e^{\alpha y}+D_2e^{-\alpha y}\end{aligned}\right\} \tag{28}$$

Inserting equations (28) into equations (27) results in eight equations in the eight unknowns $A_1, A_2, \ldots D_2$. The requirement that $A_1, A_2, \ldots D_2$ have nontrivial solutions is

$$\begin{vmatrix} 1 & \gamma_1^2 & 0 & 0 & 0 & 0 & 0 & 0 \\ 1 & \gamma_2^2 & -1 & -\gamma_2^2 & 0 & 0 & 0 & 0 \\ \frac{\rho_1}{\rho_2}(U_1-c) & -\frac{\rho_1}{\rho_2}(U_1-c)\gamma_2^2 & -\left[(U_1-c)+\frac{\beta}{\alpha}\right] & \left[(U_1-c)-\frac{\beta}{\alpha}\right]\gamma_2^2 & 0 & 0 & 0 & 0 \\ 0 & 0 & 1 & 1 & -1 & -1 & -1 & -1 \\ 0 & 0 & (U^*-c)+\frac{\beta}{\alpha} & -\left[(U^*-c)-\frac{\beta}{\alpha}\right] & -\left[(U^*-c)-\frac{\beta}{\alpha}\right] & (U^*-c)+\frac{\beta}{\alpha} & 0 & 0 \\ 0 & 0 & 0 & 0 & \gamma_2^2 & 1 & -\gamma_2^2 & 1 \\ 0 & 0 & 0 & 0 & \left[(U_1-c)-\frac{\beta}{\alpha}\right]\gamma_2^2 & -\left[(U_1-c)+\frac{\beta}{\alpha}\right] & -\frac{\rho_1}{\rho_2}(U_1-c)\gamma_2^2 & \frac{\rho_1}{\rho_2}(U_1-c) \\ 0 & 0 & 0 & 0 & 0 & 0 & \gamma_2^2 & 1 \end{vmatrix}=0 \tag{29}$$

Where $\gamma_1 \equiv e^{-\alpha h_1}$ and $\gamma_2 \equiv e^{-\alpha h_2}$. By assigning $U_1=0$ (this merely alters the real part of $c$) and operating on rows 1, 2, 3, 6, 7, and 8, equation (29) can be reduced to the determinant

$$\begin{vmatrix} c-\frac{\beta}{\alpha}+\zeta\frac{\rho_1}{\rho_2}c & \left[\zeta\frac{\rho_1}{\rho_2}c-\left(c+\frac{\beta}{\alpha}\right)\right]\gamma_2^2 & 0 & 0 \\ 1 & 1 & -1 & -1 \\ h_2\beta-c+\frac{\beta}{\alpha} & -\left(h_2\beta-c-\frac{\beta}{\alpha}\right) & -\left(h_2\beta-c-\frac{\beta}{\alpha}\right) & h_2\beta-c+\frac{\beta}{\alpha} \\ 0 & 0 & \left(\zeta\frac{\rho_1}{\rho_2}c-c-\frac{\beta}{\alpha}\right)\gamma_2^2 & \zeta\frac{\rho_1}{\rho_2}c+c-\frac{\beta}{\alpha} \end{vmatrix}=0 \tag{30}$$

where

$$\zeta \equiv \frac{\gamma_2^2+\gamma_1^2}{\gamma_2^2-\gamma_1^2}$$

On expanding and simplifying, equation (30) becomes

$$\left[c-\frac{\beta}{\alpha}\left(\zeta\frac{\rho_1}{\rho_2}+\xi\right)^{-1}\right]\left[c^2\left(\zeta\frac{\rho_1}{\rho_2}\xi+1\right)-c\left(h_2\beta-\zeta\frac{\rho_1}{\rho_2}\frac{\beta}{\alpha}+h\beta\zeta\frac{\rho_1}{\rho_2}\xi\right)+\frac{h\beta^2}{\alpha}\xi-\frac{\beta^2}{\alpha^2}\right]=0 \tag{31}$$

where

$$\xi \equiv \frac{1+\gamma_2^2}{1-\gamma_2^2}$$

One root can be seen to be wholly real:

$$c=\frac{\beta}{\alpha}\left(\zeta\frac{\rho_1}{\rho_2}+\xi\right)^{-1} \tag{32}$$

This can be identified as the root belonging to a symmetric disturbance by assigning $v_2'=v_3'=0$ at $y=0$ in equation (27). In this case equation (30) reduces to

$$\begin{vmatrix} c-\frac{\beta}{\alpha}+\zeta\frac{\rho_1}{\rho_2}c & \zeta\frac{\rho_1}{\rho_2}c-\left(c+\frac{\beta}{\alpha}\right)\gamma_2^2 \\ 1 & 1 \end{vmatrix}=0 \tag{33}$$

which yields equation (32) as before. The remaining two roots,

$$c=\frac{\beta}{\alpha}\left\{\frac{h_2\alpha+\zeta\frac{\rho_1}{\rho_2}(\xi\alpha h_2-1)\pm\sqrt{\left[h_2\alpha+\zeta\frac{\rho_1}{\rho_2}(\xi\alpha h_2-1)\right]^2-4\left(\zeta\frac{\rho_1}{\rho_2}\xi+1\right)(\alpha h_2\xi-1)}}{2\left(\zeta\frac{\rho_1}{\rho_2}\xi+1\right)}\right\} \tag{34}$$

can similarly be identified as roots belonging to an antisymmetric disturbance. One way of doing this is to set $v_2'$ at $y=h_2$ equal to $v_3'$ at $y=-h_2$ or (from eq. (28))

$$B_1+B_2\gamma_2^2-C_1\gamma_2^2-C_2=0 \tag{35}$$

Using equation (35) in place of equations (27f), (27g), and (27h) gives for the determinantal equation

$$\begin{vmatrix} 1 & \gamma_2^2 & 0 & 0 & 0 & 0 \\ 1 & \gamma_2^2 & -1 & -\gamma_2^2 & 0 & 0 \\ \frac{\rho_1}{\rho_2}(-c) & \frac{\rho_1}{\rho_2}c\gamma_2^2 & \left(c-\frac{\beta}{\alpha}\right)\gamma_2^2 & -\left(c+\frac{\beta}{\alpha}\right)\gamma_2^2 & 0 & 0 \\ 0 & 0 & 1 & 1 & -1 & -1 \\ 0 & 0 & -c+\frac{\beta}{\alpha} & c+\frac{\beta}{\alpha} & c+\frac{\beta}{\alpha} & -c+\frac{\beta}{\alpha} \\ 0 & 0 & 1 & \gamma_2^2 & -\gamma_2^2 & -1 \end{vmatrix}=0 \tag{36}$$

with roots of equation (34) for $c$ as before. That the root for the symmetric disturbance $c=(\beta/\alpha)[\zeta(\rho_1/\rho_2)+\xi]^{-1}$ is wholly real implies neutral stability. For the symmetric disturbance, then, the inviscid analysis does not yield information on wave numbers where amplification occurs, but merely suggests that the profile is relatively stable to symmetric disturbances and neutrally stable in the limit of infinite Reynolds number.

The roots corresponding to the antisymmetric disturbances (eq. (34)) are complex when

$$4\left(\zeta\frac{\rho_1}{\rho_2}\xi+1\right)(\alpha h_2\xi-1)>\left[h_2\alpha+\zeta\frac{\rho_1}{\rho_2}(\xi\alpha h_2-1)\right]^2 \tag{37}$$

The complex root having the positive imaginary part corresponds to an amplified disturbance. The denominator of the right side of equation (34), $2[\zeta(\rho_1/\rho_2)\xi+1]$, when written in full,

$$2\left(\frac{\rho_1}{\rho_2}\frac{e^{-2\alpha h_2}+e^{-2\alpha h_1}}{e^{-2\alpha h_2}-e^{-2\alpha h_1}}\frac{1+e^{-2\alpha h_2}}{1-e^{-2\alpha h_1}}+1\right)$$

is positive for $h_2<h_1$; that is, for the flame zone contained within the duct. Therefore, the amplified root of equation (34) is

$$c=\frac{\beta}{\alpha}\left\{\frac{h_2\alpha+\zeta\frac{\rho_1}{\rho_2}(\xi\alpha h_2-1)+\sqrt{\left[h_2\alpha+\zeta\frac{\rho_1}{\rho_2}(\xi\alpha h_2-1)\right]^2-4\left(\zeta\frac{\rho_1}{\rho_2}\xi+1\right)(\alpha h_2\xi-1)}}{2\left(\zeta\frac{\rho_1}{\rho_2}\xi+1\right)}\right\} \tag{38}$$

Since this is an inviscid analysis, the damped root of equation (34) can have no meaning (ref. 22) and is consequently ignored.

## RESULTS

The disturbance amplitude grows with time as $e^{\alpha c_i t}$, where $\alpha c_i$ is (from eq. (38))

$$\alpha c_i=\frac{\Delta U}{2h_2}\sqrt{\left[\frac{h_2\alpha+\zeta\frac{\rho_1}{\rho_2}(\xi\alpha h_2-1)}{\zeta\frac{\rho_1}{\rho_2}\xi+1}\right]^2-4\frac{\alpha h_2\xi-1}{\zeta\frac{\rho_1}{\rho_2}\xi+1}} \tag{39}$$

since

$$\beta=\frac{U^*-U_1}{h_2}=\frac{\Delta U}{h_2}$$

The quantity under the radical in equation (39) is independent of local $(U^*-U)/h_2$ values. This quantity is plotted in figure 2 as a function $2\alpha h_2$ for the following conditions:

$$\frac{\rho_1}{\rho_2}=1 \qquad \lim_{h_1\to\infty}\frac{h_2}{h_1}=0$$

$$\frac{\rho_1}{\rho_2}=5,\ 7 \qquad \frac{h_2}{h_1}=0.25,\ 0.50,\ 0.75$$

The first set of conditions corresponds to Rayleigh's solution for the stability of an unconfined jet. The second set of conditions represents density ratios that are expected in a flame in a duct for three flame widths. The values of the parameter $\alpha c_i(2h_2/\Delta U)$ in figure 2 go from 0 at $2\alpha h_2=0$ through a maximum, then to 0 again at a finite value of $2\alpha h_2$. For a given value of $2h_2/\Delta U$, this parameter behaves as the amplification rate $\alpha c_i$.

It is clear from figure 2 that, for constant density, the flow is more unstable the smaller $h_2/h_1$ becomes. For constant $h_2/h_1$, the flow is more unstable the smaller $\rho_1/\rho_2$ becomes. The influence of density ratio and wall proximity on the stability of the subject profile is in keeping with experimental observations of another type of profile with a flex—namely, the wake of a cylindrical rod. The stabilizing effect of density ratio is illustrated in reference 1, which notes that a flame anchored in the wake of the rod inhibits vortex shedding. The stabilizing effect of wall proximity is illustrated in reference 30, which shows that wall proximity increases the minimum Reynolds number for the occurrence of shed vortices.

The stabilizing influence of the walls is further illustrated in figure 3. Figures 3(a) and (b) show the values of $2\alpha h_2$ for neutral stability and maximum instability plotted against

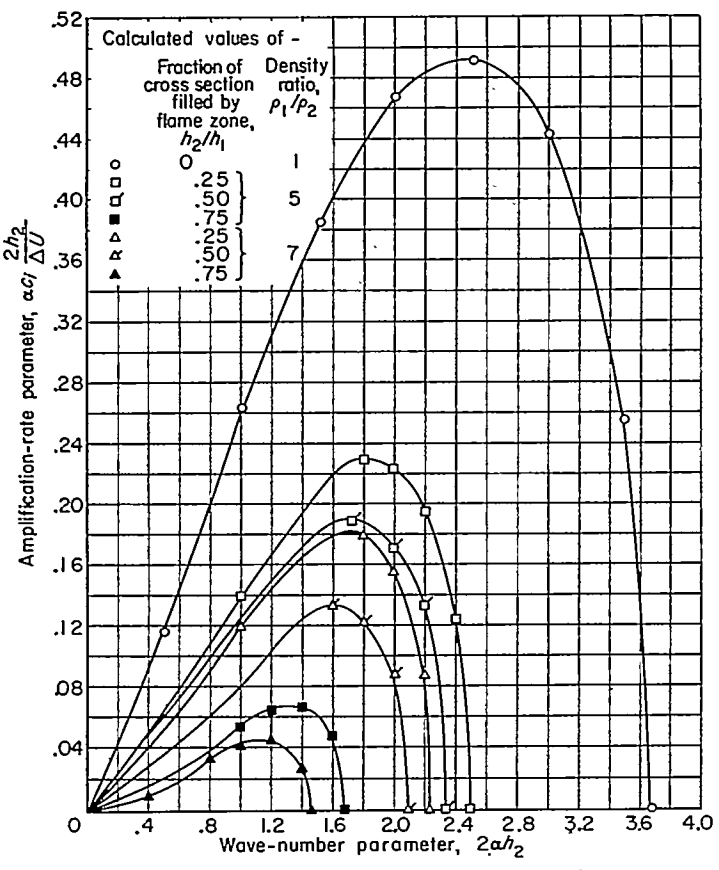


FIGURE 2.—Amplification-rate parameter for profile.

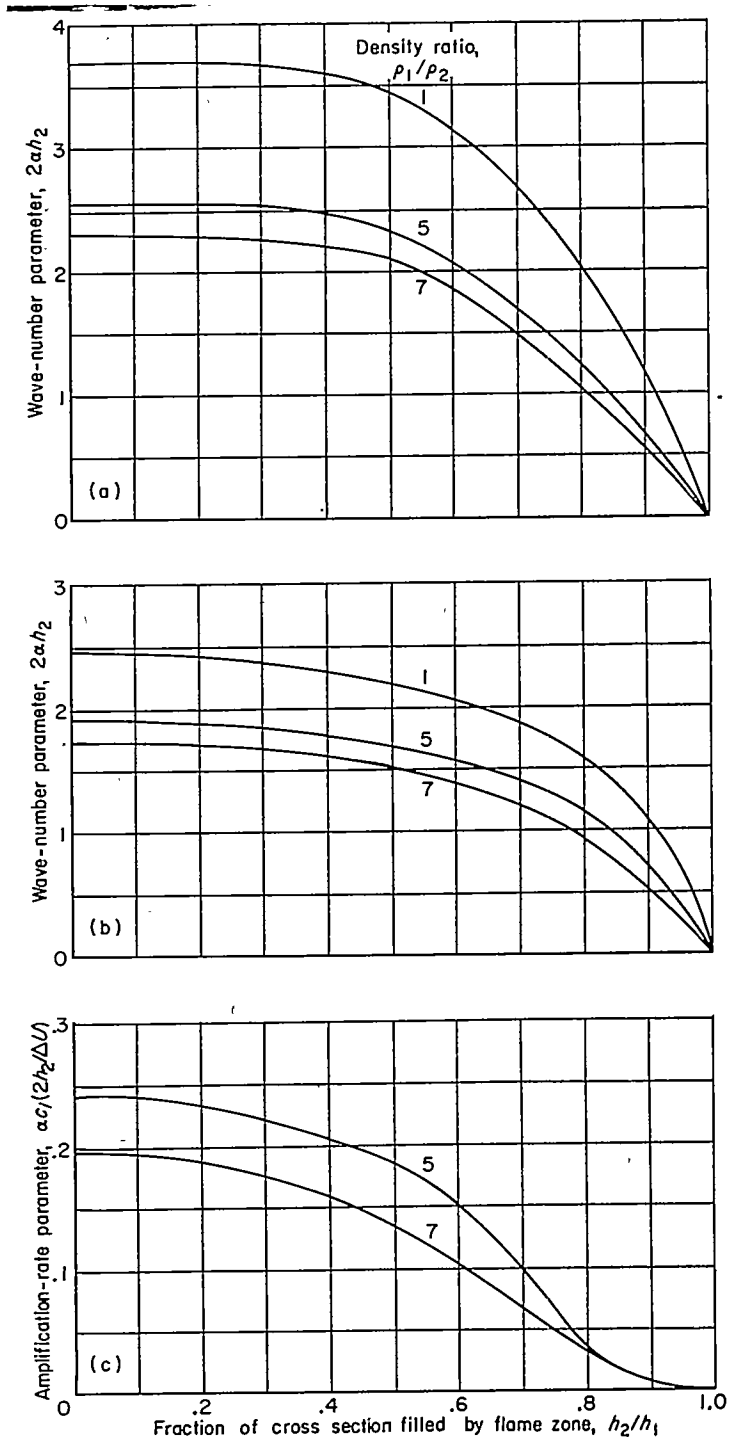


(a) Wave-number parameter for neutral stability.
(b) Wave-number parameter for maximum instability.
(c) Amplification-rate parameter for maximum instability.

FIGURE 3.—Wave-number parameter for neutral stability and maximum instability, and amplification-rate parameter at maximum instability for profile.

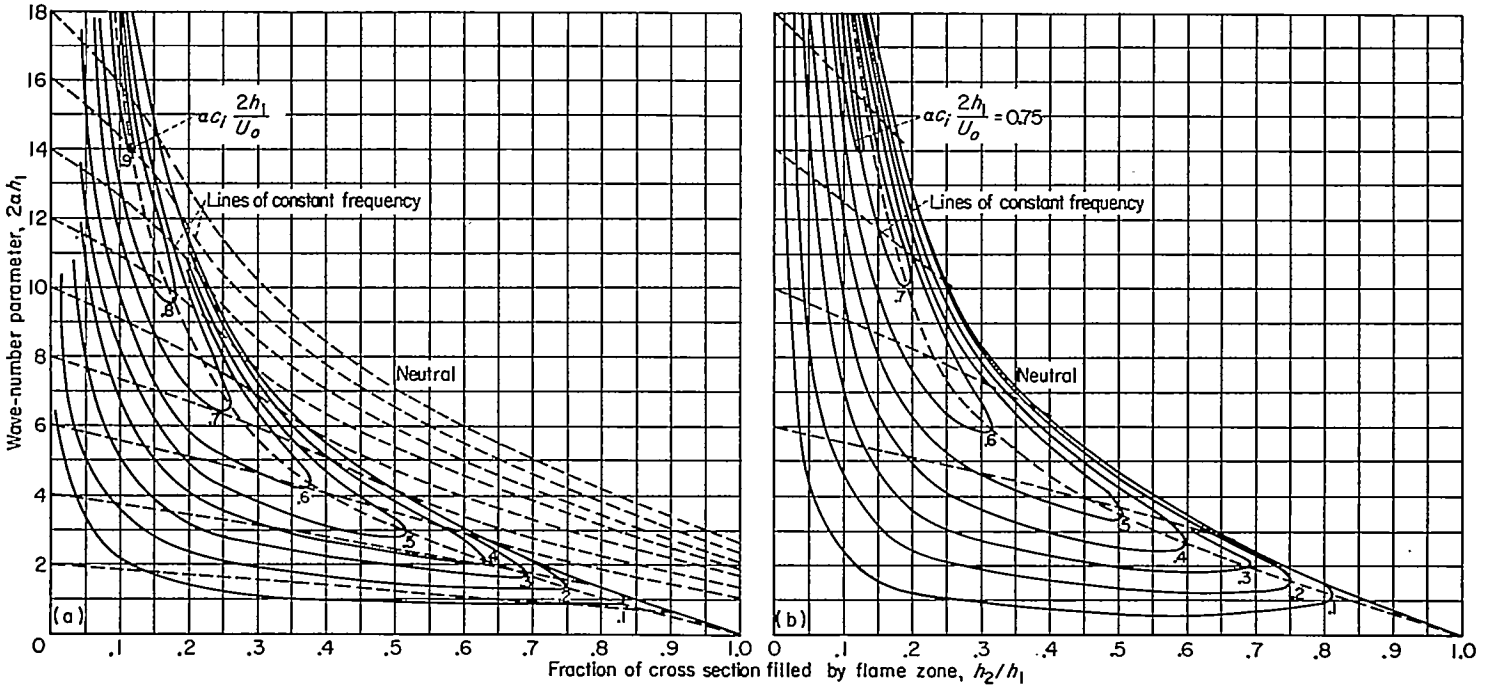


(a) Density ratio, 7. (b) Density ratio, 5.

FIGURE 4.—Stability map for flame in a duct. Contours of constant amplification rate are given by lines of constant $\alpha c_i(2h_1/U_o)$. Lines of constant frequency show path a given disturbance originating at flameholder takes as it propagates along flame zone at phase velocity.

$h_2/h_1$. Figure 3(c) shows the amplification parameter $\alpha c_i(2h_2/\Delta U)$ for maximum amplification rate plotted against $h_2/h_1$. Both the amplification rate and the range of the parameter $2\alpha h_2$ diminish as the flame fills the duct.

### CONSTRUCTION OF STABILITY MAP

In considering the effect of disturbance amplification in the flame zone, local growth-rate contours as a function of wave number and flame-width ratio $h_2/h_1$ present nearly all the important information. Such a plot is called the stability map of a flame in a duct. The map is constructed from the data of figures 2 and 3 and from the steady-state relation of $U^*/U_o$ and $U_1/U_o$ as functions of $h_2/h_1$ (eqs. (1) and (3)) in the following manner. Given: $(U_1/U_o)(h_2/h_1)$, $(U^*/U_o)$ $(h_2/h_1)$, and $[\alpha c_i(2h_2/\Delta U)](2\alpha h_2, h_2/h_1)$ for a given $\rho_1/\rho_2$. The quantity desired is $[\alpha c_i(2h_1/U_o)]$ $(2\alpha h_1, h_2/h_1)$. This quantity is obtained through suitable cross plots of figures 2 and 3 and equations (1) and (3) by setting $2\alpha h_1 = 2\alpha h_2/(h_2/h_1)$:

$$\alpha c_i \frac{2h_1}{U_o} = \alpha c_i \frac{2h_2}{U^* - U_1}\left(\frac{\frac{U^*}{U_o} - \frac{U_1}{U_o}}{h_2/h_1}\right) \tag{40}$$

The resulting stability map is shown in figure 4. Contours of constant dimensionless amplification rates $\alpha c_i(2h_1/U_o)$ are shown as functions of the dimensionless wave number $2\alpha h_1$ and dimensionless flame width $h_2/h_1$ for $\rho_1/\rho_2$ of 7 and 5. These contours are in a region bounded by $2\alpha h_1 = \infty$, 0; $h_2/h_1 = 0$; and the line of $2\alpha h_1$ for neutral stability (i.e., the critical $2\alpha h_1$ as a function of $h_2/h_1$).

### PHASE VELOCITY

A disturbance that distorts the flow and therefore distorts the flame front has a wavelength $\lambda = 2\pi/\alpha$. Such a disturbance if introduced at the flameholder travels along the flame front at the phase velocity $c_r$. This can be seen from the variation of the disturbance with $x$ distance and time; that is,

$$v' \approx e^{i\alpha(x-ct)} = e^{\alpha c_i t} e^{i\alpha(x-c_r t)}$$

In order to follow the amplification rate of a given disturbance, it is necessary to follow a disturbance of constant frequency. The relation between frequency and wavelength is

$$f = \frac{c_r}{\lambda} = \frac{\alpha c_r}{2\pi} \tag{41}$$

The quantity $\frac{c_r - U_1}{U^* - U_1}$ from equation (38) is given by

$$\frac{c_r - U_1}{U^* - U_1} = \frac{1}{\alpha h_2} \frac{h_2\alpha + \zeta\frac{\rho_1}{\rho_2}(\xi\alpha h_2 - 1)}{2\left(\zeta\frac{\rho_1}{\rho_2}\xi + 1\right)} \tag{42}$$

for

$$\left[h_2\alpha + \zeta\frac{\rho_1}{\rho_2}(\xi\alpha h_2 - 1)\right]^2 - 4\left(\zeta\frac{\rho_1}{\rho_2}\xi + 1\right)(\alpha h_2\xi - 1) < 0$$

and by

$$\frac{c_r - U_1}{U^* - U_1} = \frac{1}{\alpha h_2} \frac{h_2\alpha + \zeta\frac{\rho_1}{\rho_2}(\xi\alpha h_2 - 1) + \sqrt{\left[h_2\alpha + \zeta\frac{\rho_1}{\rho_2}(\xi\alpha h_2 - 1)\right]^2 - 4\left(\zeta\frac{\rho_1}{\rho_2}\xi + 1\right)(\alpha h_2\xi - 1)}}{2\left(\zeta\frac{\rho_1}{\rho_2}\xi + 1\right)} \tag{43}$$

for

$$h_2\alpha+\zeta\frac{\rho_1}{\rho_2}(\xi\alpha h_2-1)-4\left(\zeta\frac{\rho_1}{\rho_2}\xi+1\right)(\alpha h_2\xi-1)\geq 0$$

A plot of this quantity against $\alpha h_2$ is given for $\rho_1/\rho_2=7$ at $h_2/h_1=0.25$, 0.50, and 0.75 in figure 5(a). Also shown in figure 5(a) for comparison is $(c_r-U_1)/(U^*-U_1)$ for $\rho_1/\rho_2=5$, $h_2/h_1=0.25$ and for $\rho_1/\rho_2=1$, $h_2/h_1=0$.

Note that

$$\lim_{\alpha h_2\to 0}\frac{c_r-U_1}{U^*-U_1}=0$$

From the steady-state solutions,

$$\lim_{h_2/h_1\to 0}(U^*-U_1)=0$$

Therefore, at the flameholder $c_r=U_1=U_o$. Then it is convenient to relate the local wave number to the wave number at the flameholder by

$$\alpha=\alpha_o\frac{U_o}{c_r} \tag{44}$$

where $\alpha_o$ is the wave number at the flameholder, which is related to the frequency of the disturbance $f$ and $U_o$ by $\alpha_o=f2\pi/U_o$. By means of equations (42), (43), (44), (1), and (3), values of $\alpha(\alpha_o, h_2/h_1)$ were calculated; these are shown in figure 4 as lines of constant frequency. These lines enable one to follow the local amplification rate of a disturbance of given frequency from the flameholder to some station downstream and are so employed in a later section.

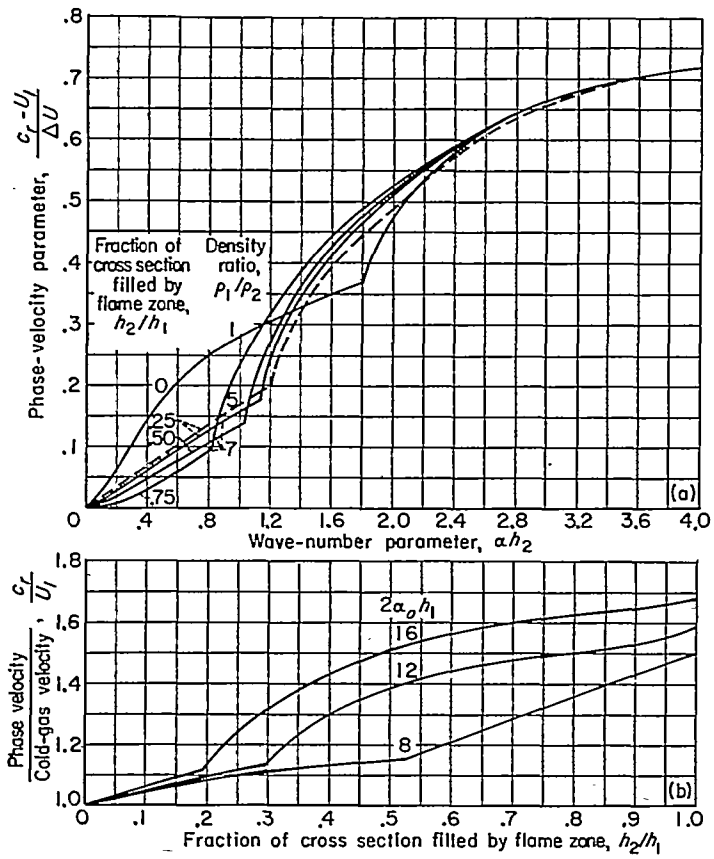


(a) Phase-velocity parameter for amplified and neutral disturbances as function of wave-number parameter.

(b) Ratio of phase velocity to cold-gas velocity at three frequencies as function of $h_2/h_1$ for density ratio of 7.

FIGURE 5.—Phase-velocity parameters.

An additional calculation for the phase velocity was made for later comparison with experimental data. In figure 5(b) is shown a plot of $c_r/U_1$ against $h_2/h_1$ for $\rho_1/\rho_2$ of 7 and $2\alpha_o h_1$ of 8, 12, and 16. These data enable direct comparison of measured values of phase velocity with values predicted from the stability analysis.

### DISTURBANCE GROWTH

A qualitative picture of the nature of the disturbances propagating at phase velocity is shown in figure 6. The streamline distributions are given for a neutral disturbance in a reference plane moving at the phase velocity $c_r$; in this frame of reference, the streamlines are no longer a function of time. Motion is relative to the "eyes" of the disturbance centers. In the hot flame core, the gas moves faster than $c_r$; in the colder gas outside the flame, the gas moves slower than $c_r$.

To picture what happens to an amplified disturbance, imagine the $y$-amplitude of the wrinkles in figure 6 to be

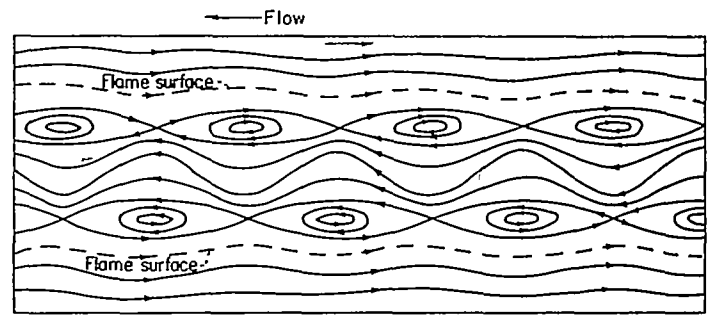


FIGURE 6.—Streamlines of neutral disturbance moving at phase velocity.

growing from right to left. In addition, the flame width is increasing gradually, as is the phase velocity; and therefore the $x$- and $y$-spacing of the "eyes" is increasing in the direction of flow until a neutral situation is reached. At each $x$-station the disturbance has a local growth rate $\alpha c_i$ that acts over a short time $\Delta t$. Then (since $x$ is related to time by $dx=c_r dt$), at any time $t$ after the disturbance originated at the flameholder, the amplitude is

$$v'=v'_o e^{\int_0^t \alpha c_i dt} \tag{45}$$

where $v'_o$ is the amplitude of the disturbance at the flameholder on the centerline of the profile.[2]

Up to this point, the independent variables have been the dimensionless wave number $2\alpha h_2$ and flame width $h_2/h_1$. In order to evaluate equation (45), it is necessary to use the relation

$$\frac{dx}{dt}=c_r \tag{46}$$

and some assumption concerning the variation of $h_2/h_1$ with $x$. Two simple assumptions are used that bracket the variation of $h_2/h_1$ with $x$ found by experiment and facilitate the integra-

[2] The linking of the parallel-flow solutions by conserving $v'$ along the centerline is the simplest but not necessarily the best of several available choices.

tion of equation (45). These assumptions are (1) that the flame is linear:

$$\frac{\mathrm{d}\frac{h_2}{h_1}}{\mathrm{d}\frac{x}{h_1}}=K_2 \tag{47}$$

and (2) that the change in fraction burned with distance is linear:

$$\frac{\mathrm{d}F}{\mathrm{d}\frac{x}{h_1}}=K_1 \tag{48}$$

A qualitative comparison of the way these assumptions describe a flame surface is given in the following sketch:

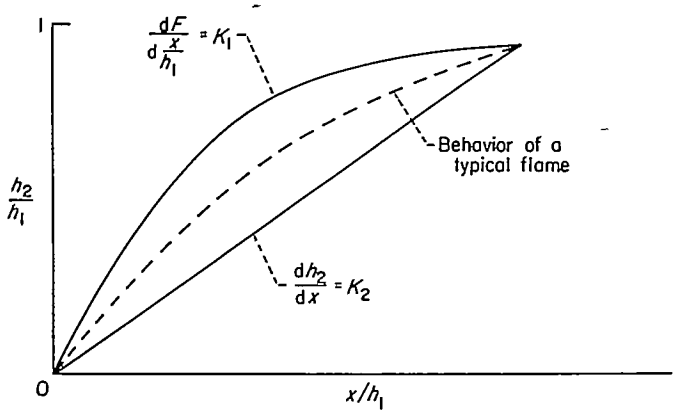


Sketch (e)

Inserting equations (46) and (47) in equation (45) results in

$$v'=v_o'\left(e^{\frac{1}{2}\int_0^{h_2/h_1}\alpha c_i\frac{2h_1}{U_*}\frac{U_*}{c_r}\mathrm{d}\frac{h_2}{h_1}}\right)^{1/K_2} \tag{49}$$

The term in parentheses is called the gain $G$, which is independent of the value of the propagation rate $K_2$.

A similar derivation can be made for the alternative form of heat release; that is, for

$$\frac{\mathrm{d}F}{\mathrm{d}\frac{x}{h_1}}=K_1$$

which yields

$$v'=v_o'\left(e^{\frac{1}{2}\int_0^{F}\alpha c_i\frac{2h_1}{U_*}\frac{U_*}{c_r}\mathrm{d}F}\right)^{1/K_1} \tag{50}$$

where the term in parentheses $G'$ is independent of the value of $K_1$.

The values of $G$ and $G'$ can be obtained by graphical integration. They give relative values of amplification of a disturbance of given frequency when integrated along a constant-frequency line in figure 4. Figure 7 gives the results of such an integration carried from $h_2/h_1$ of 0 to 1 for a range of $2\alpha_o h_1$ and for the following conditions: $G$ is given as a function of $2\alpha_o h_1$ for $\rho_1/\rho_2$ of 5 and 7, and $G'$ is given as a function of $2\alpha_o h_1$ for $\rho_1/\rho_2$ of 7. It is apparent that, for the conditions examined, there is a most-amplified frequency

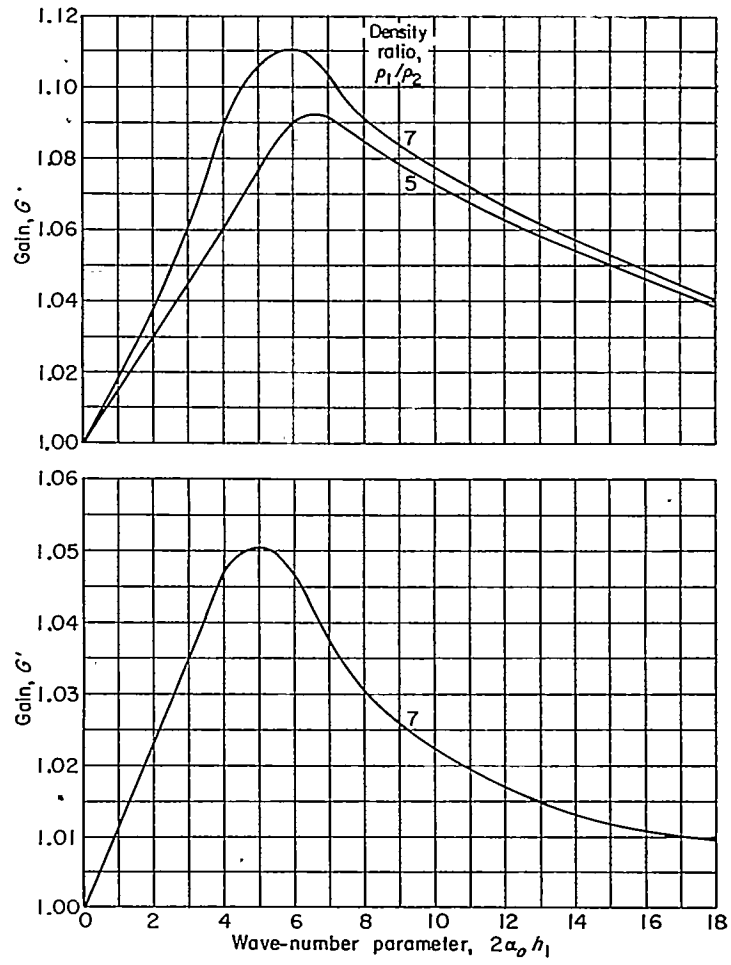


FIGURE 7.—Gains for flame filling the duct.

corresponding to a value of $2\alpha_o h_1 \approx 6$. Recall that $f=2\alpha_o h_1 U_o/2\pi 2h_1$ or the most-amplified frequency is approximately $f \approx U_o/2h_1$. This frequency does not depend upon a rate of flame spreading; it was obtained by assuming that a mode of flame spreading is specified. Approximately the same frequency obtains for the two modes of flame spreading specified.

Not only is the most-amplified frequency in figure 7 at $\rho_1/\rho_2$ of 5 very near that for $\rho_1/\rho_2$ of 7, but also the numerical values of the gains are very nearly the same. This latter occurrence is due to two opposing influences: For a given $U^*-U_1$, the profile having the lower value of $\rho_1/\rho_2$ has a higher amplification rate, and a disturbance of given frequency is amplified over a wider range of $h_2/h_1$. On the other hand, at any value of $h_2/h_1$, $U^*-U_1$ is smaller for the smaller $\rho_1/\rho_2$.

The growth of the disturbances for fractional values of $h_2/h_1$ (or $F$) was calculated by taking the integral in equation (49) or (50) to fractional values of $h_2/h_1$ (or $F$). The results are shown in figure 8, in which the gains $G$ and $G'$ are plotted against $h_2/h_1$ or $F$ for values of $2\alpha_o h_1$ from 2 to 18. For some values of $h_2/h_1 < 5$, there are frequencies higher than those corresponding to $2\alpha_o h_1 \approx 6$ that locally exhibit a maximum gain. The fact that for values of $h_2/h_1 < 0.5$ there is a local amplification that depends on frequency is used later in comparing analysis with experiment. As $h_2/h_1$ decreases, the frequency that is most amplified increases.

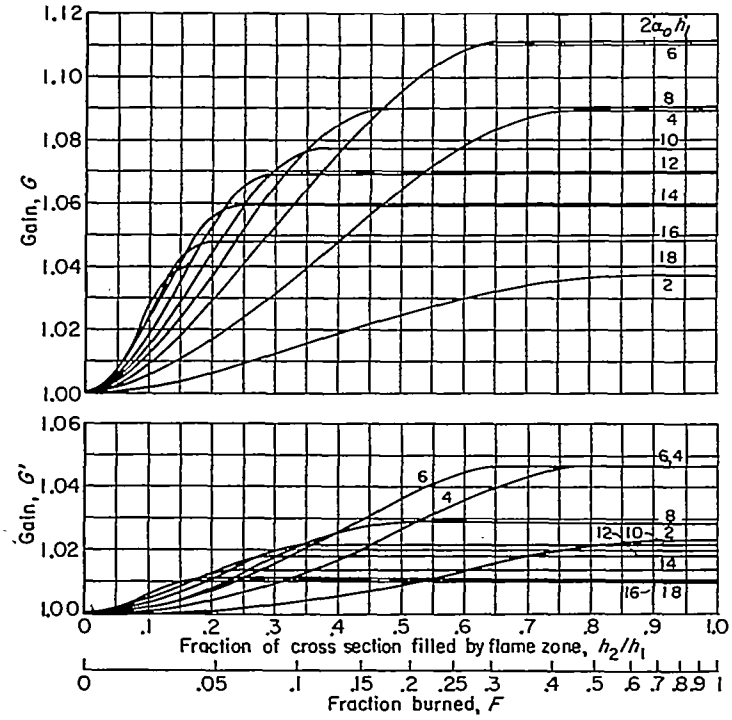


FIGURE 8.—Gains as function of $h_2/h_1$ for family of initial wave-number parameters. Density ratio, 7.

### DISTURBANCE VELOCITY DISTRIBUTION IN $y$-DIRECTION

The way the disturbance velocity $v'$ varies along the axis of the duct is shown in figure 8. In reducing the results of this analysis to measurable quantities, a qualitative picture of the way the disturbance velocity $v'$ varies across the duct is needed. Such a picture can most easily be obtained by considering a neutrally stable disturbance.

From equations (18) and (28),

$$\frac{v'_{2,y}}{v'_o}=\frac{1}{\gamma_y}\frac{\frac{B_1}{B_2}+\gamma_y^2}{\frac{B_1}{B_2}+1}\quad 0\leq y\leq h_2 \tag{51}$$

where $v'_{2,y}$ is the disturbance velocity at $y$ in region 2, $v'_o$ is the disturbance velocity at the centerline, and $\gamma_y\equiv e^{-\alpha y}$. In the region $h_2\leq y\leq h_1$, $v'_{1,y}/v'_{2,h_2}$ can be obtained from equations (18), (27), and (28) in the form

$$\frac{v'_{1,y}}{v'_{2,h_2}}=\frac{-\gamma_1^2+\gamma_y^2}{-\gamma_1^2+\gamma_2^2}\frac{\gamma_2}{\gamma_y} \tag{52}$$

The ratio $B_1/B_2$ can be obtained from the equation represented by the first row in the determinantal equation (30)

$$\left(c-\frac{\beta}{\alpha}+\zeta\frac{\rho_1}{\rho_2}c\right)B_1+\left(-c-\frac{\beta}{\alpha}+\zeta\frac{\rho_1}{\rho_2}c\right)\gamma_2^2B_2=0$$

or

$$\frac{B_1}{B_2}=-\gamma_2^2\left[\frac{\left(\zeta\frac{\rho_1}{\rho_2}-1\right)-\frac{\beta}{\alpha c}}{\left(\zeta\frac{\rho_1}{\rho_2}+1\right)-\frac{\beta}{\alpha c}}\right] \tag{53}$$

Recall that $\beta/\alpha c$ in equation (30) is the same as $(1/\alpha h_2)[(U^*-U_1)/(c-U_1)]$, which for real values of $c$ is given in equations (42) and (43).

A series of calculations was made to obtain the representative behavior of $v'_{h_2}/v'_o$ across the duct, and the results are shown in figure 9 for $\rho_1/\rho_2$ of 7. The critical $h_2/h_1$ is taken as the value where for a given frequency the imaginary part of $c$ becomes 0. Figure 9(a) shows the value of $v'_{h_2}/v'_o$ at the critical $h_2/h_1$ plotted against initial wave number $2\alpha_o h_1$. For $2\alpha_o h_1>8$ (i. e., for $(h_2/h_1)_{cr}<0.46$) the value of $v'_{h_2}/v'_o\approx 0.2$. The ratio decreases at $2\alpha_o h_1<8$ (i. e., for $(h_2/h_1)_{cr}>0.46$) as the flame approaches the wall.

In figure 9(b) the value $v'_{h_2}/v'_o$ is given for a fixed frequency corresponding to $2\alpha_o h_1=12$ following a disturbance along the duct from the flameholder ($h_2/h_1=0$) to the station where the flame touches the wall. The dashed portion is interpolated between $h_2/h_1=0$ (where $v'_{h_2}=v'_o$) and $h_2/h_1=(h_2/h_1)_{cr}$ (where the calculation starts). It is obvious from this curve that, if $v'_{h_2}$ is measured instead of $v'_o$, the apparent growth rate is not as rapid for $h_2/h_1<(h_2/h_1)_{cr}$ as for $v'_o$, simply because of the velocity distribution. Also, for $h_2/h_1>(h_2/h_1)_{cr}$ there is an apparent decay in $v'_{h_2}$ owing to this distribution, despite the fact that the value of $v'_o$ is neutrally stable. This latter point is employed in comparing the analytical with the experimental results.

The significance of figure 9 is summarized as follows:

(1) Although the inviscid treatment eliminates consideration of damping, it is clear that at the flame front the velocity amplitude diminishes at $h_2/h_1>(h_2/h_1)_{cr}$ because of the velocity distribution.

(2) In some instances, even though the flow is unstable and the disturbance velocity amplitude is increasing along

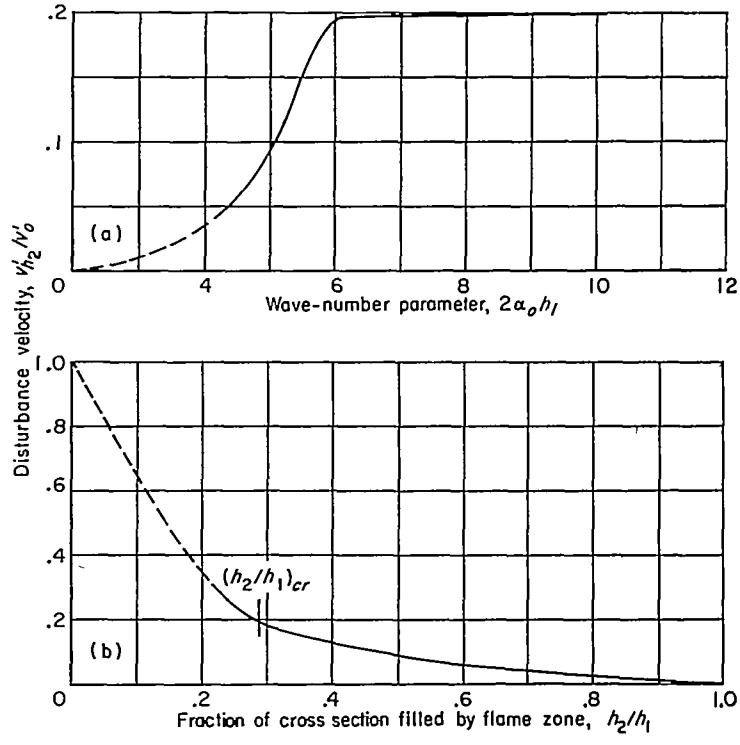


(a) At critical $h_2/h_1$.
(b) For wave-number parameter of 12.

FIGURE 9.—Disturbance-velocity distributions. Density ratio, 7.

the center of the flame, the disturbance-velocity amplitude at the flame front may not necessarily be increasing.

(3) The disturbance that is most amplified at the center of the profile (i.e., $2\alpha_c h_1=6$) is not necessarily the most amplified at the flame front, owing to the velocity distribution; the frequency of the latter is somewhat greater than that of the former.

### RELATION OF THEORETICAL RESULTS TO MEASURABLE QUANTITIES

In the experimental phase, current instrumentation techniques impose limitations on what can be measured. For example, the velocity $v'_o$ cannot be measured directly by hot-wire techniques because the flame temperature is too high ($\approx 4000°$ R). The purpose of this section is to collect certain results of the foregoing analysis that lend themselves to direct measurement.

**Flame slope.**—In equations (49) and (50) the growth of a disturbance $v'/v'_o$ is found to be proportional to a calculable quantity, gain, raised to a power $1/K$. The quantity $K$ is alternatively $K_2=\mathrm{d}(h_2/h_1)/\mathrm{d}(x/h_1)$ or $K_1=\mathrm{d}F/\mathrm{d}(x/h_1)$, depending on the mode of flame propagation assumed. For both modes, $K$ is smaller the more gradual the rate of flame spreading. To a first approximation, then, the amplification of a disturbance increases as the ratio of propagation velocity to flow velocity decreases. This trend can be verified experimentally.

**Phase velocity.**—One quantity that can be measured immediately is the phase velocity $c_r$. A plot of $c_r/U_1$ for three frequencies is given in figure 5(b). Thus, for a given flow setting, the absolute magnitudes of $c_r/U_1$ can be compared and the variation with frequency and with $h_2/h_1$ can be examined.

**Flame-front displacement.**—The transverse velocity $v'$ acting at the flame surface $y=h_2$ causes a wavy wrinkle to appear in the surface. If a quantity $h$ is defined as the distance from crest to valley of these wrinkles, this quantity equals twice the $y$ amplitude of the streamlines of the flow at the flame front. If a neutral case is considered and the distribution of $v'$ in the flame zone is approximated by

$$v'=v'_c+(v'_o-v'_c)\left(1-\frac{y}{y_c}\right)$$

the equations of the streamlines are given by

$$\frac{y}{y_c}\approx 1-\epsilon\cos\alpha x\pm\sqrt{1-2\Psi^*+2k\cos\alpha x}$$

where

$k$ $\dfrac{v'_c}{(U^*-c)\alpha y_c}$

$v'_c$ amplitude of disturbance velocity at $y_c$

$v'_o$ amplitude of disturbance velocity at centerline

$y_c$ coordinate where $U=c$

$\epsilon$ $\dfrac{v'_o-v'_c}{(U^*-c)\alpha y_c}$

$\Psi^*$ dimensionless stream function, $\dfrac{1}{(U^*-c)y_c}\displaystyle\int_0^y U\,\mathrm{d}y$

At $h_2\leqq h_{2,cr}$, $2\Psi^*$ varies between 0.96 and 0.99. Because $2k$ can be taken arbitrarily small, for $2k/(1-2\Psi^*)\ll 1$,

$$\frac{y}{y_c}=1-\epsilon\cos\alpha x\pm\sqrt{1-2\Psi^*}\left[1+\frac{k\cos\alpha x}{(1-2\Psi^*)}\right]$$

Because $y>y_c$, the plus sign is chosen so that

$$\frac{y}{y_c}=1+\sqrt{1-2\Psi^*}+\left(\frac{k}{\sqrt{(1-2\Psi^*)}}-\epsilon\right)\cos\alpha x$$

$$\approx 1+0.2+\frac{1}{\alpha y_c}\left[\frac{\dfrac{v'_c}{U_o}}{\dfrac{U^*-U_c}{U_o}(0.2)}-\frac{\dfrac{v'_o}{U_o}-\dfrac{v'_c}{U_o}}{\dfrac{U^*-U_o}{U_o}}\right]\cos\alpha x$$

$$\approx 1.2+\frac{\dfrac{v'_o}{U_o}}{\alpha y_c\dfrac{U^*-c}{U_o}}\left(\frac{6v'_c}{v'_o}-1\right)\cos\alpha x$$

But $v'_c/v'_o$ is a weak function of $\alpha$ and $h_2/h_1$ and is approximately 0.2.

Employing the identity

$$\frac{U^*}{U_o}-\frac{c}{U_o}=\left(\frac{U^*}{U_o}-\frac{U_1}{U_o}\right)\left(1-\frac{c-U_1}{U^*-U_1}\right)$$

and a value of $(c-U_1)/(U^*-U_1)$ from figure 5(a),

$$\frac{U^*}{U_o}-\frac{c}{U_o}\approx\left(\frac{U^*}{U_o}-\frac{U_1}{U_o}\right)(0.85)$$

where the quantity $(U^*/U_o)-(U_1/U_o)$ is a function of $\rho_1/\rho_2$ and $h_2/h_1$ only. Thus,

$$\frac{y}{y_c}\approx 1.2+\frac{0.2\dfrac{v'_o}{U_o}}{0.85\,\alpha y_c\dfrac{U-U_o}{U_o}}\cos\alpha x$$

at the flame front. The coefficient of $\cos\alpha x$ is $\frac{1}{2}h$, the flame-front wrinkle amplitude. It can be seen that $h$ will behave qualitatively like $v'$. Without going into further detail, then, some predictions can be made from the theory that may be verified by experiment. First, $h$ may be expected to behave qualitatively as shown in the following sketch:

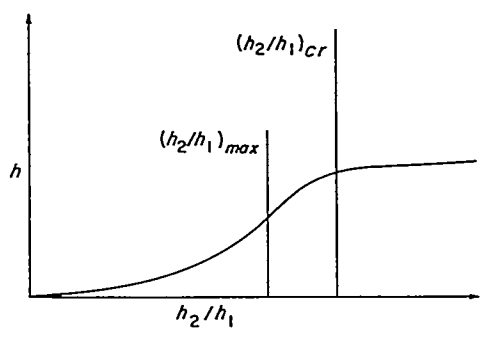


Sketch (f)

The shape of the curve in sketch (f) can be used to locate the approximate $x$-position of $(h_2/h_1)_{cr}$. There is a point of inflection where $v'_{h_2/h_1}$ reaches a maximum and a knee as $v'_{h_2/h_1}$ ceases to grow. The knee position falls between the $h_2/h_1$ for maximum amplification and $(h_2/h_1)_{cr}$. Thus, the data that can be sought are the absolute values of $h_2/h_1$ where the knee occurs for a given frequency and the relative

positions of the knee for different frequencies.

**Flame propagation.**—As stated in the introduction, one of the reasons for pursuing the stability analysis is to find a disturbance frequency that permits the greatest increase in flame spreading with the smallest expenditure of energy. In this section a model of flame propagation is constructed that permits extrapolating the behavior of $v'$ from the stability analysis to a measurable behavior of flame propagation. The flame front is assumed to be a zone in which the density goes from $\rho_1$ to $\rho_2$ in a distance that is short compared with the disturbance wavelength. This front is propagating into the gas of density $\rho_1$ at a rate $V_{T,u}$; that is, the undisturbed turbulent flame speed. Owing to the normal propagation of the front, an initially wavy surface becomes a cusped surface. Assuming such a surface composed of cylindrical arcs

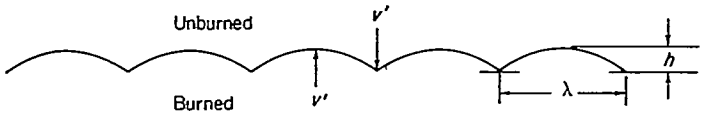


Sketch (g)

permits a calculation of the flame-front stretching due to a displacement $h$. If the undisturbed area $S_u=\lambda$ and the disturbed area $S_d$ are approximately equal to arc length,

$$\frac{S_d}{S_u}\approx\sqrt{1+\left(\frac{2h}{\lambda}\right)^2} \tag{54}$$

An equilibrium $h$ is reached when

$$\frac{S_d}{S_u}=\sqrt{\frac{1+\frac{2v'}{V_{T,u}}}{1+\frac{v'}{V_{T,u}}}} \tag{55}$$

Then $S_d/S_u$ behaves roughly as $\left(1+\frac{1}{2}\frac{v'}{V_{T,u}}\right)$ for small amplitude. Equation (54) contains a nonlinear term $4h^2/\lambda^2$. The development so far as been a linear one. The linear development would be expected to furnish only a first approximation for amplitudes large enough so that $4h^2/\lambda^2$ is no longer negligible compared to unity.

The sequence of events that leads to a prediction of $S_d/S_u$ is as follows:

(1) The flame is initially wrinkled by the velocity $v'$ acting at the flame surface.

(2) As the wrinkles grow, the flame shape shifts from a sine wave to a cusped surface, owing to normal propagation.

(3) After a certain time an equilibrium is reached between the disturbance velocity $v'$ and the undisturbed propagation velocity $V_{T,u}$.

The ratio of the disturbed surface to the undisturbed surface when equilibrium is reached is, for small disturbances,

$$\frac{S_d}{S_u}=\left(1+\frac{1}{2}\frac{v'}{V_{T,u}}\right)=\frac{V_{T,d}}{V_{T,u}} \tag{56}$$

Before this equilibrium value of $S_d/S_u$ is reached, the flame surface is given by (again for the neutral case)

$$\frac{y_{h_2}}{y_c}\approx 1.2+\frac{0.2\,v_o'}{\Delta U\alpha y_c}\cos\alpha x$$

But $2h/\lambda$ of equation (54) is given by

$$\frac{2h}{\lambda}\approx\left(\frac{y_{h_2}}{y_c}-1.2\right)\frac{y_c 2\alpha}{\pi}$$

$$\approx\frac{v_o'}{\Delta U}\,\frac{0.4}{\pi}\cos\alpha x$$

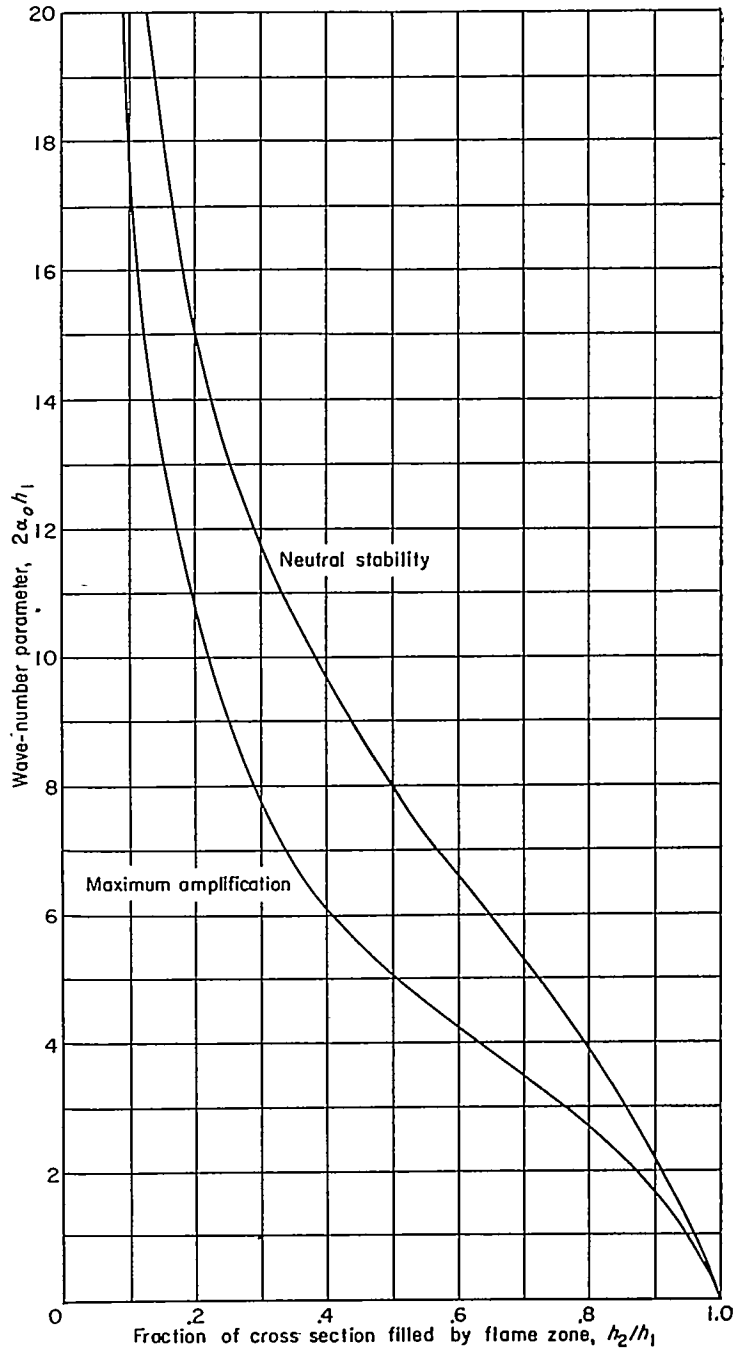


FIGURE 10.—Frequencies that give maximum increase in local flame speed. Density ratio, 7.

Thus, in the transient case as in the equilibrium case (eq. (55)), $S_d/S_u$ behaves as $v'$. The quantity $S_d/S_u$ when measured locally should behave like $G$ in figure 8, if the effect of distribution is neglected. When the latter effect is taken into account, $v'$ for fixed $2\alpha_o h_1$ measured at $h_2$ achieves a maximum value somewhere between $h_2/h_1$ for maximum amplification and neutral stability.

Thus, at any station $h_2/h_1$, there should be a frequency of disturbance that would cause the greatest increase in flame speed, and at this station the increase in flame speed should be greater for greater values of $v'/V_{T,u}$.

Figure 10 gives a plot of $2\alpha_o h_1$ against $h_2/h_1$ for maximum amplification and for neutral stability. For any value of $h_2/h_1$, the frequency giving the greatest $v'/V_{T,u}$ (at the flame surface) has a value of $2\alpha_o h_1$ that falls between these curves. The lag in time required for the flame to become wrinkled initially will move the curve for maximum $S_d/S_u$ to slightly higher $2\alpha_o h_1$ values. The curves given should be considered the lower limits of $2\alpha_o h_1$ for maximum $S_d/S_u$, and they serve as a basis for comparison with the experimental data.

### EFFECT OF FLAMEHOLDER

When a flame is anchored in a duct, some form of flameholder must be used. The most common form of flameholder studied in recent years is the cylinder with axis normal to the stream. The cross section of the cylinder has assumed many different shapes. Properties of the flow in the wake are common to all the shapes studied. In this section some of these properties are used to deduce the effect of a flameholder on the flow field and on its stability far from the flameholder.

**Steady-state velocity distribution.**—The properties of the flow field in the immediate wake of the flameholder as described in references 1 and 31 are shown in sketch (h):

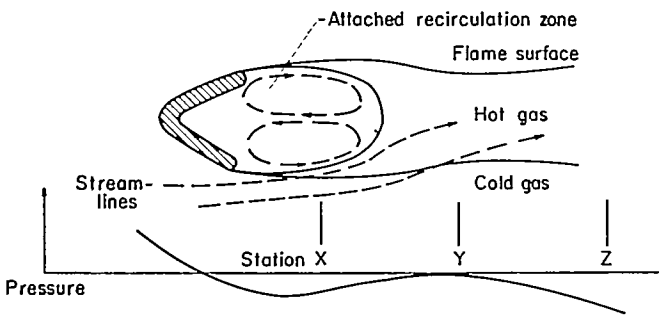


Sketch (h)

Two eddies are attached in the wake of the flameholder. The gas in this zone is hot; it acquires energy from the downstream hot gas and delivers energy to the outside cold gas by diffusion. At some position on the surface of the recirculation zone, sufficient energy is acquired by the cold gas for ignition to occur and a flame to propagate into the cold-gas stream as shown in sketch (h). The pressure measured at the walls has an axial distribution that is shown qualitatively in sketch (h) (refs. 1 and 31).

If the static pressure is assumed constant across the duct at any axial station, the effect of the first positive, then vanishing, then negative pressure gradient upon gases of unlike densities permits an estimation of the velocity profile downstream of the flameholder. The velocity profiles at stations X, Y, and Z of sketch (h) are shown in sketch (i):

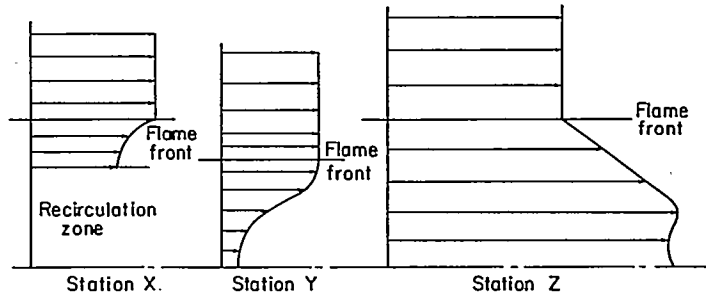


Sketch (i)

At station X the pressure gradient in the axial direction has been positive for a small distance and is still positive at X. This fixes the sense of the velocity difference between cold and hot gases on either side of the flame and the sense of the velocity gradient of the hot gas at the flame front. At station Y the gas has a positive-pressure-gradient history, again fixing the sense of the velocity difference, and at Y the pressure gradient vanishes, causing the velocity gradient at the flame front to vanish. At station Z the gas has a negative-pressure-gradient history from Y sufficient to cause the sense of velocity difference and gradient at the flame front as shown. The gas particle at the position of the velocity maximum passed through the flame at station Y.

If the profile is approximated by straight-line segments with a corner at this velocity maximum as shown in sketch (j),

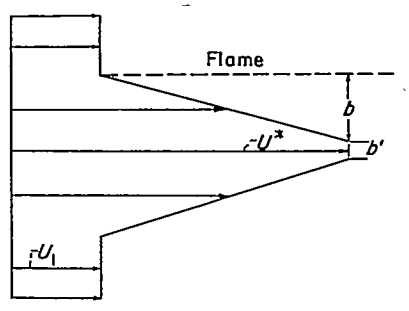


Sketch (j)

some quantitative relation based on the continuity equation and experimental observations can be obtained. From continuity,

$$\frac{1}{2}b'U^*=V_w l_w \frac{\rho_1}{\rho_2} \tag{57}$$

and

$$b\frac{U^*+U_1}{2}=V_F l_F \frac{\rho_1}{\rho_2} \tag{58}$$

where

$l_F$ axial length from station Y to station of interest downstream of Y (sketch (h))
$l_w$ axial length of wake to station Y
$V_F$ mean flame speed over $l_F$
$V_w$ mean flame speed over $l_w$

Combining equations (57) and (58) gives

$$\frac{b'}{2b}=\frac{U^*+U_1}{2U^*}\frac{V_w l_w}{V_F l_F} \tag{59}$$

In order to obtain an order of magnitude of $b'/2b$ of interest in the stability analysis, the terms on the right side of equation (59) are given the following values: $(U^*+U_1)/U^*=1.5$ (from ref. 1 for $F=0.25$, $\rho_1/\rho_2=6$); $V_w/V_F\approx 1/(V_T/V_L)\approx 1/2.5$; and $l_w\approx 4d$ (from ref. 1). Defining $l$ as $l_w+l_F$,

$$\frac{l_w}{l_F}=\frac{1}{\frac{l}{l_w}-1}=\frac{4}{\frac{l}{d}-4}$$

equation (59) becomes

$$\frac{b'}{2b}=\frac{1.2}{\frac{l}{d}-4} \qquad \left(\frac{l}{d}>4\right) \tag{60}$$

At a station $l/d=8$ (from eq. (60)),

$$\frac{b'}{2b}=0.6$$

Farther downstream, at $l/d=24$, for example,

$$\frac{b'}{2b}=0.06$$

The foregoing stability analysis is for a profile in which $b'=0$.

From this section it can be seen that, near the flameholder ($l/d=8$), the hot-gas velocity distribution differs in shape from the _/_ profile neglecting the flameholder. At this station, 60 percent of the flame-zone width has a flat distribution. Remote from the flameholder ($l/d=24$), 6 percent of the hot-gas width has a flat velocity distribution. The magnitude and direction of the error incurred in neglecting this flattening are estimated in the following section.

**Comparison of stability of _/_ and _/‾_ profiles.**—Amplification rates as a function of $2\alpha h_2$ are compared in figure 2

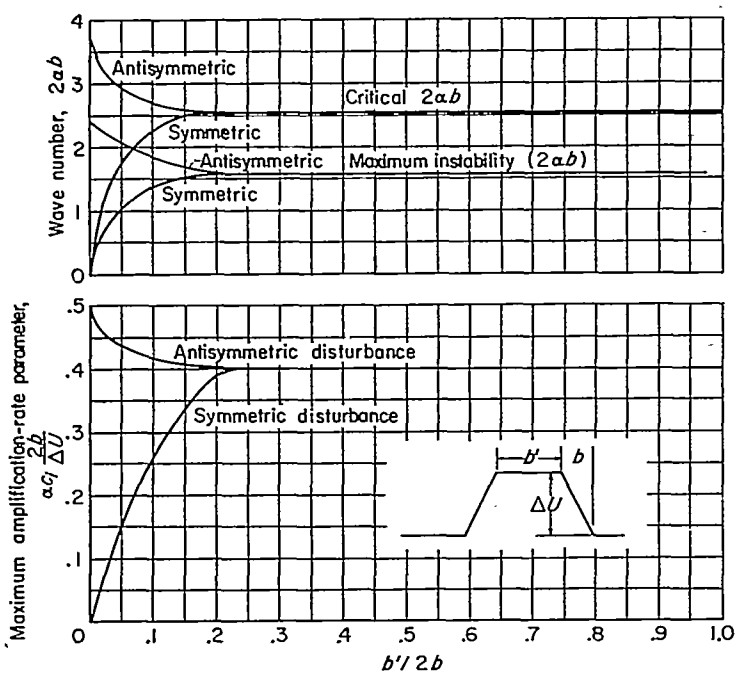


FIGURE 11.—Effect of velocity profile on amplification-rate parameter and on wave-number parameters for neutral stability and maximum instability.

for several values of $\rho_1/\rho_2$ and $h_2/h_1$. The effect of increasing $\rho_1/\rho_2$ and $h_2/h_1$ is stabilizing; that is, the magnitude of the amplification rates and the range of $2\alpha h_2$ over which positive values exist are reduced. The plots of amplification rate against $2\alpha h_2$ are affine. It appears reasonable that, in examining the effect of truncating the profile, an examination at a single value of $\rho_1/\rho_2$ and $h_2/h_1$ would yield representative results.

The conditions considered here are the ones formulated by Rayleigh in equations (24) and (25) (p. 387, ref. 15), which correspond to $\rho_1/\rho_2=1$ and $h_2/h_1=0$ (or $h_1=\infty$). Calculations were made in which $b'/2b$ was taken as a parameter in such a way that the results yield values of $\alpha c_i(2b/\Delta U)$ and $2\alpha b$ at maximum instability and a critical value of $2\alpha b$ where $\alpha c_i$ vanishes. The results of these calculations are shown in figure 11. When $b'=0$, the results correspond to those of figure 2; the flow is unstable to antisymmetric disturbances and neutrally stable to symmetric disturbances. As $b'/2b$ increases, the amplification rate and the critical values of $2\alpha b$ decrease for the antisymmetric disturbances. The flow gradually becomes unstable to symmetric disturbances as $b'/2b$ increases. At $b'/2b<0.2$, the flow is as unstable to symmetric as to antisymmetric disturbances and possesses the same critical values of $2\alpha b$. The values of $b'/2b$ of interest here are of the order 0.6 to 0.06. The flame half-width $h_2$ is $b'/2+b$. In the following table the values of the important parameters $\alpha c_i(2h_2/\Delta U)$, $(2\alpha h_2)_{max\ c_i}$, and $(2\alpha h_2)_{cr}$ are compared for $b'/2b=0$, 0.06, and 0.6 for antisymmetric disturbances:

| $\frac{b'}{2b}$ | $\alpha c_i\left(\frac{2h_2}{\Delta U}\right)_{max}$ | $(2\alpha h_2)_{max\ c_i}$ | $(2\alpha h_2)_{cr}$ |
|---|---|---|---|
| 0 | 0.492 | 2.44 | 3.69 |
| .06 | .508 | 2.49 | 3.71 |
| .6 | .688 | 3.28 | 4.57 |

For a given $2h_2/\Delta U$, the amplification rate is increased as the hot-gas velocity is progressively truncated. The wave-number range over which the flow is unstable is widened. Both of these effects bespeak a greater instability of flow. On the other hand, it can be easily demonstrated that, for a given $\Delta U$, $h_2/h_1$ is greater when the profile is truncated, so that the destabilizing effect of the flameholder is partially but not completely attenuated.

The difference between the parameters calculated at $b'/2b=0$ and 0.6 shows that near the flameholder the amplification rates may be of the order of 20 percent higher for some wave numbers than were those previously found. Because the flame zone must start with a finite width dependent upon the flameholder width, those frequencies having wave numbers $2\alpha d\mathscr{K}$ that exceed $2\alpha d\mathscr{K}_{cr}$ are suppressed. Here, $\mathscr{K}$ is some proportionality factor less than unity. Certainly, neglect of the effect of a finite-size flameholder facilitates generalizing the results of the stability analysis. The investigations of this section indicate that, for flameholders small compared with duct width, such neglect appears warranted in a large part of the flame zone.

## SUMMARY OF THEORETICAL RESULTS

1. The flow field of a flame in a duct is unstable to antisymmetric disturbances having wavelengths of the order of 2.5 times the local flame width and greater. As $h_2/h_1$ approaches unity, this critical wavelength approaches $\infty$.

2. The amplification rate depends directly upon the magnitude of the velocity difference (apex velocity minus cold-gas velocity) and inversely upon the flame width. For fixed values of these quantities, the maximum amplification rate decreases with increasing values of $\rho_1/\rho_2$ and $h_2/h_1$, going to zero for $h_2/h_1=1$.

3. When the history of a disturbance is followed through the course of an entire flame, a wave number for maximum disturbance growth is found. This maximum growth is for such a wave number at the flameholder that $2\alpha_o h_1=6$, which corresponds to a frequency $f=U_o/2h_1$. The actual growth is substantially independent of density ratio because of two compensating factors:

(a) The amplification rate is lower for a higher density and given velocity difference.

(b) The velocity difference is greater for a higher density ratio.

4. The disturbances achieve their terminal amplification at a value of $h_2/h_1$ roughly inversely proportional to the frequency of the disturbance. Thus, higher frequencies achieve their amplification near the flameholder; lower frequencies, remote from the flameholder.

5. The magnitude of the terminal amplification depends upon the inverse of flame slope or roughly $(V_T/U_o)^{-1}$. The amplification that can be achieved for the maximum of $2\alpha_o h_1=6$ is about $(1.1)^{U_o/V_T}$. For example, for $V_T/U_o=1/20$, amplification is eightfold. For $V_T/U_o=1/100$, amplification is 14,000-fold.

6. The disturbance propagates with a phase velocity up to 60 percent greater than the cold-gas velocity.

7. The flameholder inhibits the growth of antisymmetric disturbances having higher frequencies but permits symmetric disturbances to be amplified near the flameholder. At 8 diameters downstream of the flameholder, the stability picture is substantially that obtained by neglecting the flameholder.

## EXPERIMENT: EXAMINATION OF DISTURBANCE GROWTH IN A V-FLAME

### INTRODUCTION

The effect of imposing controlled disturbances on a V-flame anchored in a duct was investigated experimentally for two reasons:

(1) To gain quantitative information on the mechanism of the breakdown of the flame-generated shear region that would explain the occurrence of flame-amplified turbulence

(2) To find a type of excitation that promotes flame propagation without causing the sort of shell failure that combustor resonance causes

The method of excitation consists in exciting a column of gas in the flameholder support tube. This method offers a control on the amplitude when excitation is accomplished with a speaker, but could be accomplished by means of an edge tone excited by the flowing stream for application in an engine. Only the speaker excitation is used here. The sound issues from a port at the flameholder and disturbs the flame at the flameholder. The two types of ports used operated as follows:

(1) Sound issued from a port just upstream of one flameholder edge, causing the fluctuating flow about the flameholder to be quasi-antisymmetric.

(2) Sound issued from the center of the flameholder, causing the fluctuating flow at the flameholder to be symmetric.

The principal disadvantage in this form of excitation is that, for some frequencies, modes of burner cavity resonance are excited. An objective in the experimental work, therefore, was to determine whether an observed flame-front distortion accompanying an imposed disturbance was due to flame-zone instability or to some form of duct resonance.

No effort was made to determine effects of variations in fuel-air ratio or fuel type. The primary variable investigated was the frequency of excitation. The only attempts at correlating the results are the comparison with the results of the preceding stability analysis. The chief frustration encountered is the impossibility of obtaining a laminar V-flame at velocities where values of $V_T/U_o$ are sufficiently low for the preceding theory to be valid. The reason for this

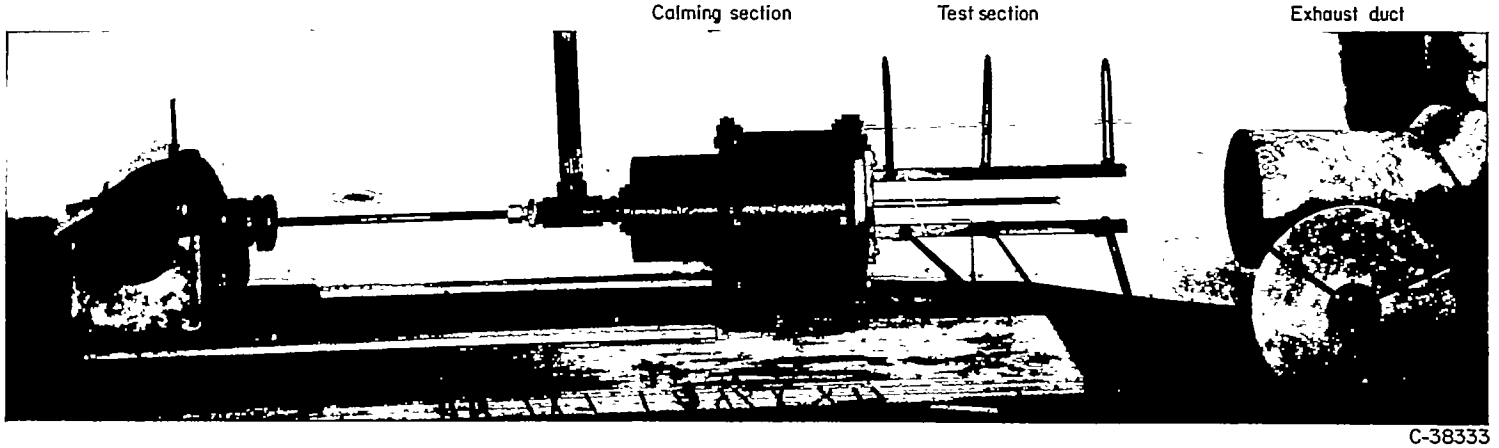


C-38333

FIGURE 12.—Combustor.

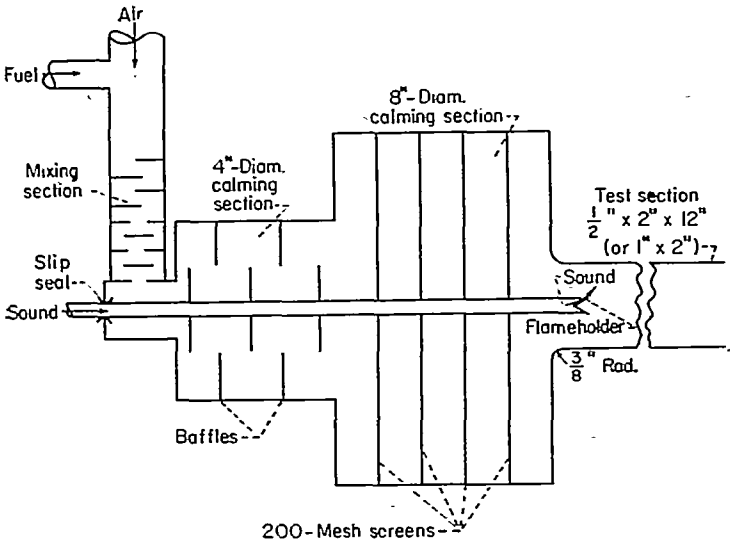


FIGURE 13.—Schematic drawing of combustor.

difficulty is the instability of the boundary layer, which separates from the flameholder and undergoes transition to turbulent motion quite close to the point of separation. All the results are obtained with the flow already somewhat turbulent.

The principal instrument used in measuring flame speeds is the photomultiplier probe, first applied in a rigorous way to the study of turbulent flame speeds by Clark and Bittker (ref. 32). An independent confirmation of the method is obtained by comparing combustion efficiency measured by the photomultiplier probe and by momentum pressure drop.

## APPARATUS

### BURNER TEST SECTION

A photograph of the burner (fig. 12) shows the important components. Air and propane were filtered, metered, and mixed before entering the two-stage calming section (fig. 13). In this section the mixture passed through six banks of 200-mesh screen and then through a ⅜-inch-radius nozzle plate into the ½- by 2-inch (or alternatively 1- by 2-in.) rectangular glass-walled test section. The top and bottom walls of this test section were ½- by ½-inch (alternatively ½- by 1-in.) brass stock. The side walls were ¼-inch Vycor plates resting on brackets and held against the ½-inch top and bottom pieces by clamps.

The exhaust system consisted of a 6-inch-diameter pipe connected to a hood and a blower to force the gases out. A 4- to 6-inch spacing was maintained between the test section and the exhaust duct, and between the exhaust duct and the hood; there was no indication of resonance due to the exhauster.

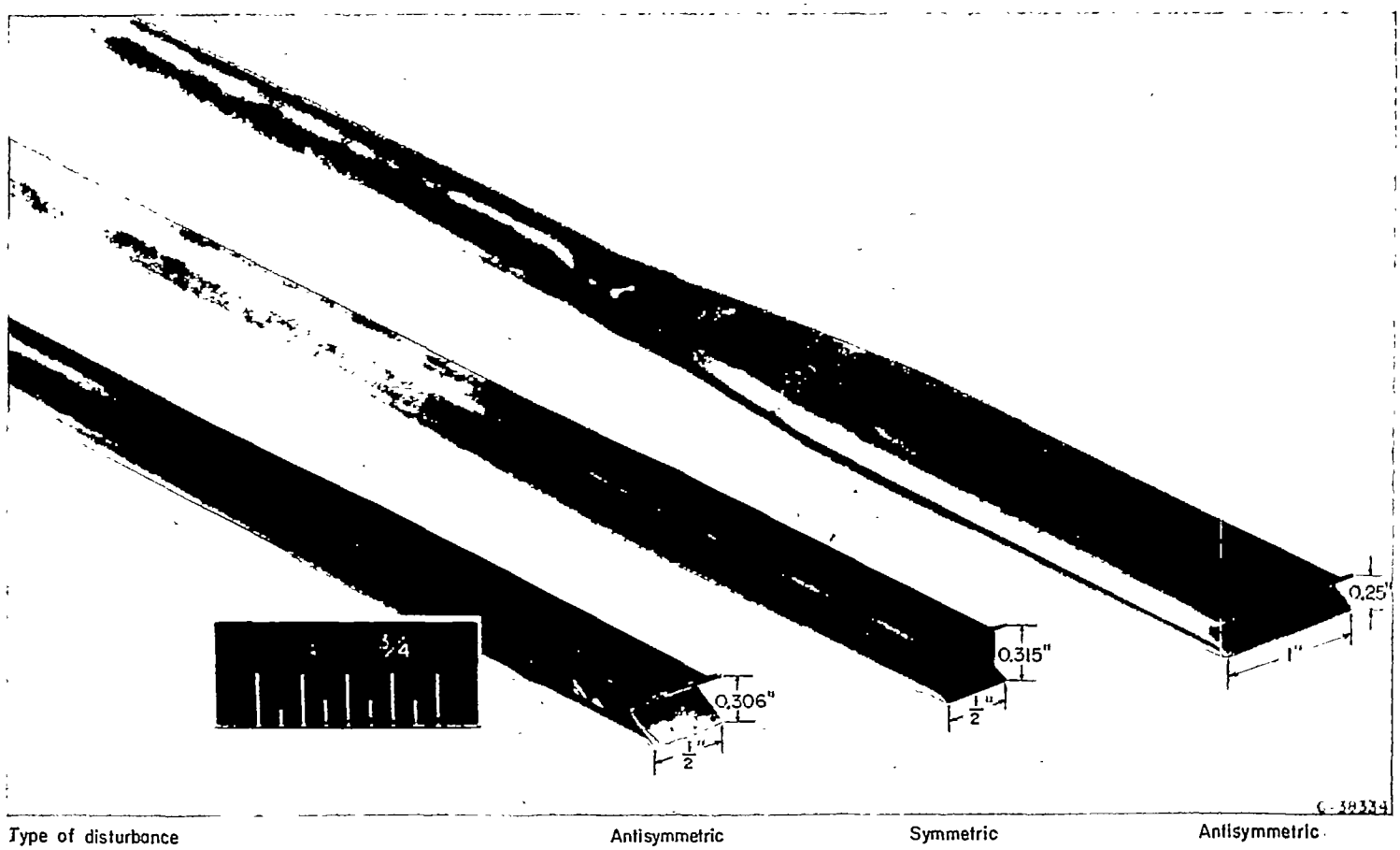


FIGURE 14.—Flameholders.

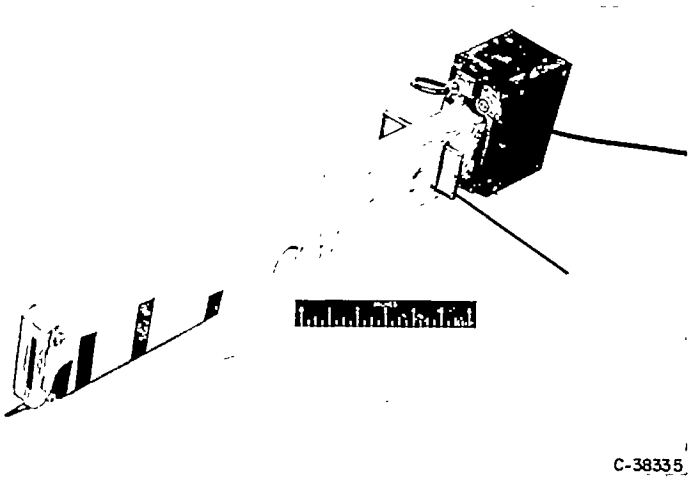


FIGURE 15.—Photomultiplier probe.

The flameholder was a flat hollow paddle 36 to 38 inches long with a 60° gutter on one end and a ⅜-inch tube leading to a piston-type loudspeaker on the other. The three flameholders used in this program are shown in figure 14. The flameholders used to supply the disturbances were resonators that had resonant frequencies every 190 to 200 cycles when coupled to the speaker. The flameholder designed to produce antisymmetric disturbances allowed the sound to issue from a slot just upstream of one edge of the flameholder; the one designed to give symmetric disturbances allowed the sound to issue from the center. The flameholders pictured were approximately 0.25 to 0.30 inch thick. In one test a 0.50-inch gutter was tacked onto the 0.306-inch antisymmetric flameholder to examine the effect of flameholder size.

In no case was the distribution of $v'$ downstream of the flameholder measured. It is not known how much the experimental distribution differs from the measured theoretical distribution. The essential features in both experimental and theoretical disturbances are that antisymmetric disturbances cause the flow to flap back and forth at the centerline of the duct, while symmetric disturbances cause it to dilate about the centerline.

### AUXILIARY EQUIPMENT

**Sound-producing system.**—The speaker was supplied a sinusoidal signal from a signal generator through a power amplifier. The speaker and flameholder could be positioned as desired.

**Flow metering.**—Air and propane were metered through rotameters.

**Hot-wire equipment.**—An NACA constant-temperature, frequency-compensated, hot-wire anemometer was used (ref. 33). Spectra and $u'$ were measured at various locations in the duct. Measurements of $u'$ were made primarily with a vacuum-tube voltmeter. Two spot checks were made against a root-mean-square computer, and the correction factor was found to be approximately unity. Spectra were measured with a wave analyzer.

**Pressure measurements.**—Velocity surveys were made using 0.018-inch hypodermic tubing, or 0.030-inch stainless tubing, for impact tubes. Measurements were read on a water micromanometer. Velocity measurements were made at the plane of exhaust with room pressure as static.

**Photomultiplier probe.**—The photomultiplier tube was installed in a probe as shown in figure 15. Light reached the photomultiplier tube after passing through two vertical slots, which were ¼ and 1/16 inch wide and 2 feet apart, and through filters when desired. Photomultipliers were supplied by a ripple-free regulated d-c source.

Alternating-current and direct-current voltmeters having identical input resistances were used where indicated.

**Shadowgraph system.**—The optical arrangement used in taking shadowgraph pictures is shown in figure 16. The light source could be used continuously or as a 4-microsecond flash. The camera was focused 1.5 feet in front of the test section. The shutter and flash were manually synchronized.

**Stroboscope.**—A stroboscope consisting of a slotted aluminum disk and a synchronous motor was used to view the disturbed flame in the preliminary phases of the investigation. The stroboscope can be seen in the lower right corner of figure 12.

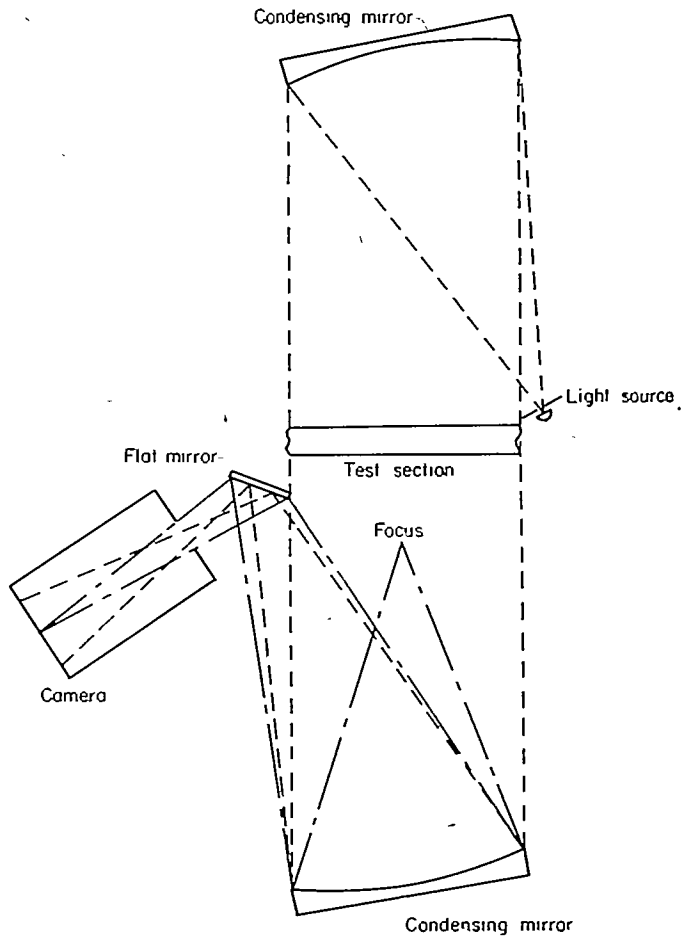


FIGURE 16.—Schematic drawing of shadowgraph apparatus.

PROPERTIES OF SYSTEM

**Velocity profiles upstream of flameholder.**—Velocity profiles measured 3 and 12 inches downstream of the nozzle are shown in figure 17. The flameholder was positioned so that each measurement was taken upstream of the gutter. Measurements were also taken at the plane of the nozzle, and no variation greater than ½ foot per second from 55 feet per second was found. These measurements are for a nominal flow setting of 50 feet per second.

Flame photographs and flame-speed measurements were made at nominal velocities of 50 and 100 feet per second in ½- and 1-inch-wide test sections; the profiles of figure 17 therefore represent the highest percentage of boundary layer encountered.

**Velocity profile in wake; no flame.**—Velocity profiles in the wake of a 0.306-inch-wide, 60° gutter at a nominal

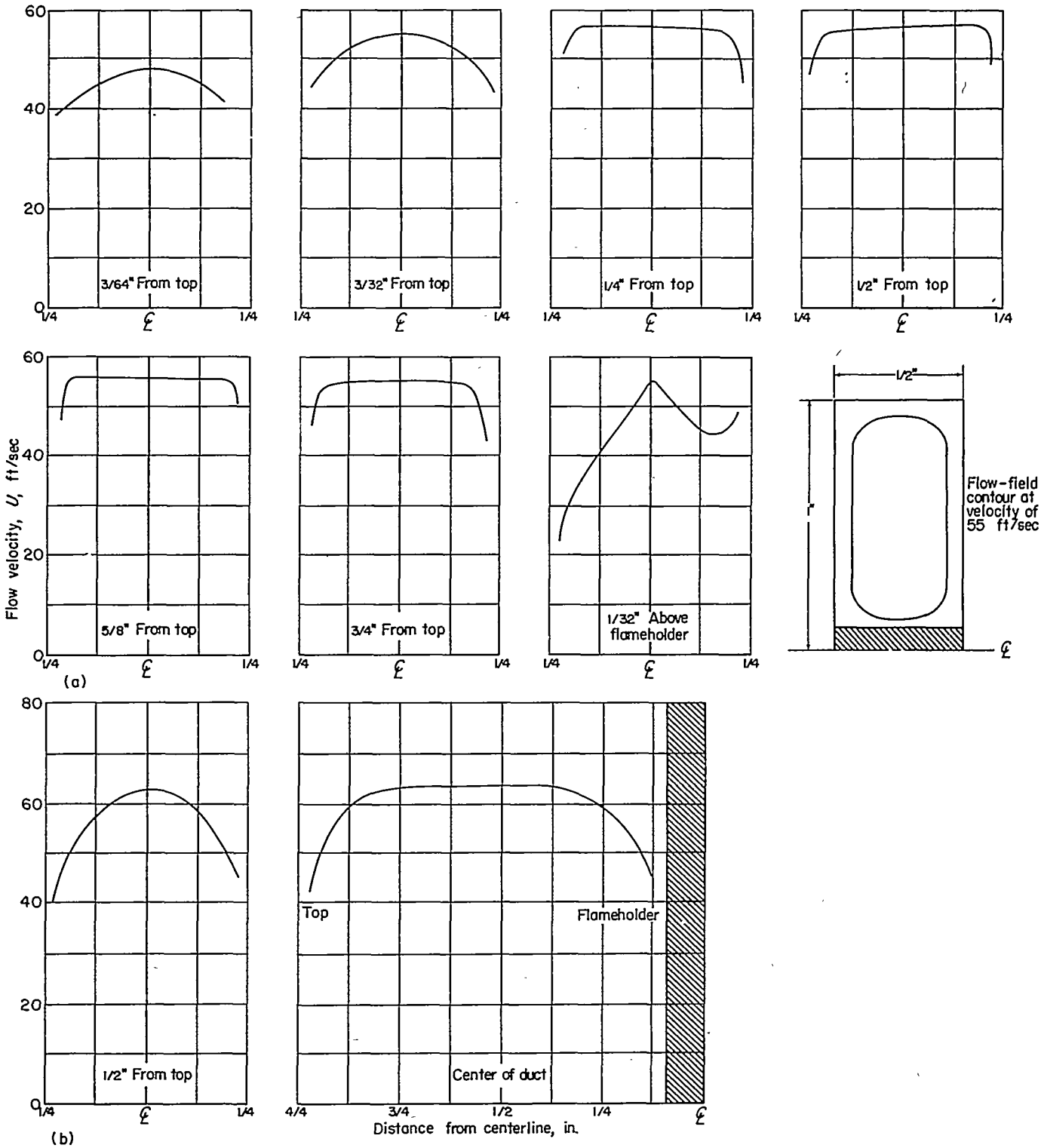


(a) Profiles 3 inches downstream of nozzle.
(b) Profiles 12 inches downstream of nozzle.

FIGURE 17.—Time-averaged velocity profiles with cold flow. Nominal velocity, 50 feet per second.

velocity of 46 feet per second are shown in figure 18. This set of profiles shows a comparison of the spreading of a wake with and without an antisymmetric disturbance at 200 cycles per second. The only amplitude measurement available for this disturbance is a root-mean-square $u'$ of 5 feet per second, measured ⅛ inch above the lip of the flameholder.

The effect of other frequencies on wake spreading was examined by placing total-pressure tubes 3 inches downstream of the flameholder at the center of the wake and varying the frequencies. The results are interpreted in the following manner. The velocity is read while disturbances are being introduced. The distance from the wake at which this velocity is attained without the sound (say $x$) is found. An index of the lengths required to accomplish equal degrees of mixing without and with the disturbance is then the ratio $x/3$. This ratio is plotted against frequency in figure 19.

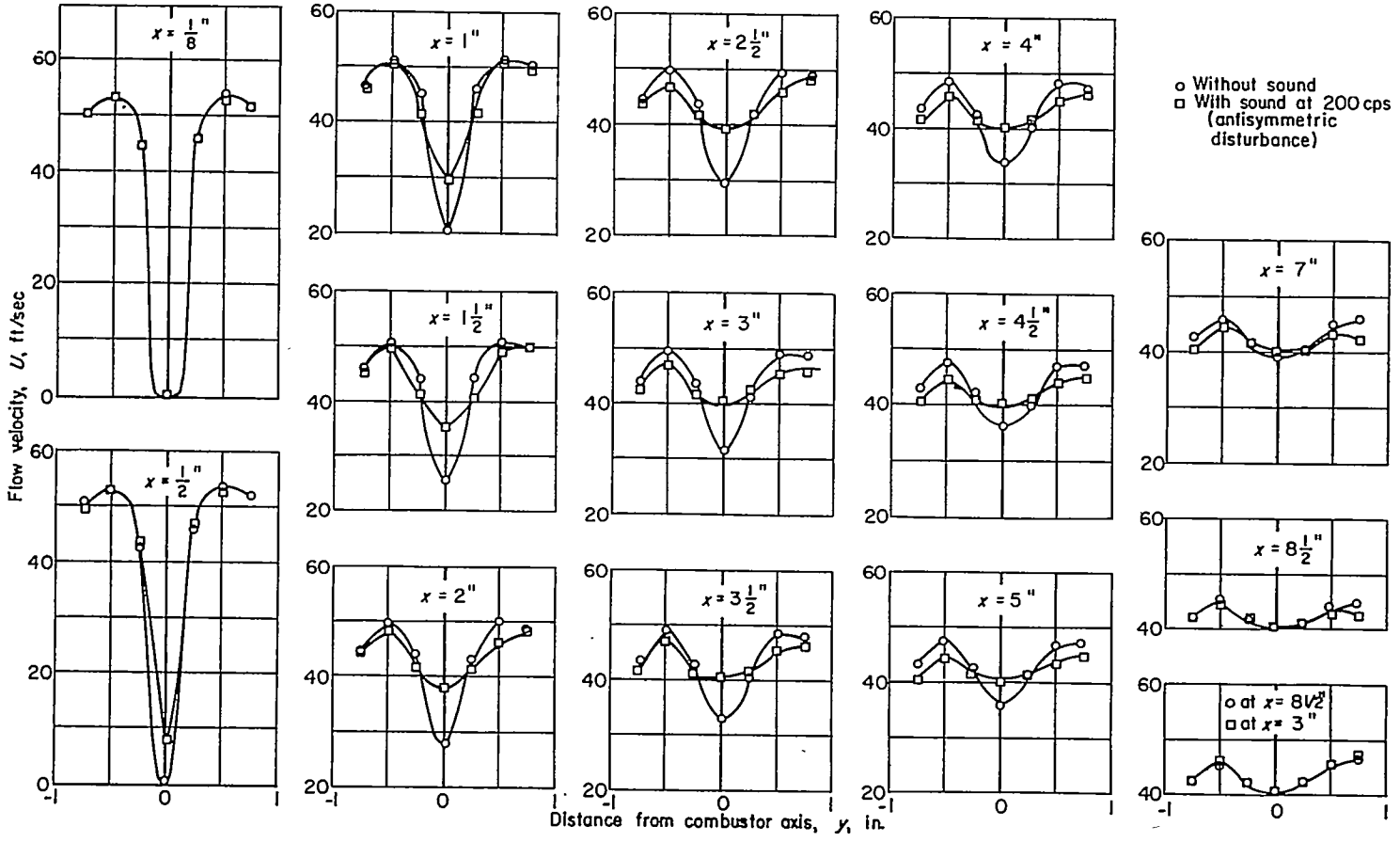


FIGURE 18.—Velocity profiles in wake of 0.306-inch flameholder.

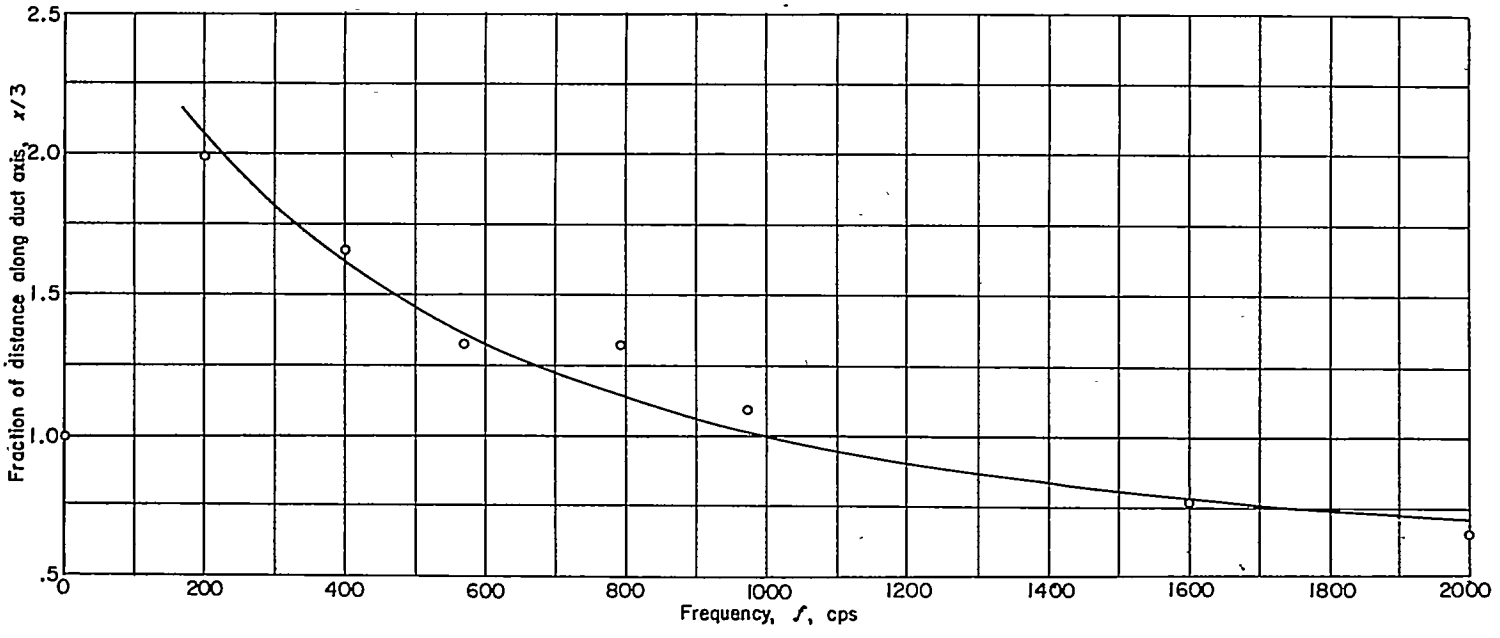


FIGURE 19.—Axial length required to achieve mixing to arbitrary extent.

The fact that the apparent diffusion rate decreased at frequencies greater than 1000 cycles per second indicated a decrease in form drag for frequencies greater than 1000 cycles per second. Static measurements at the base of the gutter showed no change in base pressure for the higher-frequency disturbances. Those lower frequencies that increased mixing also decreased base pressure (i. e., increased form drag). This probably means that the velocity is increased in the wake for frequencies less than 1000 cycles per second. There seems little hope, however, of reducing flameholder drag by imposing high-frequency disturbances of this kind.

**Turbulence intensity and spectra.**—The turbulence component $u'$ in the direction of flow was measured with 0.0002- by 0.08-inch tungsten wires, using the NACA constant-temperature anemometer amplifier. The wire was oriented parallel to the flameholder tips. No flame was present for these measurements. The results are presented in the following table:

| Distance from nozzle lip, $x$, in. | Nominal velocity, $U$, ft/sec | Distance from top wall, $y$, in. [a] | Vertical distance from station, in. | Turbulence component, $u'$, ft/sec | Scale of turbulence, $L$, in. |
|---|---|---|---|---|---|
| 0 | 50 | ½ | ¼ | 0.306 | ---------- |
| | 100 | ½ | ¼ | .420 | ---------- |
| 6 | 50 | ⅛ | ¼ | 1.38 | 0.2 |
| | | ⅛ | ⅛ | 1.68 | ---------- |
| | | ¼ | ¼ | .818 | .15 |
| | | ¼ | ⅛ | .978 | ---------- |
| | | ½ | ¼ | 1.021 | .15 |
| | | ¾ | ¼ | 3.35 | .17 |
| | 100 | ⅛ | ¼ | 2.44 | ---------- |

[a] At $x=0$, $y$ measured from centerline; at $x=6$, $y$ measured from flameholder lip.

The spectra measured at several stations were compared with spectra found representative for isotropic turbulence (refs. 33 and 34). A typical plot is shown in figure 20. The scale $L$ is estimated as the one whose spectrum most nearly corresponds to the measured spectrum (refs. 33 and 34). This scale [3] where determined is given in the preceding table.

The apparent transition from laminar to turbulent flow in the boundary layer on the flameholder surface occurred if the flameholder was about 1 inch or more from the test-section nozzle; the disturbance velocity in the boundary was roughly that in the nozzle itself. With the flameholder within 1 inch of the nozzle, eddies were shed at 420 cycles per second when no flame was present. With the flameholder 1 inch or more from the nozzle, transition occurred upstream of the flameholder lip, and no clearly defined eddy-shedding frequency was found in the wake.

With a flame anchored on the flameholder, no eddy shedding was observed without external excitation. The flame appeared turbulent for flameholder positions greater and less than 1 inch from the nozzle. Therefore, the transition

[3] This is the scale that would be used for calculating a turbulent burning velocity from existing theory (ref. 8). It is of interest herein because of the scale of disturbance the flame amplifies; $L \approx 1$.

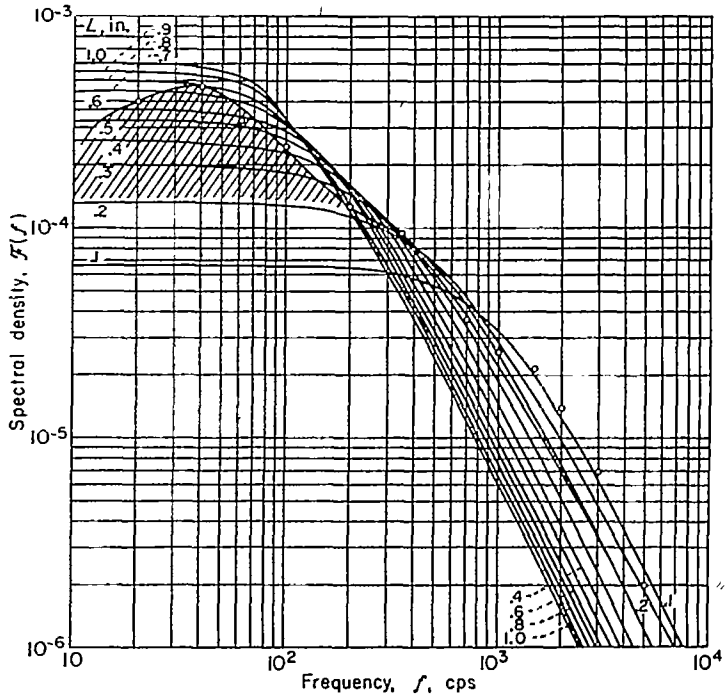


FIGURE 20.—Turbulence spectra for flow velocity of 50 feet per second; $\mathcal{F}(f)=(4L/U)/\{1+[(2\pi/U)Lf]^2\}$, measured ⅛ inch above flameholder lip.

to turbulence in the separated boundary evidently affects the turbulent flame appearance in about the same manner as transition in the attached boundary layer. The lean-blowout fuel-air ratio was adversely affected when the transition was moved from the attached to the free boundary layer.

In an effort to obtain a laminar flame zone, some exploratory work was done to move the transition point farther downstream of the point of separation from the flameholder. Small unheated cylindrical rods (as in ref. 3) placed about 1 inch from the nozzle entrance were used as flameholders. It was possible to move the transition point about 1 inch downstream of the flameholder (at 50 ft/sec). Lean blowout, however, was moved to a fuel-air ratio so rich that excessive heating occurred in the glass walls, which impaired the use of the shadowgraph system. In the transient period immediately after ignition while the walls were still cool, a clear picture of the flame could be observed. Studying the flame for a length of time was not possible with this arrangement. Therefore, turbulent transition at or upstream of the flameholder lip was accepted.

### CALIBRATION OF DISTURBANCE AMPLITUDE WITH SPEAKER INPUT

Because of the interaction between the standing-wave tube supplying the sound to the flameholder and the standing waves in the test section, it was necessary to calibrate the sound input with the flameholder at the position and velocity to be used in the burning tests. For most runs the flameholder was placed midway between acoustically open ends in the test section in order to suppress velocity disturbances at the flameholder due to all even modes of vibration of the test section.

The inputs were set in the following manner: The flameholder position and flow velocity to be used in a burning run were set. The hot wire was placed 1/8 inch above and 1/8 inch upstream of the flameholder lip, to center it over the port from which the sound issued. Resonant frequencies were excited in the flameholder support tube. The input to the speaker required to give the desired $u'$ at the wire was recorded for each frequency. The wire was removed, fuel was introduced and ignited, and the burning run was made. The distribution of $v'$ resulting from this sort of excitation was not explored. The change in the nature of interaction between test sections and the standing-wave tube with and without combustion was not explored but was presumed to be small, since only about 30 percent of the combustible mixture was burned in the test section.

### RATIO OF TURBULENT TO LAMINAR FLAME SPEED DETERMINED BY PHOTOMULTIPLIER PROBE

Photomultiplier tubes have been used to sense transient area changes in a laminar flame distorted by sound (refs. 35 and 36) and to study Bunsen flames that were alternately laminar and turbulent by comparing the average intensity of light emitted from the flame (ref. 32). Turbulent and laminar flames having identical mixture ratios and feed rates produced identical quantities of light (ref. 32). Therefore, it appears that the photomultiplier tube, if used with caution, can become an average-heat-release-rate meter.

In the following discussion, the local heat-release rate is characterized by the ratio of turbulent to laminar flame speed $V_T/V_L$. This ratio is defined as the heat released per unit time divided by the heat that a pair of laminar flames alined with the axis of the duct would release per unit length per unit time. The relation is illustrated by considering the way the quantities are measured:

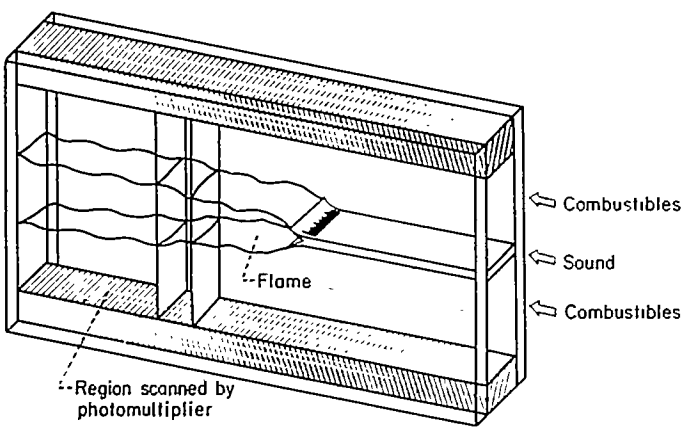


Sketch (k)

In the test section shown in sketch (k), flame fronts are anchored on the top and bottom of the flameholder and appear to span from wall to wall. The photomultiplier scans a narrow region of the test section. The voltages read from the photomultiplier-tube output are recorded at the same fuel-air ratio for a turbulent flame and for a laminar flame. The flame-front half-angle is measured, and each voltage is multiplied by the cosine of the half-angle. The ratio of the resulting product for the turbulent flame to that for the laminar flame is defined as $V_T/V_L$. In the region of interest, the cosine of the half-angle was approximately 1 for the turbulent flames, so that, in effect, the unit length of the flame fronts becomes the unit length of the combustor.

In obtaining the laminar flame, the same fuel and air rotameter settings were used as for the turbulent flame, but a large fraction of the mixture was bled off upstream of the flameholder. Three banks of 200-mesh screen were installed just upstream of the flameholder, and the resulting flame appeared laminar. The flame did not span from wall to wall near the flameholder; therefore, the voltage recorded for this region was quite low. Far downstream of the flameholder the flame front became twisted so that it represented a flame depth greater than the wall-to-wall depth. In between these two regions was one in which the flame appeared to touch the walls and to have negligible twist. The voltage recorded by the photomultiplier probe as it scanned this region was nearly constant. The extreme voltages recorded in this region envelop a band within which the true voltage corresponding to a pair of laminar flames was thought to lie.

In order to pinpoint an exact value for the laminar voltage as well as to verify the method (the zone of uncertainty is quite small), an auxiliary determination of $V_T/V_L$ was made. Photomultiplier-probe voltages were read at seven equally spaced stations along the combustor from flameholder to exhaust nozzle, and an average voltage was calculated. Simultaneously, the momentum pressure drop across the flame zone was measured. With the help of Scurlock's results (ref. 1), the fraction of combustible burned $F$ was determined from the measured momentum pressure drop. Then an average $V_T$ was calculated from

$$F=\frac{(\text{Length})\ (2)\ (V_T)\ (\text{depth})}{(U_o)\ (\text{depth})\ (\text{height})}$$

where length, depth, and height are the dimensions of the combustor. With this $V_T$, the measured average voltage, and the value for laminar flame speed $V_L$ taken from reference 37, voltage corresponding to a laminar flame was obtained from

$$\frac{E_L}{V_L}=\frac{E_T}{V_T}$$

where $E_L$ and $E_T$ are the photomultiplier voltages for laminar and turbulent flames. This voltage lies within the zone of uncertainty found by direct viewing of the laminar flame. These results are reported more fully in the section Examination of Method.

The fact that reference 32 was cited does not mean that any photomultiplier calibration was obtained from that work. Reference 32 established that (for a given combustor at a given composition and flow rate) a photomultiplier voltage is proportional to the heat released within sight of the photomultiplier tube and is independent of the existence or nonexistence of turbulence. The agreement of the two methods

for determining $V_T/V_L$ justifies this use of the photomultiplier probe.

It was hoped initially to follow the amplitude of a flame wrinkle by measuring the a-c component of the photomultiplier signal. The reasoning was that the flame would be wrinkled sufficiently for its local instantaneous slope to serve as a detectable index of flame-wrinkle amplitude. This slope, of course, would appear as an increased voltage at the photomultiplier because the length of the flame cutting across the field of view would be increased. The data showed an amplitude more dependent on the distance from the duct exhaust than on the distance from the flameholder. The sound waves introduced as the source of excitation at the flameholder reflected from the exhaust of the combustor. Therefore, the a-c component read by the probe was largely influenced by the time-varying displacement of local flame zones due to plane waves of sound. The filter a-c signals for two frequencies as a function of distance from the flameholder are compared in figure 21. One set was obtained from the photomultiplier probe with burning, the other set from a hot-wire anemometer without burning.

The photomultiplier probe was used only to survey for the

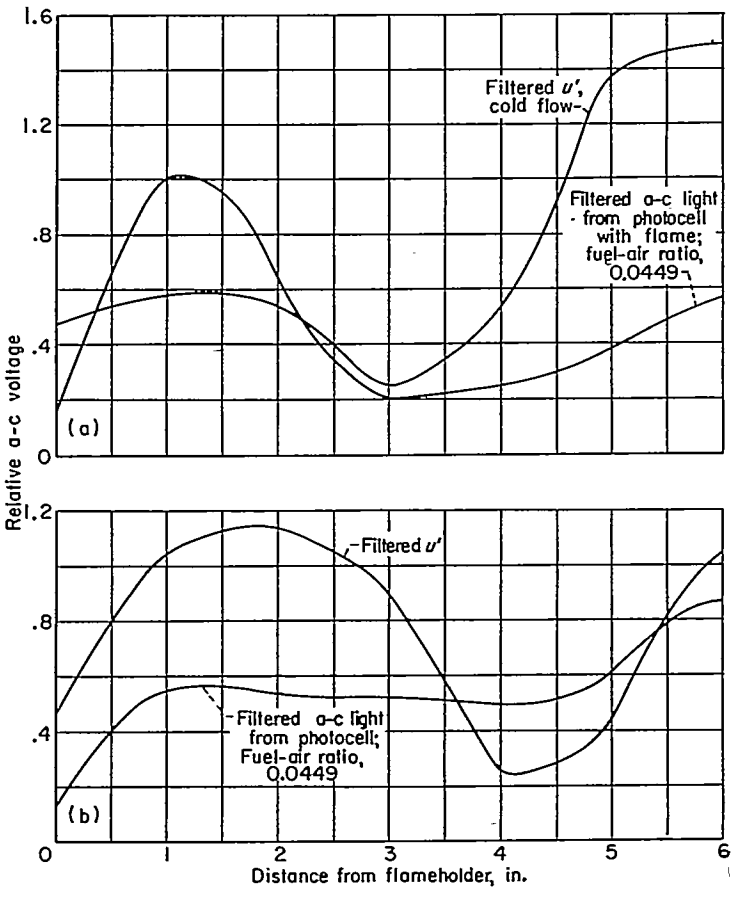


(a) Frequency, 570 cps.
(b) Frequency, 1500 cps.

FIGURE 21.—Comparison of hot-wire and photomultiplier measurements showing effect of plane waves near exhaust of duct. Flow velocity, 50 feet per second.

effect of disturbances on local $V_T/V_L$ values on a time-average basis.

## RESULTS

The analytical part of this paper suggests certain beha ior that can be examined experimentally. Accordingly, tests are included that furnish the necessary data for a comparison with the results of the analysis. One of the primary variables studied was the effect of the frequency of excitation on disturbance growth. The frequency range of interest happened to include some of the resonant frequencies of the combustion-gas volume as well as the spontaneous eddy-shedding frequency of the flameholder in cold flow. The effect of combustor resonance or spontaneous eddy-shedding was also examined.

Certain precautionary measures were taken in choosing geometry and operating conditions. To guard against burner resonance, the combustor was kept short, so that only about 30 percent of the combustible was consumed. Spontaneous burner resonance sometimes occurred when this value was exceeded. The conditions were kept within the Reynolds number reported in reference 1 to be free of spontaneous eddy-shedding when a flame is anchored on the flameholder. Although these measures precluded the occurrence of spontaneous oscillations due to these two causes, they could not prevent the system from favoring certain frequencies within the range of interest. These influences, then, received special attention.

Markstein has shown that instabilities of a laminar flame front cause the front to assume a cellular structure under certain conditions (ref. 4). The occurrence of such cells clearly could confuse an interpretation of the results. Consequently, the data were taken solely at conditions where the cells do not spontaneously arise.

### EXAMINATION OF METHOD

With the flameholder 6 inches from the open end of the duct and 6 inches from the tunnel entrance, runs were made at three fuel-air ratios at 50 feet per second over a range of disturbance frequencies. The 0.306-inch-wide gutter with antisymmetric disturbances was used. The change in impact pressure with and without combustion was measured by a single impact tube upstream of the flameholder. Since the difference is of the order of inches of water and the rate of mass flow is constant, it is assumed that the difference is entirely due to a change in static pressure. The fraction burned was calculated from Scurlock's results (ref. 1) and the measured pressure drop. Concurrently, the light intensity at seven stations along the flame was measured and averaged.

The fraction burned is compared with the average voltage (which is proportional to the average intensity) in figure 22 by plotting both against the frequency of disturbance for the three fuel-air ratios examined. The following table indicates the amount of scatter in the ratio of fraction burned to mean voltage:

| Fuel-air ratio | $F/E_T$ for frequency, $f$, cps, of— | | | | | Average $F/E_T$ |
|---|---|---|---|---|---|---|
| | 0 | 380 | 470 | 760 | 1500 | |
| 0.0444 | 0.137 | 0.131 | 0.134 | 0.137 | 0.131 | 0.134 |
| .0515 | .1017 | .1070 | .1035 | .1063 | .1035 | .105 |
| .0580 | .0818 | .0817 | .0853 | .0858 | .0852 | .084 |

From the relation

$$\frac{F}{E_T}=\frac{2V_T\times\text{length}\times\text{depth}}{U_o\times\text{height}\times\text{depth}\times E_T}$$

(where length, height, and depth are dimensions of the combustor), an average value of $V_T/E_T$ is calculated. From the average values in the preceding table for $F/E_T$ at each fuel-air ratio, the following values of $V_T/E_T$ were obtained:

| Fuel-air ratio | $V_T/E_T$, (ft/sec)/volt |
|---|---|
| 0.0444 | 1.115 |
| .0515 | .880 |
| .0580 | .709 |

For these fuel-air ratios and the inlet temperature and pressure used, a laminar flame speed was obtained from reference 37. Then the voltage that would correspond to a laminar flame was calculated from

$$E_L=\frac{V_L}{V_T/E_T}$$

The values of $V_L$ from reference 37, the value of $E_L$ calculated from the preceding relation, and the zone of $E_L$ measured directly by viewing a pair of laminar flames in the test section are as follows:

| Fuel-air ratio | $V_L$ (ref. 37) | $E_L=\frac{V_L}{V_T/E_T}$ | $E_L$ by direct measurement |
|---|---|---|---|
| 0.0444 | 0.74 | 0.663 | 0.658 to 0.682 |
| .0515 | 1.10 | 1.25 | 1.15 to 1.39 |
| .0580 | 1.32 | 1.862 | ---------- |

The $E_L$ taken from values of $V_L/(V_T/E_T)$ that resulted from momentum-pressure-drop measurements fall within the limits of $E_L$ by direct measurement and are used as the calibration of the photomultiplier probe. Local values of $V_T/V_L$ reported subsequently are defined by the ratio of voltage read at that station to this $E_L$ for the applicable fuel-air ratio.

### COMPARISON OF FLAME SPEED WITH FLAME APPEARANCE

Shadowgraphs were taken at the same conditions used in the preceding comparison between average voltage and $\Delta p$. Some of these shadowgraphs, along with the distribution of

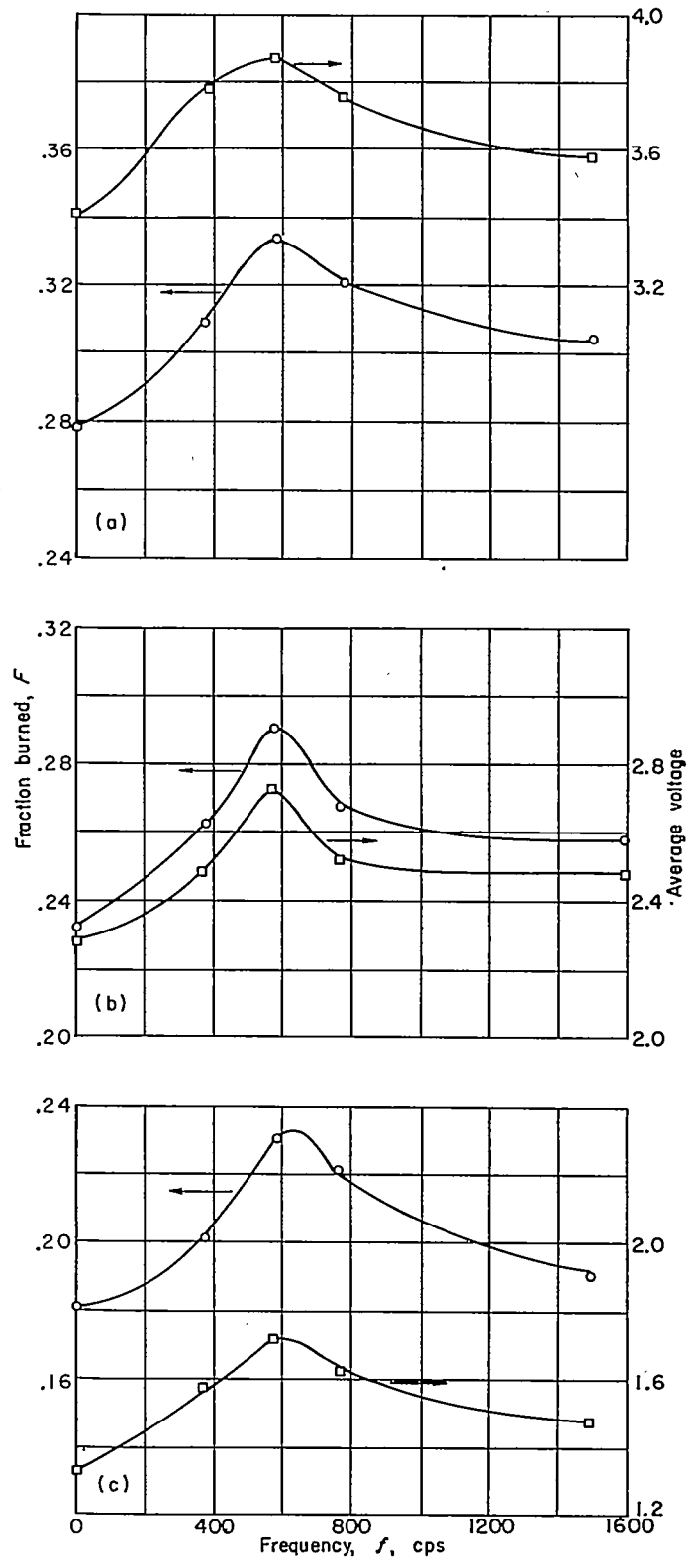


(a) Fuel-air ratio, 0.0580.
(b) Fuel-air ratio, 0.0515.
(c) Fuel-air ratio, 0.0444.

FIGURE 22.—Comparison of fraction burned obtained by momentum-pressure-drop measurement with average voltage obtained by photomultiplier survey. Flow velocity, 50 feet per second; length, 6 inches; disturbance velocity, 2.38 feet per second; antisymmetric disturbance.

$V_T/V_L$ for each, are presented in figure 23. In most of these photographs the gross disturbance caused by the input sound can be identified. If a line drawn along the turbulent flame front is faired through all but these gross wrinkles, its length divided by the length of a line faired along the undisturbed surface should be equal to

$$\left(\frac{S_d}{S_u}\right)_{pg} \equiv \frac{\text{Area of flame disturbed at frequency } f}{\text{Area of undisturbed flame surface}}$$

A similar ratio is available from the average voltages obtained by the photomultiplier survey in figure 22, defined by

$$\left(\frac{S_d}{S_u}\right)_{pm} = \frac{(E_T)_d}{(E_T)_u}$$

The $(S_d/S_u)_{pg}$ obtained by the former method and the $(S_d/S_u)_{pm}$ obtained from the photomultiplier readings are compared in the following table:

| Frequency, $f$, cps | Fuel-air ratio | | | |
|---|---|---|---|---|
| | 0.0444 | | 0.0515 | |
| | $\left(\frac{S_d}{S_u}\right)_{pm}$ | $\left(\frac{S_d}{S_u}\right)_{pg}$ | $\left(\frac{S_d}{S_u}\right)_{pm}$ | $\left(\frac{S_d}{S_u}\right)_{pg}$ |
| 0 | 1 | 1 | 1 | 1 |
| 380 | .18 | 1.15 | 1.09 | 1.11 |
| 570 | 1.304 | 1.185 | 1.19 | 1.12 |
| 770 | 1.23 | 1.23 | 1.10 | 1.18 |
| 1500 | 1.10 | 1.085 | 1.09 | 1.07 |

In general, the correlation is good. It may be significant that, at 570 cps, $(S_d/S_u)_{pm}$ is about 10 percent greater than $(S_d/S_u)_{pg}$. At this frequency, it is relatively easy to measure the area; that is, experimental scatter should not be as great as 10 percent. The evidence suggests the generation of additional turbulence in the flame, other than the growth of the low-frequency-imposed disturbance. It is regrettable that a laminar stabilized flame could not be obtained in this equipment, because this frequency could conceivably cause a transition point from laminar to turbulent flow.

For each plot in figure 23, $u'$ is a constant, so that $u'/V_L$ decreases with increasing fuel-air ratio. Also, $V_T/V_L$ decreases, for the most part, with increasing fuel-air ratio and, therefore, with decreasing $u'/V_L$.

At a given distance $x$, the ratio $(S_d/S_u)_{pm}$ defined by $\frac{(V_T/V_L)_d}{(V_T/V_L)_u}$ descends with ascending fuel-air ratio. This is in keeping with the interpretation in the stability analysis. The following table gives the values of $S_d/S_u$ at 570 cps for the three fuel-air ratios:

| $x$, in. | Fuel-air ratio | | | | | |
|---|---|---|---|---|---|---|
| | 0.0444 | | 0.0515 | | 0.0580 | |
| | $\frac{S_d}{S_u}$ | $\frac{u'}{V_{T,u}}$ | $\frac{S_d}{S_u}$ | $\frac{u'}{V_{T,u}}$ | $\frac{S_d}{S_u}$ | $\frac{u'}{V_{T,u}}$ |
| 1 | 1.522 | 2.025 | 1.129 | 1.220 | 1.076 | 1.055 |
| 2 | 1.183 | 1.437 | 1.205 | 1.107 | 1.122 | .962 |
| 3 | 1.166 | 1.376 | 1.175 | 1.08 | 1.119 | .937 |
| 4 | 1.177 | 1.358 | 1.151 | 1.058 | 1.147 | .913 |
| 5 | 1.197 | 1.352 | 1.129 | 1.038 | 1.116 | .873 |

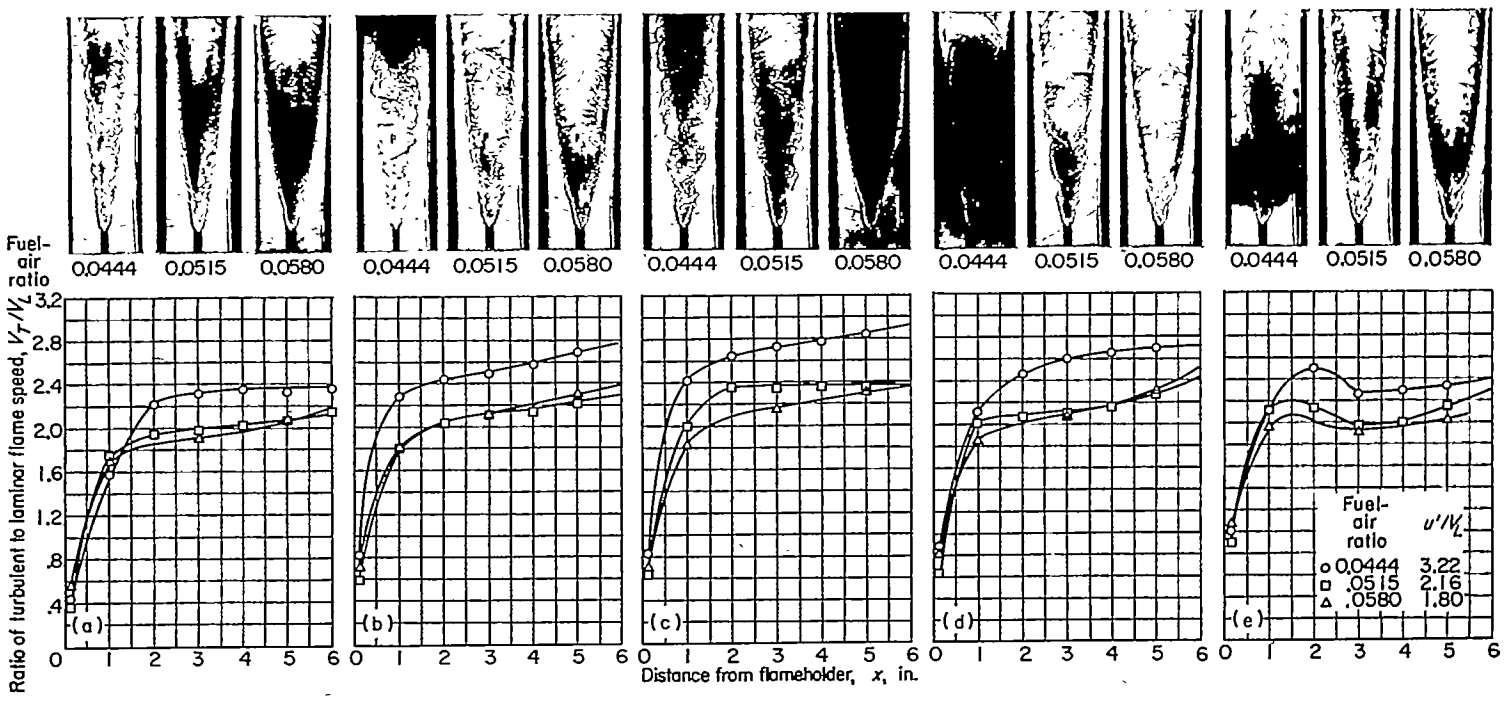


(a) No disturbance.
(b) Antisymmetric disturbance at 380 cps.
(c) Antisymmetric disturbance at 570 cps.
(d) Antisymmetric disturbance at 760 cps.
(e) Antisymmetric disturbance at 1500 cps.

FIGURE 23.—Comparison of flame appearance and $V_T/V_L$ for three fuel-air ratios for 0.306-inch flameholder. Flow velocity at plane of flameholder, 50 feet per second.

### DISTRIBUTION OF LOCAL $V_T/V_L$ VALUES WITH RESPECT TO VARIOUS FREQUENCIES

The ratio of turbulent to laminar flame speed $V_T/V_L$ is plotted against distance from the flameholder in figure 24(a), and $V_T/V_L$ is cross-plotted against frequency at several stations in figure 24(b). Great care was taken in keeping fuel-air ratio, velocity, and plate voltage to the photocell constant throughout the run. The 0.306-inch flameholder, modified to prevent leakage about the edges, was used. The disturbance velocity measured as described earlier gave $u'$ of 2.16 feet per second for all frequencies.

In order to compare these data with theory, the following computations were made:

(1) From the preceding calibration the fraction burned was calculated as a function of combustor length for the upper envelope of the $V_T/V_L$ curves for the disturbed flames.

(2) An idealized $h_2/h_1$ against length was obtained from this fraction burned using Scurlock's results (ref. 1).

(3) Increments of length over which a given frequency has a maximum $V_T/V_L$ were read from figure 24(a).

(4) These increments were plotted against $h_2/h_1$ and compared with the theoretical plot taken from figure 10. Recall

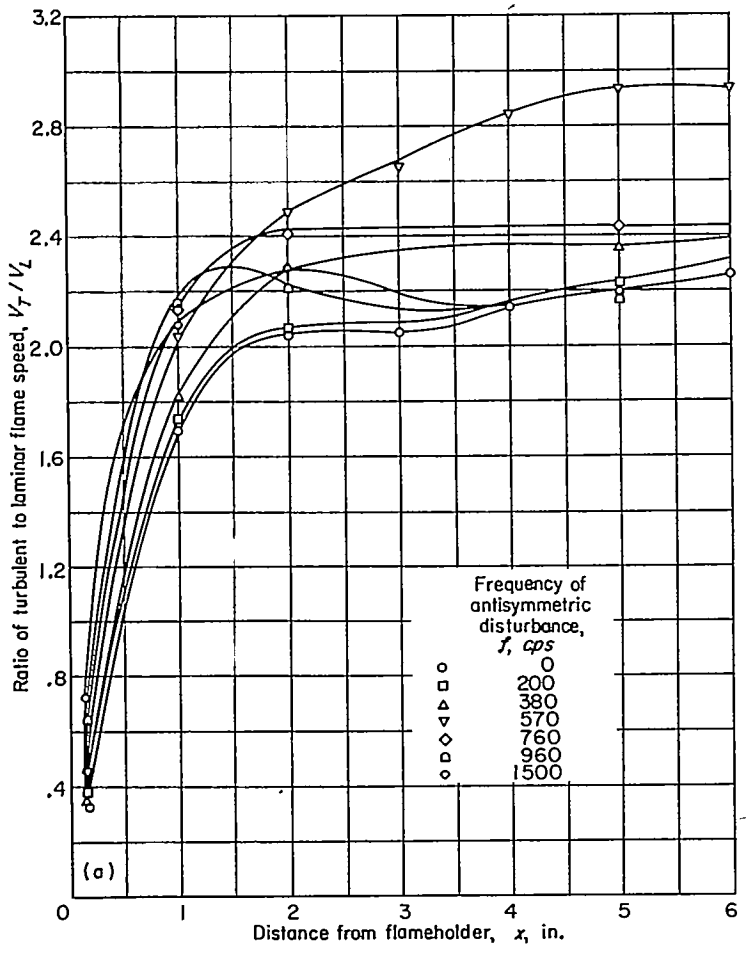


(a) Variation of flame-speed ratio with distance from flameholder. Test-section depth, ½ inch.

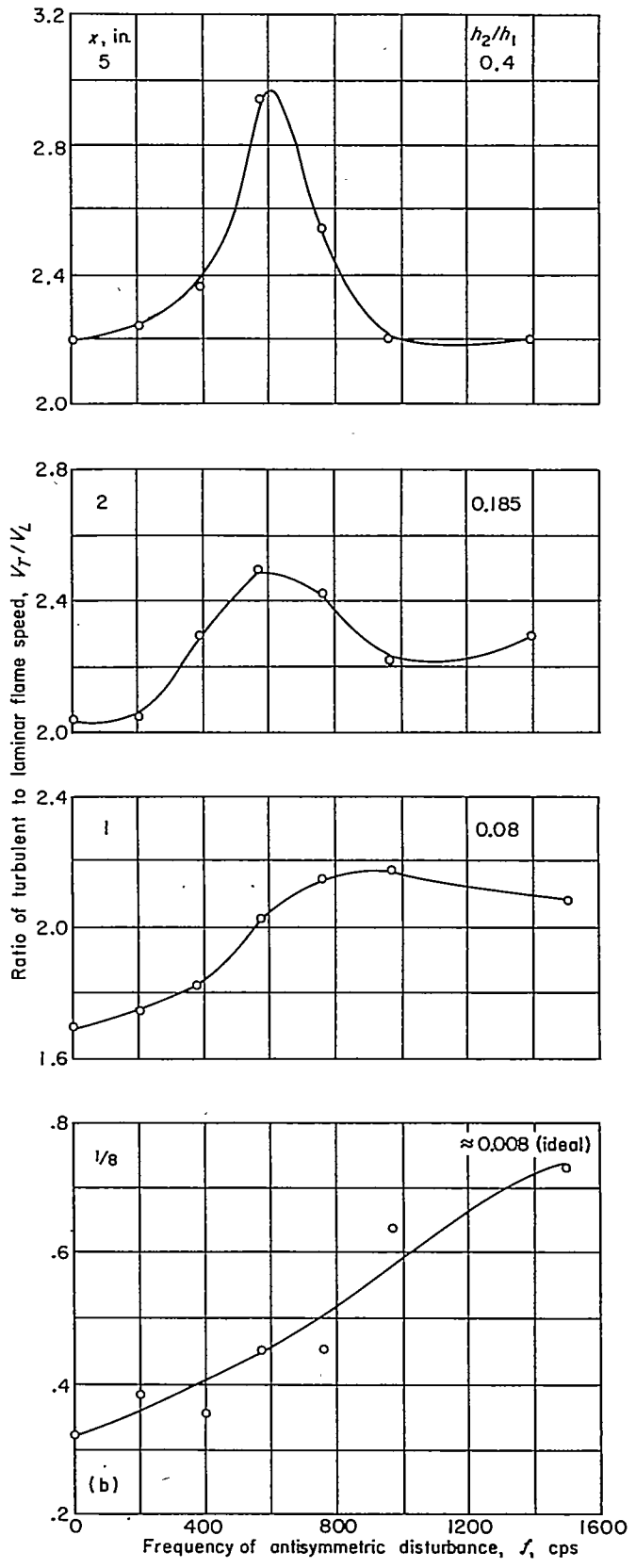


(b) Variation of flame-speed ratio with frequency for various distances from flameholder. Test-section depth, 1½ inches.

FIGURE 24.—Effect of antisymmetric-disturbance frequency on flame-speed distribution with 0.306-inch flameholder. Flow velocity, 50 feet per second; fuel-air ratio, 0.0444; disturbance velocity, 2.16 feet per second.

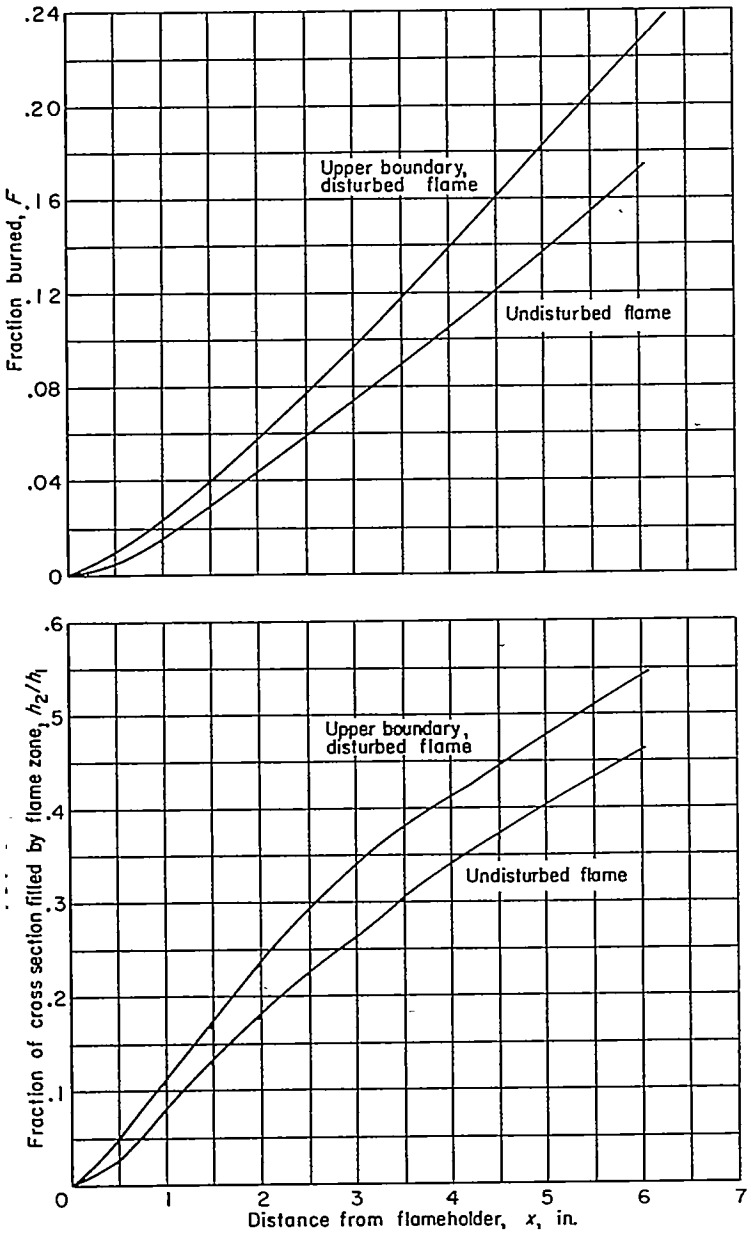


FIGURE 25.—Distribution of fraction burned and idealized $h_2/h_1$ for data of figure 24(a).

that $f=\frac{2\alpha_o h_1 U_o}{2\pi 2h_1}$. Results of steps (1) and (2) are shown in figure 25, and steps (3) and (4) in figure 26.

Similar data taken at the lower amplitude ($u'=1.44$ ft/sec) gave similar results.

### DISTURBANCE-DISPLACEMENT GROWTH

In this section the actual disturbance-displacement growth is compared with that of qualitative theory (sketch (f)).

In an effort to produce low disturbance amplitudes, the glass walls of the test section were reduced to 6 inches in length and the flameholder was moved to ⅝ inch downstream of the nozzle entrance. At this position the speaker inputs were calibrated with the hot wire as previously discussed, and shadowgraphs were taken for several low amplitudes. As mentioned in the section on turbulence intensity and spectra, the flameholder boundary layer underwent

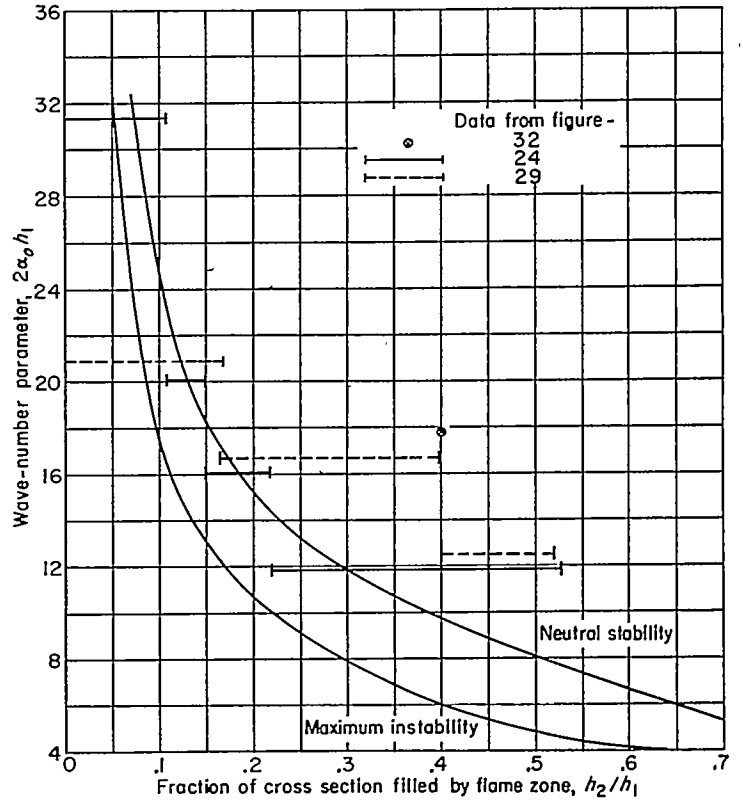


FIGURE 26.—Frequency giving maximum increase in flame speed as function of $h_2/h_1$ compared with results of stability analysis.

transition in the separated layer. The photographs of figure 27(a) show that, at these low intensities, the apparent width of the flame was not appreciably altered. The mean flame width measured from a direct photograph was used to determine $h_2/h_1$.

The displacement $h$ was measured as the distance from surrounding crests to a given trough in the flame surface. Measurements were made on both sides of the flame for each photograph. The data for two amplitudes and two frequencies obtained in this manner are shown in figures 27(b) to (d). The dashed curve is the qualitative curve from sketch (f).

The knee should occur between $(h_2/h_1)_{max}$ and $(h_2/h_1)_{cr}$ as discussed in the section Relation of Theoretical Results to Measurable Quantities. The vertical lines in figure 27 are drawn through these two values. With the general shape of the qualitative curve known, it can be seen that a line faired through the data points would exhibit a knee in the region bounded by $(h_2/h_1)_{max}$ and $(h_2/h_1)_{cr}$. Comparison of figures 27(c) and (d) shows that the knee moves to increased values of $h_2/h_1$ as frequency is reduced. Both the value of $h_2/h_1$ where the knee occurs and the variation of this value with frequency agree with the results of the analysis.

### DISTURBANCE PHASE VELOCITIES

From the photographs of figure 27(a), values of $c_r/U_1$ were determined, again using the mean flame width to furnish $h_2/h_1$. The quantity $U_1/U_o$ was then determined from Tsien's results (eq. (3)). Wavelengths were measured from trough to trough, and the mean position of a pair of troughs located

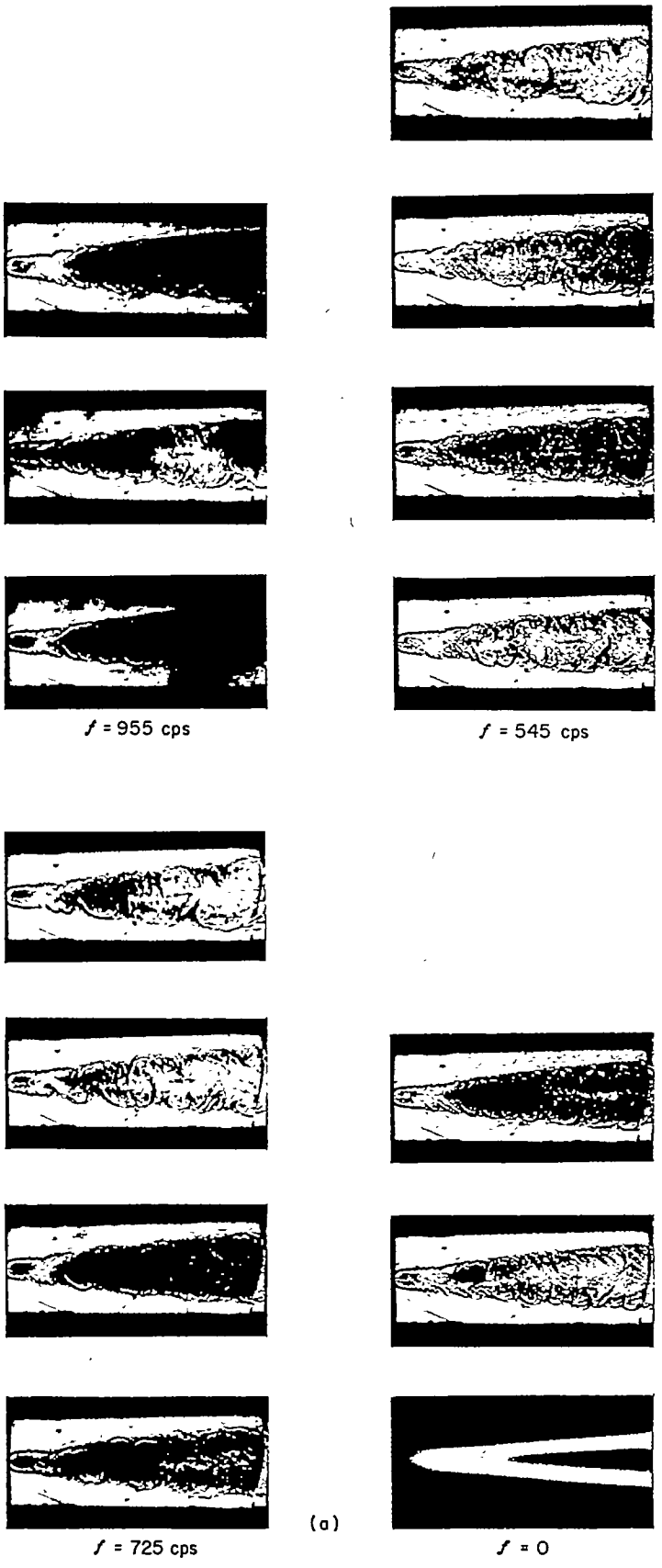


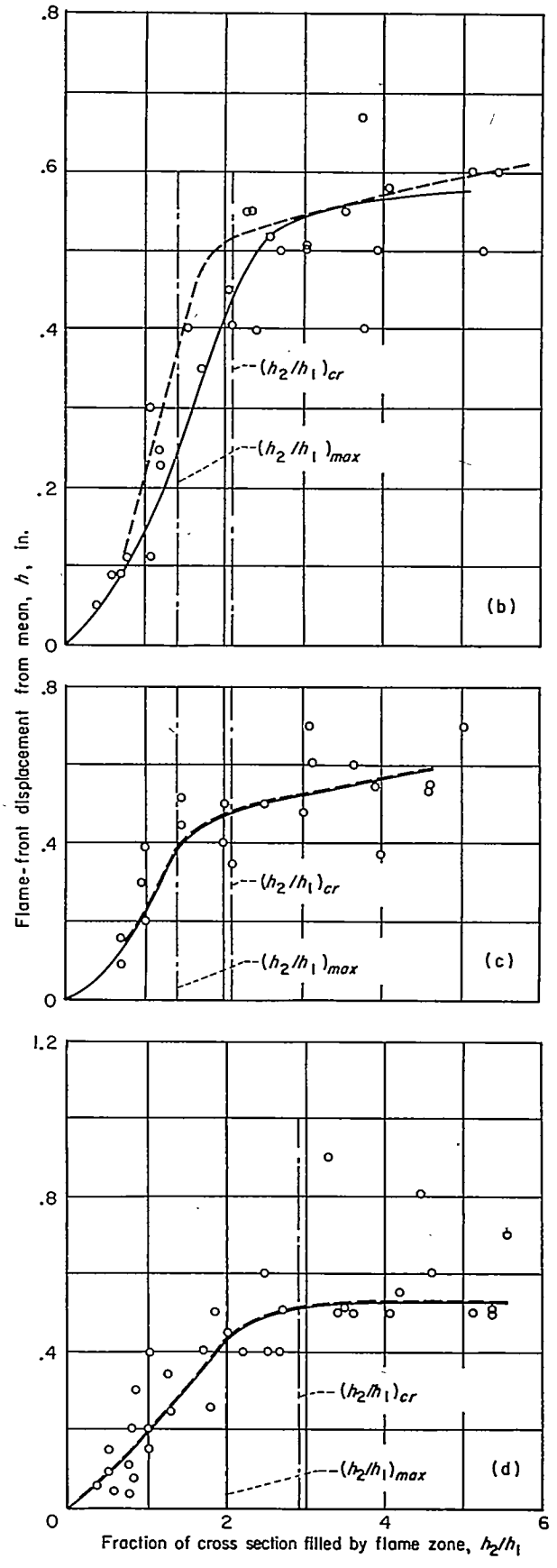


(a) Flame shadowgraphs for disturbance velocity of 0.75 foot per second at various frequencies.

(b) Disturbance velocity, 0.60 foot per second; frequency, 725 cps.
(c) Disturbance velocity, 0.75 foot per second; frequency, 725 cps.
(d) Disturbance velocity, 0.75 foot per second; frequency, 545 cps.

FIGURE 27.—Displacement measure on flame front for small-amplitude disturbances. Flow velocity, 50 feet per second; fuel-air ratio, 0.0484; turbulent disturbance velocity, 0.303 foot per second.

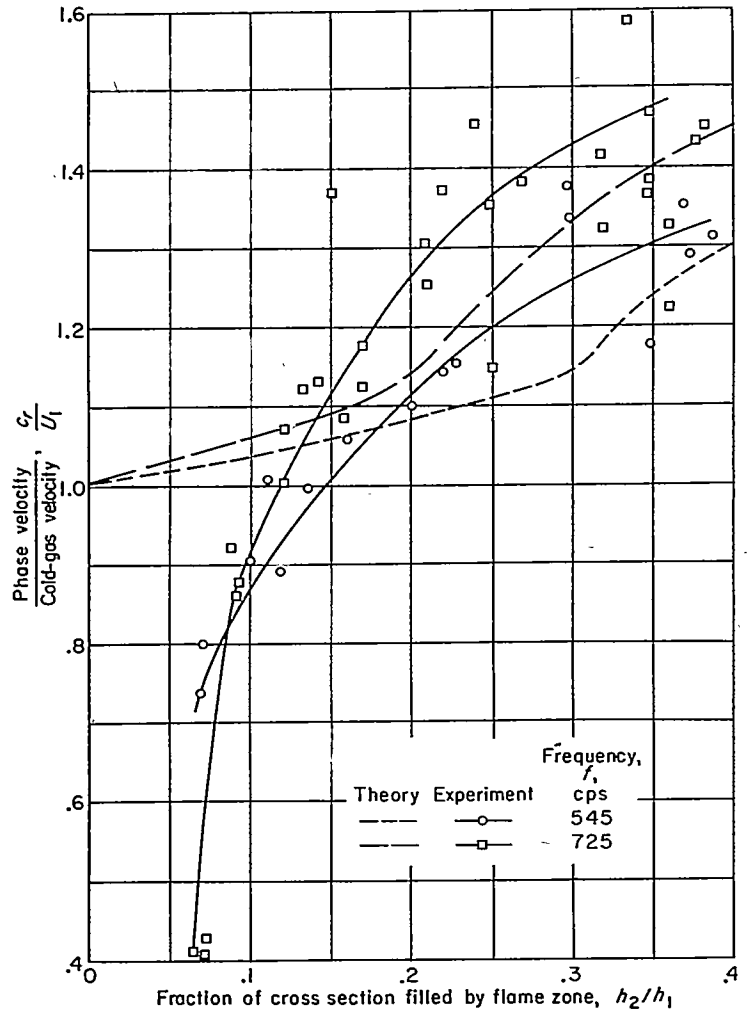


FIGURE 28.—Propagation velocities for small-amplitude disturbance.

the applicable value of $h_2/h_1$. The results are shown for two frequencies in figure 28.

The dashed lines are the values of $c_r/U_1$ obtained from figure 5(b), which is based on the results and interpretation of the stability analysis. The scatter of the experimental data is wide, but the magnitude and trends of the data remote from the flameholder are quite good. Values of $c_r/U_1$ less than unity are obtained for values of $h_2/h_1<1.5$, which implies flow reversal within this region.

### EFFECT OF TEST-SECTION DEPTH

A single run was made to determine the effect of the test-section depth on the results. The data obtained with the 1-inch-deep combustor at a velocity of 50 feet per second and a fuel-air ratio of 0.0493 are shown in figure 29. The turbulence at the center of the duct was half that of the ½-inch duct. Combustor depth seems to have some influence on the turbulent flame speed but not on the effect of imposed disturbances.

The undisturbed flame speed in the 1-inch duct reached almost twice laminar flame speed in a longer time than in the ½-inch duct. The effect of imposed disturbance on amplification as a function of frequency remains the same,

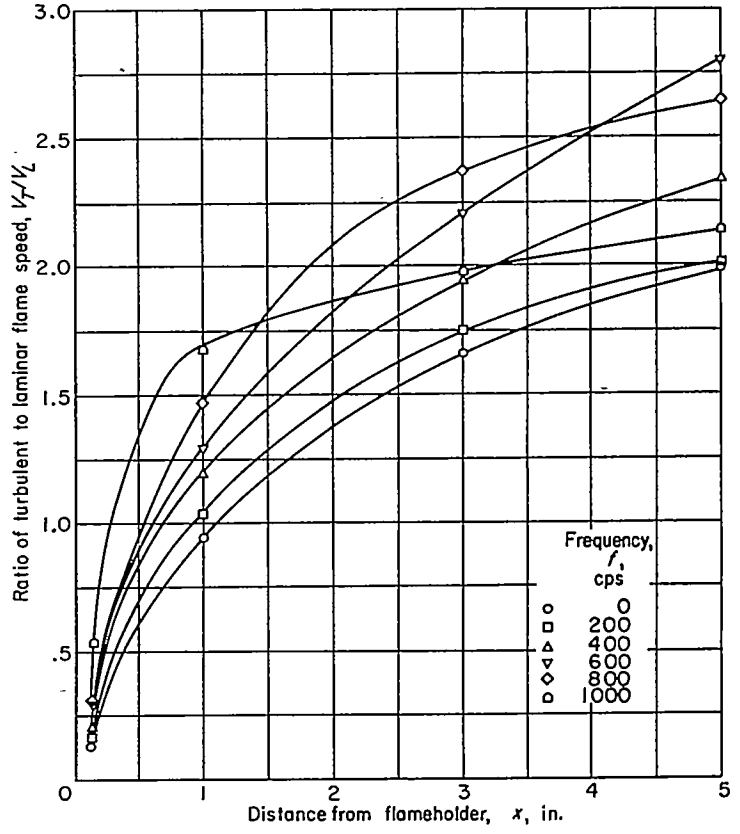


FIGURE 29.—Flame-speed distribution in 1-inch-deep test section. Flow velocity at plane of flameholder, 50 feet per second; fuel-air ratio, 0.0493; ¼-inch flameholder.

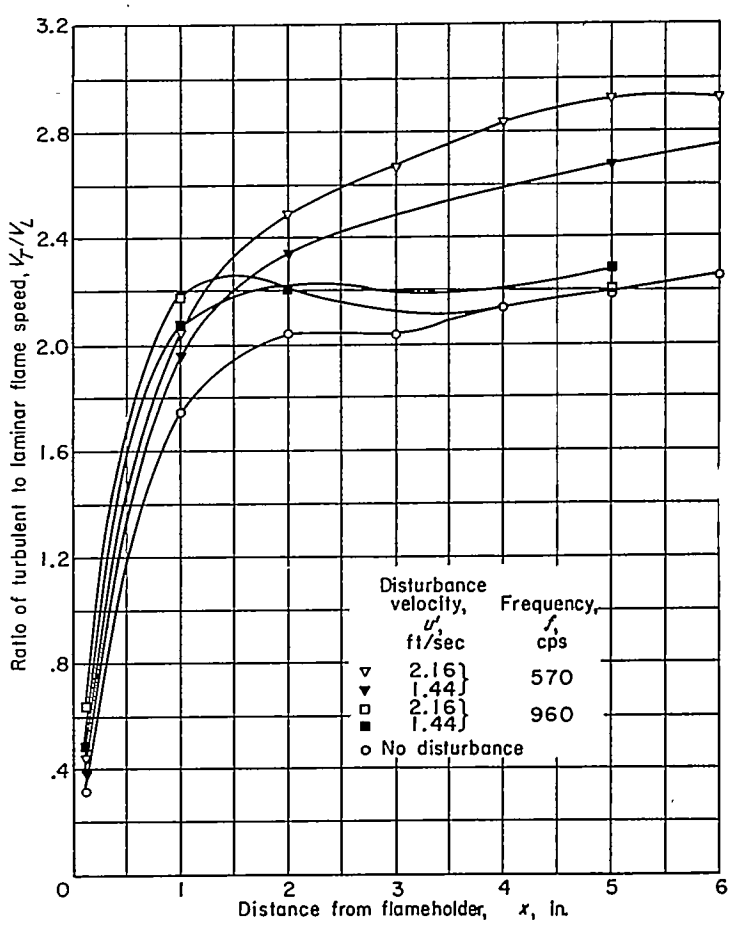


FIGURE 30.—Effect of amplitude on flame-speed distribution. Flow velocity, 50 feet per second; fuel-air ratio, 0.0444. ⟶

however. This can be seen from a comparison of figures 29 and 24(a). The range over which a given frequency dominates, taken from this run, is also plotted in figure 26.

### EFFECT OF AMPLITUDE

The effect of amplitude on single frequencies is shown in figure 30, where flame speeds for two levels of excitation (570 and 960 cps) are compared. For the lower frequency, the increase $\Delta(V_{T,d}/V_{T,u})$ varies directly as $u'$. For the higher frequency, the curves cross. Thus, the effect of low excitation is felt farther along the flame than that of higher excitation. This behavior is not data scatter and was checked repeatedly. The same sort of thing occurs at 1500 cps, although not so markedly. The reason for this anomalous behavior is not immediately apparent.

### EFFECT OF FLAMEHOLDER SIZE

Flame appearance and $V_T/V_L$ are compared for two flameholder sizes at a velocity of 50 feet per second and a fuel-air ratio of 0.0444 in figure 31. The data for a ½-inch flameholder and a variety of excitation frequencies (fig. 31(a)) show that the 570-cps excitation is again the dominant one, but not so markedly as before. The effect of flameholder size can be summarized from figures 31(b) to (d) as follows:

(1) Flame speed is noticeably decreased with the larger flameholder.

(2) The impact of the 570-cps frequency is not nearly so great in the ½-inch flameholder as in the 0.306-inch flameholder.

The decrease in flame speed with increase in flameholder size might be explained by the theory that (1) the wake region is longer and (2) the growth of the higher frequencies is therefore somewhat inhibited by this long, relatively stable wake.

### EFFECT OF VELOCITY

Momentum-pressure-drop and flame-speed readings were taken over a range of frequencies, using a 0.306-inch flameholder, a velocity of 100 feet per second, and fuel-air

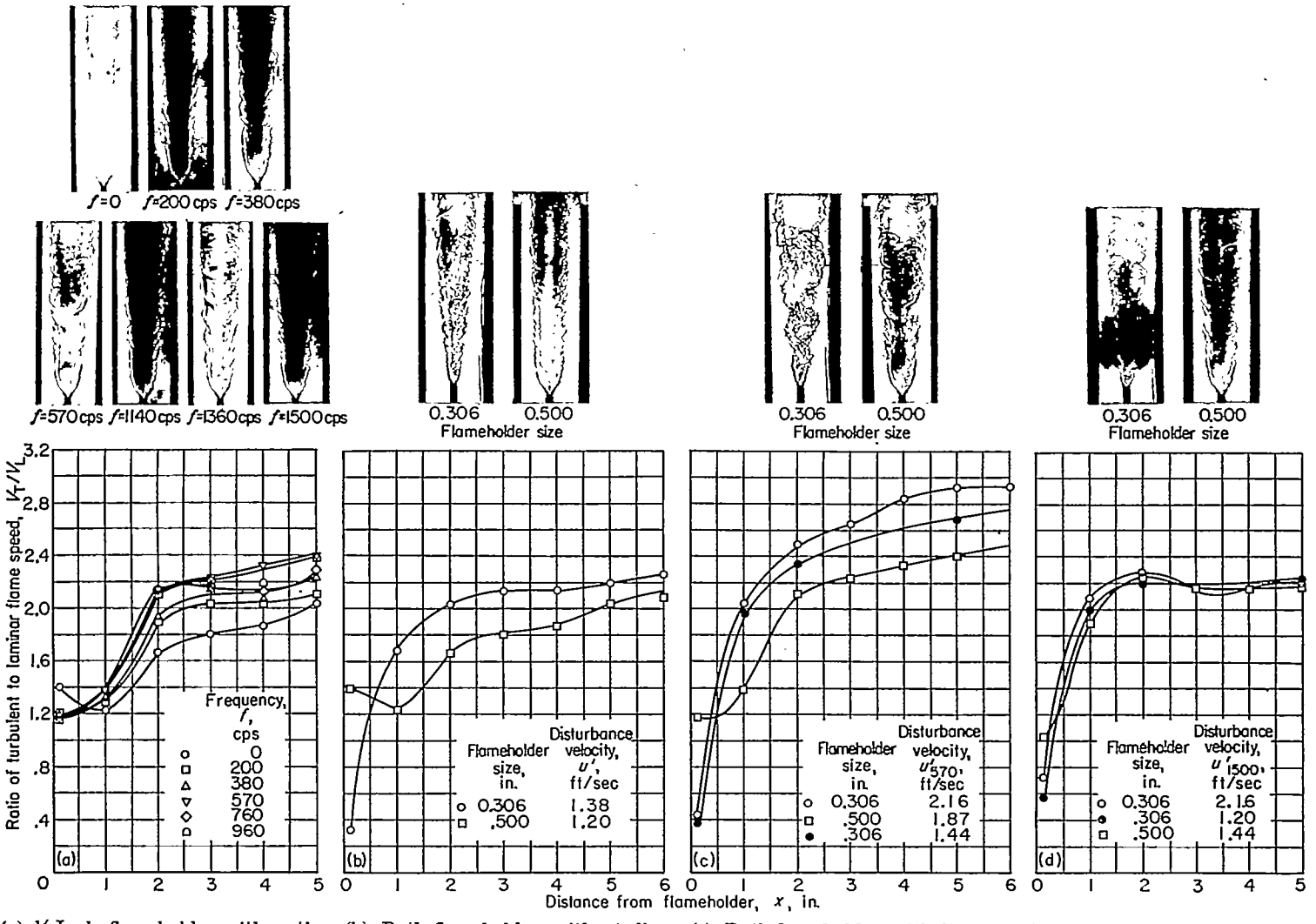


(a) ½-Inch flameholder with antisymmetric disturbances. Disturbance velocities, feet per second: $u'_l$, 2.22; $u'_T$, 1.2; and $u'_f$, 1.87.

(b) Both flameholders without disturbance.

(c) Both flameholders with disturbance at 570 cps.

(d) Both flameholders with disturbance at 1500 cps.

FIGURE 31.—Comparison of flame appearance and $V_T/V_L$ for ½- and 0.306-inch flameholders. Flow velocity, 50 feet per second; fuel-air ratio, 0.0444.

ratio of 0.0493. The results are shown in figure 32. The metering systems drifted slightly at this setting, making it difficult to hold fuel flow steady and causing some scatter in the determination of $V_L$.

The most sensitive frequency at 100 feet per second was 1700 cps, which is about three times the frequency observed at 50 feet per second. Clearly the effect is not allied with a spontaneous eddy-shedding frequency. The fraction burned is not so great as at 50 feet per second. Also, the flame speed increased sharply up to the end of the duct. These two factors tend to emphasize the higher frequencies within the limited duct length, and seem to be directly related to the instability of the flame zone. The single data point at 1700 cps is included in figure 26. This run was directed toward finding a frequency other than 570 cps for maximum effect, mainly to prevent duct resonance. Shadowgraph photographs of the flames show the antisymmetric disturbance.

The possible effect of duct resonance on these results must be considered. The modes of resonance likely to occur in a combustor are the "organ-pipe" or longitudinal modes, the transverse modes, and a single mode coupling the combustion chamber with the volume upstream of the nozzle. In the configuration studied, the longitudinal modes have frequencies, roughly, of 250 or 500 cps plus multiples of 500. The transverse modes have a minimum frequency of 3000 cps, so they are not considered here. The last type of oscillation gives a frequency of the order of 45 to 90 cps and is below the range of interest.

A longitudinal mode could affect the results in two dis-

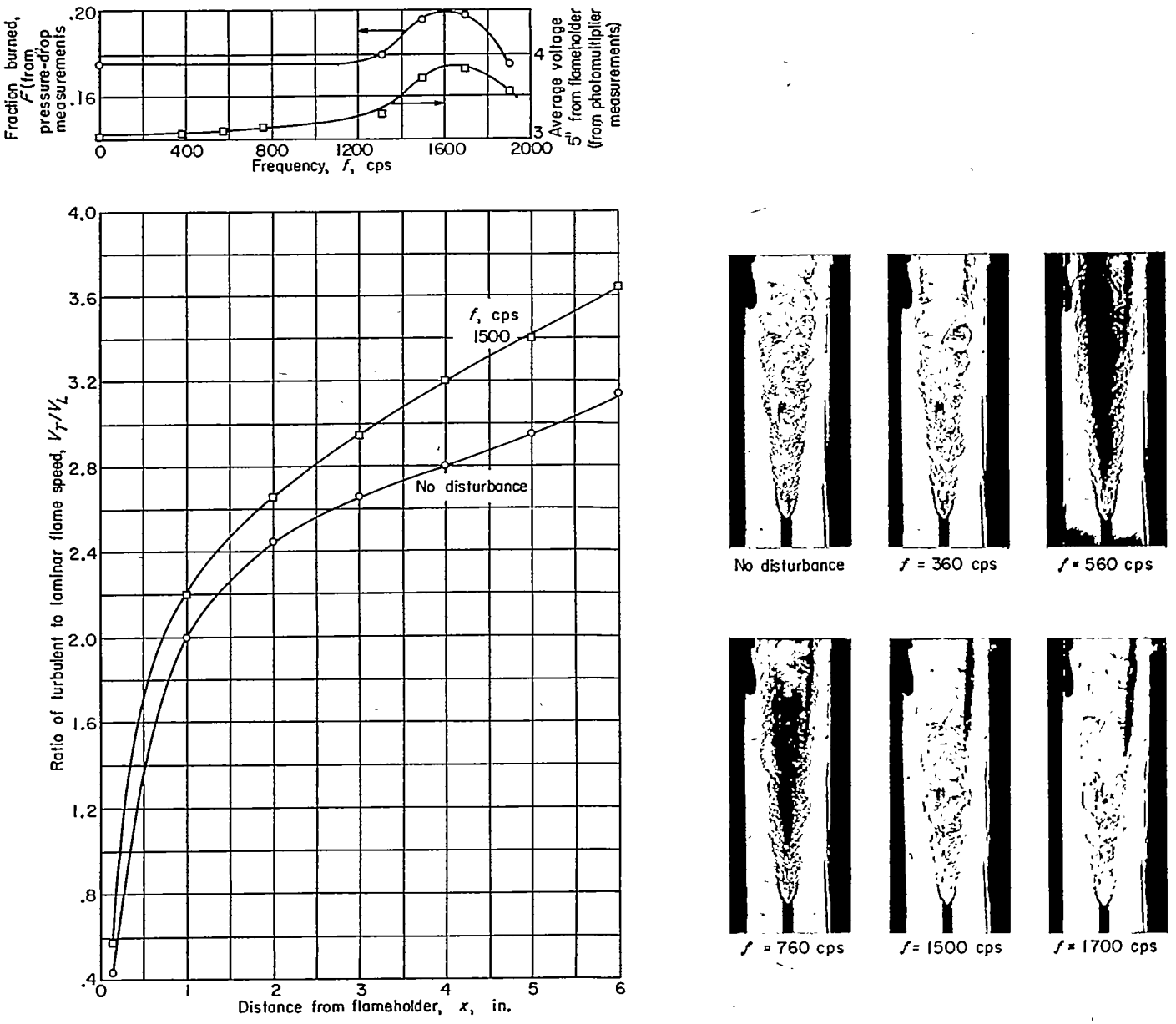


FIGURE 32.—Comparison of fraction burned with average voltage, distribution of $V_T/V_L$, and shadowgraphs with 0.306-inch flameholder. Flow velocity, 100 feet per second; fuel-air ratio, 0.0493; antisymmetric disturbance.

tinct ways: (1) If the flameholder were placed in a standing wave system at a pressure node, the time-varying velocity past the flameholder would cause large initial disturbances that would be symmetric with respect to the duct axis. (2) If the flameholder were placed at a pressure loop, there would be a coupling between the combustor and flameholder resonance that would be initially compensated for by the input calibration already discussed. If the nature of duct resonance shifts the resonant frequencies so that this compensation is no longer adequate, the input $u'$ is no longer constant for all the frequencies.

Since the photographs of figure 32 show the disturbances to be antisymmetric, the first manner of coupling is rejected. To explore the second manner of coupling, the input $u'$ for the frequencies on either side of the most sensitive ones (i. e., 1500 to 1700 cps; see fig. 32) was increased by a factor of 3. In no case was it possible to increase the fraction burned as much as the 1500- to 1700-cps disturbances increased it. Thus, the results shown in figure 32 are due to the sensitivity of the flame zone to the imposed disturbance and are not due to duct resonance.

### SYMMETRIC DISTURBANCES

A symmetric disturbance was used for tests with a 0.315-inch flameholder, velocity of 50 feet per second, and a fuel-air ratio of 0.0444. No separate calibration of input sound was attempted, the inputs of the antisymmetric-disturbance tests being used. The results are shown in figure 33. Comparisons with flame speeds obtained with antisymmetric disturbances are given. There was a leak of approximately 1/16 inch past one edge, which provided an additional flame surface and increased the apparent mean flame speed near the flameholder but did not disturb the results at some distance from the flameholder. In general, symmetric and antisymmetric disturbances gave roughly comparable shifts in flame speed near the flameholder. At a distance from the flameholder, antisymmetric disturbances increased the flame speed more than symmetric disturbances. These results are in accordance with sketch (f).

## DISCUSSION

Ten questions raised by the analytical and experimental phases of the investigation are discussed in this section.

**1. In what respects do the experimental results and the interpretations of the stability analysis agree?**—The areas of agreement are summarized in the following table:

| Interpretation of stability analysis | Investigation of sensitivity of a flame in a duct to transverse velocity disturbance |
|---|---|
| (1) The flow is stable to symmetric disturbances, unstable to antisymmetric disturbances. A qualification is made near a flameholder where the two types of disturbances are equally unstable. | (1) The flame seems about equally unstable to symmetric and antisymmetric disturbances near flameholder, is more unstable to antisymmetric disturbances far from flameholder. |
| (2) In moving along the flame at phase velocity, a disturbance of given frequency grows until the flame width becomes about 0.4 of the wavelength; then an apparent decay of the disturbance begins. | (2) A disturbance of given frequency first grows, then decays. The critical flame width where decay starts is slightly smaller than that predicted. |
| (3) There is a most-amplified frequency having a wave number of $5<2\alpha_c h_1<7$. | (3) There is a most-amplified frequency which, for the lengths investigated, corresponds to $2\alpha_c h_1 \approx 12$. |
| (4) The phase velocity ranges from a velocity equal to the cold-gas velocity at the flameholder up to 1.5 times the cold-gas velocity far from the flameholder. | (4) The phase velocity behaves much as predicted except near the flameholder, where it is lower than the cold-gas velocity. |
| (5) The amplification depends on $v'/V_{T,u}$ for a given $dh_2/dx$. | (5) The amplification depends on $v'/V_{T,u}$ for a given $dh_2/dx$. |

The details of the system that would define more exactly the shortcomings of the stability analysis as well as the adequacies await the development of a transient-velocity

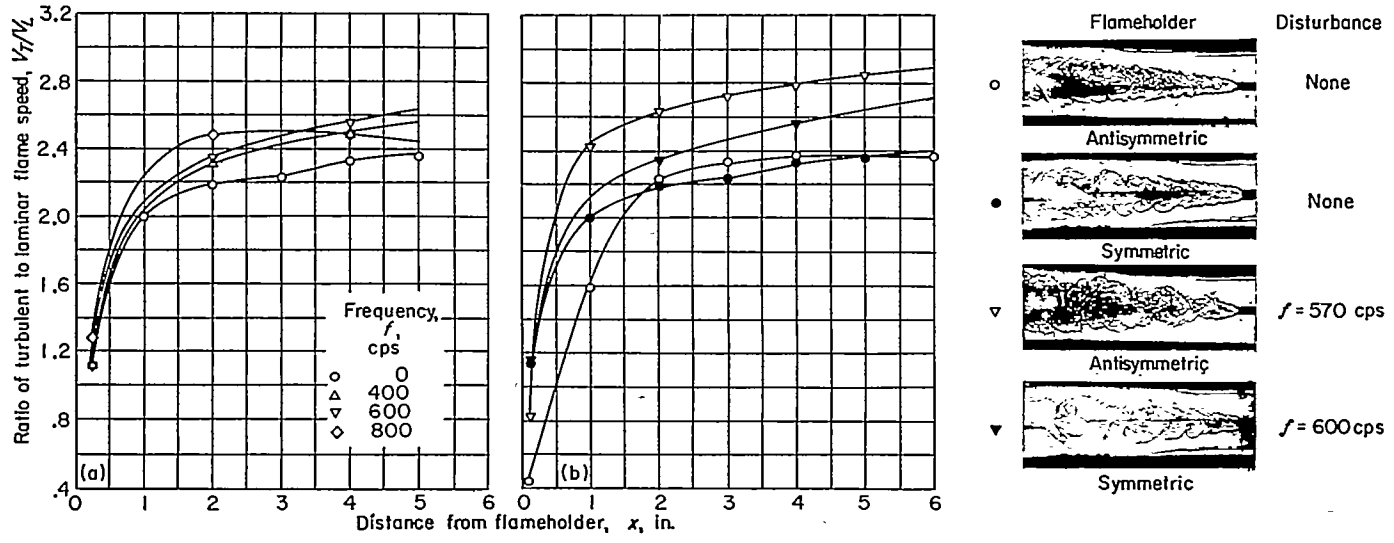


(a) Symmetric disturbances. Disturbance amplitude, unknown; input same as for figure 24 (a).

(b) Comparison of symmetric and antisymmetric flameholders with and without disturbance.

FIGURE 33.—Comparison of $V_T/V_L$ obtained with flameholders for producing symmetric and antisymmetric disturbances. Flow velocity, 50 feet per second; fuel-air ratio, 0.0444.

measuring technique that can be used in a flame zone. In at least one instance there was evidence that a form of transition took place (see Comparison of Flame Speed with Flame Appearance). The stability analysis cannot indicate when this takes place.

**2. Would the same distribution of displacement and $V_T/V_L$ with distance from the flameholder obtain if no growth occurred in the flame zone?**—This seems unlikely. For example, if the input disturbance distribution simulates a source at the corner of the flameholder, only near the flameholder would there be a marked transverse velocity component. The highest frequencies would show the greatest increase in flame speed.

**3. Do eddies shed?**—They certainly seem to. In figure 34 photographs of a lean flame, both shadowgraphs and direct

Direct photograph of flame through stroboscope; frequency, $f$, 600 cps

Shadowgraph of excited flame; frequency, $f$, 760 cps

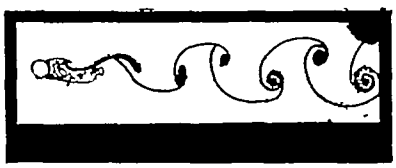

C-41538

Eddy trail

FIGURE 34.—Comparison of photographs of excited flame with eddy trail.

photographs taken through the stroboscope, are compared with a smoke-trace photograph of eddies shedding from a rod at a Reynolds number of 73 (ref. 30). The appearance of flame clearly indicates that eddy-shedding is present.

As the fuel-air ratio is increased, the range over which these eddies appear near the flameholder narrows. Figure 35 shows a plot of frequencies at which eddies appeared against fuel flow from lean to rich blowout. These data were obtained by exciting the flame at frequencies at which the constant-speed stroboscope would permit observation; that is, approximately every 100 cps.

Eddies are characterized by lobes of flame of about equal size on either side of the flameholder. These are contrasted to mere sinuosity of the flame. At 700 cps the lobes appeared symmetric, indicating duct resonance at this frequency. At 800 cps the lobes were antisymmetric and were observed throughout the fuel-air-ratio range. At the lean fuel-air ratios, most of the disturbances produced eddy-shedding.

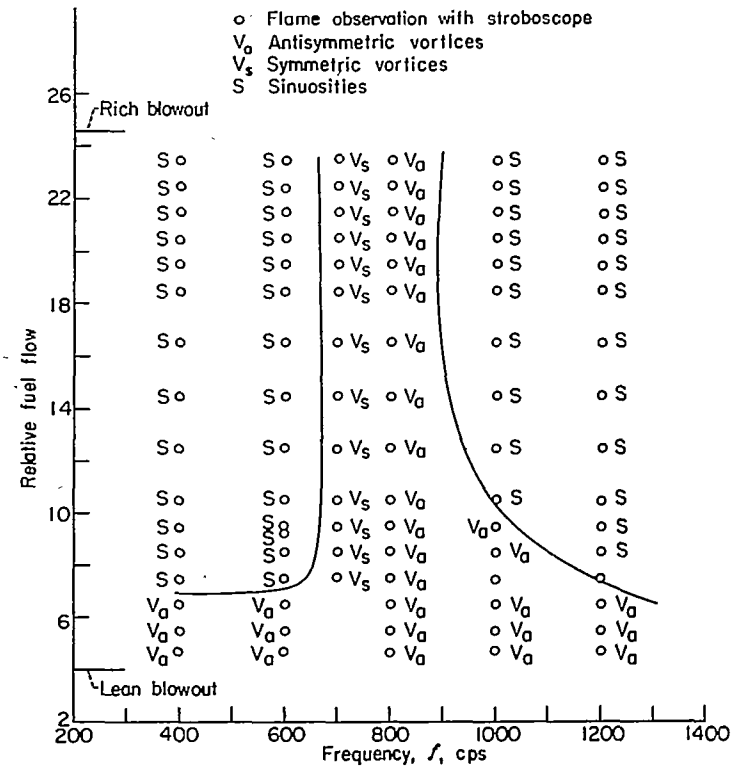


FIGURE 35.—Observations of vortex shedding excited by antisymmetric disturbances.

**4. Does the turbulent-flame propagation velocity depend upon upstream turbulence?**—It should. Bolz and Burlage (ref. 11) and Mickelsen and Ernstein (ref. 12) have shown turbulent flame speeds to be in fair agreement with Scurlock's theory (ref. 8), omitting flame-generating turbulence effects. These data were obtained in turbulent "soap-bubble" flames. Thus, in addition to the effect of the instabilities mentioned here, the incident turbulence should have an effect.

The most important point, however, is that the instability merely acts as an amplifier for a relatively narrow range of frequencies, the output within limits of the linearized theory being proportional to the input. Part of the input is, of course, the turbulent motion. The other, and in some cases the most important part, is the role played by the sound in the duct which, upon hitting the flameholder, produces a transverse velocity that may be subsequently amplified. In that this sound is related to the incident turbulence, the turbulence has an effect.

Some data on an effect of incident turbulence were obtained while exploring the properties of the system. Figure 36 shows a plot of $E_T$ against distance from the flameholder $x$ for two flameholder positions and two fuel-air ratios. The table in the section on turbulence intensity and spectra shows that the turbulence intensity increases from inlet nozzle to exhaust and from the wall to the interior of the test section. Taking as representative the value of $u'$ measured $\frac{3}{16}$ inch above the flameholder lip, the values of the turbulence parameter $u'/V_L$ vary over a factor of 2 for the two flameholder positions. It is apparent that, everywhere except near the flameholder, there is little effect of the initial $u'/V_L$ values measured. The data are insufficient for pin-

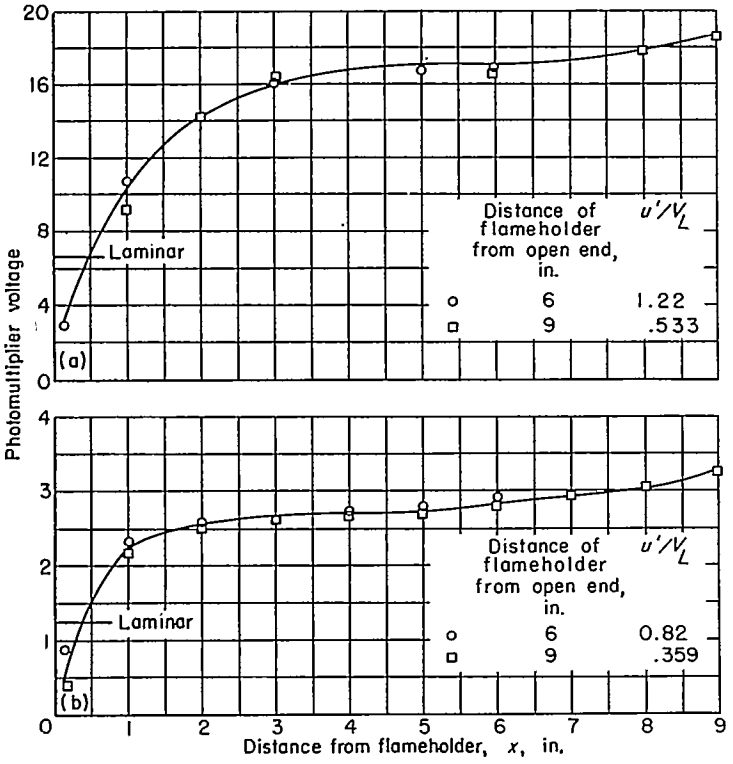


(a) Fuel-air ratio, 0.0444.
(b) Fuel-air ratio, 0.0515.

FIGURE 36.—Comparison of relative flame speeds at two flameholder positions. Flow velocity, 50 feet per second.

pointing the cause of this lack of effect. Two surmises appear warranted:

(1) The flame was noisier at the 9-inch position than at the 6-inch position because of flame-duct interaction; $u'$ was measured in the absence of a flame.

(2) The turbulence found upstream of the flameholder was due to transition in the boundary layer. The $u'$ in the boundary layer was growing for both positions measured. It is thought that the growth of this $u'$ is accelerated when the boundary layer separates from the flameholder and quite rapidly achieves a value that would be relatively insensitive to $u'$ prior to separation.

Additional data on the effect of upstream turbulence were obtained by putting three banks of 200-mesh screen just upstream of the flameholder. Shadowgraphs of the flame in this case with and without a 560-cps disturbance are shown in figure 37. Also plotted in this figure is $V_T/V_L$ measured with and without screens. In the absence of imposed disturbances, $V_T/V_L$ is lower with the screens than without. Although the conditions were set for 50 feet per second, leaks were found between the mixing section and the flameholder for this run so that the velocity was not known. The reduction in $V_T/V_L$ is thought to be primarily due to the reduction in $u'$ by the presence of the screens.

It is of interest to compare the flame-speed data obtained in this investigation with data taken in a similar apparatus. Figure 38 shows a comparison of $V_T/V_L$ obtained by photomultiplier tube with $V_T/V_L$ obtained by Scurlock (ref. 8) by measuring a mean flame width. Because $V_L$ was taken as a property of the mixture, the values of $V_T/V_L$ near the flameholder are low. The values of $V_T/V_L$ obtained with the relatively high turbulence appear higher than those obtained by Scurlock. The possible displacement of the absolute magnitudes of $V_T/V_L$ due to the different methods used would not warrant interpreting these data to give a quantitative dependence on turbulence intensity.

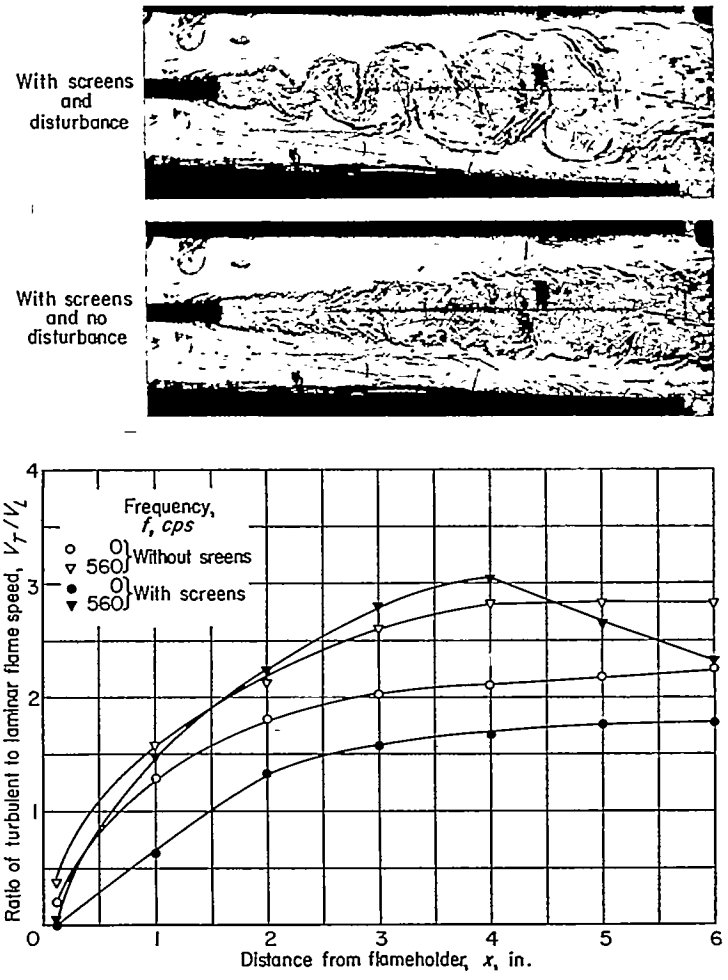


FIGURE 37.—Comparison of flame speeds with and without banks of 200-mesh screens upstream of flameholder.

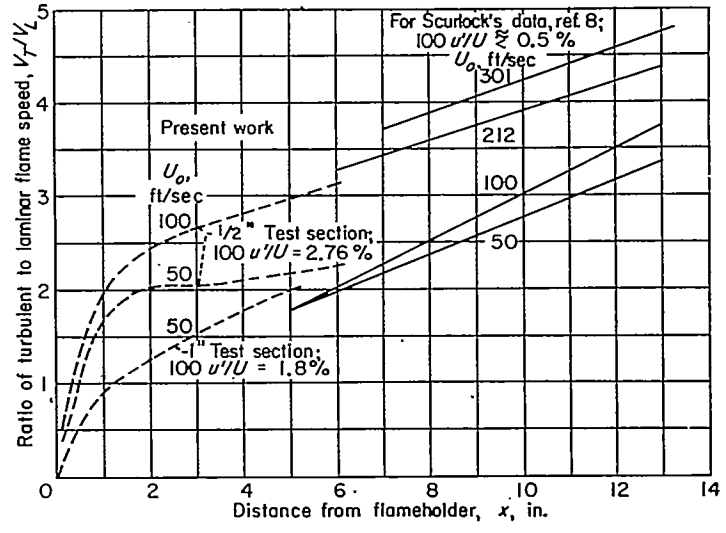


FIGURE 38.—Comparison of $V_T/V_L$ taken in ½-inch- and 1-inch-wide ducts with Scurlock's data.

**5. How does $V_T/V_L$ obtained from area measurements compare with $V_T/V_L$ taken from photomultiplier data?**—The shadowgraphs indicate considerable wrinkling of the flame surface. In addition, it appears that density gradients exist within the outer envelope of flame surface, implying heat release there.

Since no single continuous flame surface is apparent, measuring flame area from these pictures seems impossible. For the sake of comparison, however, some relative surface extension should be of interest to those who would formulate a theory of turbulent flame propagation. Such measurements were made in the following manner: The negatives of a group of photographs were used to project an image of the flame on a screen. The image of a 6-inch test section was 2½ feet long. A map measure was used to find the length of the outer envelope of the group of flame images, ignoring the obvious density gradients within the outer envelope. Lengths were measured on the top and bottom surface of each flame, averaged, and divided by projected length. The resulting quotient is defined as $\overline{(V_T/V_L)}_{ps}$.

In the following table, the ratios so obtained are compared with the average $V_T/V_L$ obtained from a photomultiplier survey $\overline{(V_T/V_L)}_{pm}$:

| $U_o$, ft/sec | Flame-holder size, in. | Fuel-air ratio | Excitation frequency, $f$, cps | $\overline{(V_T/V_L)}_{pm}$ | $\overline{(V_T/V_L)}_{ps}$ | $\frac{\overline{(V_T/V_L)}_{pm}}{\overline{(V_T/V_L)}_{ps}}$ | Photograph from figure |
|---|---|---|---|---|---|---|---|
| 50 | 0.306 | 0.0444 | 0 | 2 | 1.436 | 1.39 | 23(a) |
| | | | 570 | 2.54 | 1.77 | 1.43 | 23(c) |
| | | 0.0515 | 0 | 1.82 | 1.40 | 1.30 | 23(a) |
| | 0.500 | 0.0444 | 0 | 1.735 | 1.36 | 1.28 | 31(a) |
| 100 | 0.306 | 0.0493 | 0 | 2.46 | 1.65 | 1.49 | 32(b) |

In general, the trends indicated by the $\overline{(V_T/V_L)}_{pm}$ are followed by the $(V_T/V_L)_{ps}$. In view of the obvious internal structure and three-dimensional nature of the wrinkles, no argument for or against the wrinkled flame as an adequate turbulent flame model can be introduced.

**6. How can flame speeds be predicted on the basis of these results?**—The most promising method of predicting flame speeds would be based on an incident and amplified spectra, as recommended by Markstein (ref. 4). For example: If the incident $v'$ spectrum corresponds to a scale of turbulence $L$ of 0.15 inch and each frequency is amplified as the theory states, the spectra at $h_2/h_1=0.5$ and 0.25, for $1/K_2\approx 20$ would correspond to the ones shown in figure 39. Between the two spectra would be a continuously shifting spectrum. What is needed, then, is a model of flame propagation that would allow for a continuously shifting spectrum of turbulence. This model should have the advantage of allowing for the appearance of discrete frequencies that dominate the rest of the spectrum.

An interesting point comes up in regard to spectra. It is seen experimentally as well as theoretically that very little effect is derived from exciting the flame at a frequency less than $(2/3)(U/2h_1)$ or greater than $4U/2h_1$ (see figs. 22, 32, and 7). Therefore, for the present conditions (i. e., velocity of 50 ft/sec, 2-in. duct) the energy in the spectrum of turbulence below 200 cps apparently will not increase flame spreading.

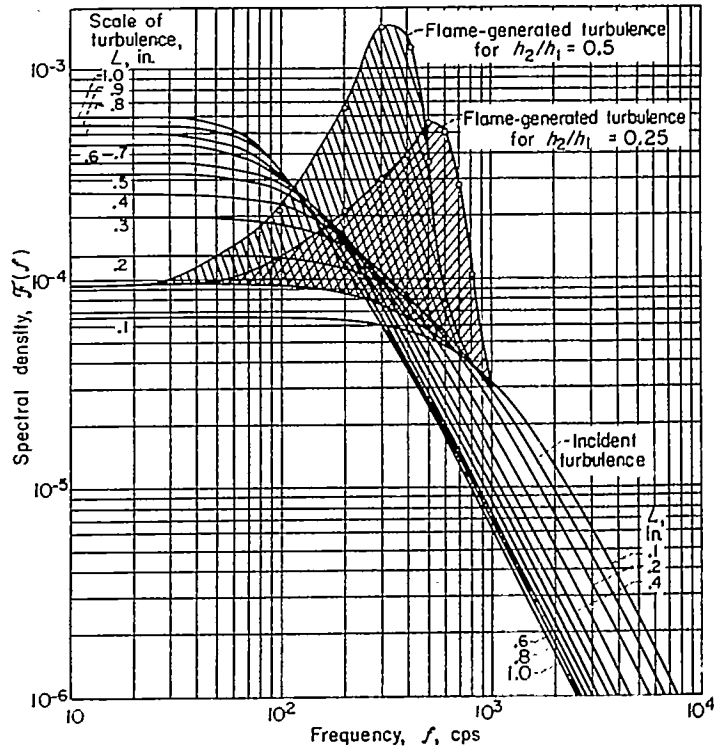


FIGURE 39.—Spectra of incident and flame-amplified turbulence; $\mathcal{F}(f)=(4L/U)/\{1+[(2\pi/U)Lf]^2\}$.

A plot of the percentage of energy in the turbulence at all frequencies below $f$ against $fL/U$ from reference 38 is shown in figure 40. For an assumed scale $L=(1/6)2h_1$, the frequency below the frequency $(2/3)(U/2h_1)$ represents about 35 percent of the total turbulence energy. This amount of energy is contained in disturbances with frequency too low to be amplified to any usable extent by the flame zone. Similarly from figure 40, the energy in the spectrum below the frequency $f=4U/2h_1$ [or $f(L/U)\approx 0.66$] is 85 percent of the total turbulence energy. Thus, about 15 percent of the turbulence energy is at frequencies too high to be appreciably amplified by the flame zone.

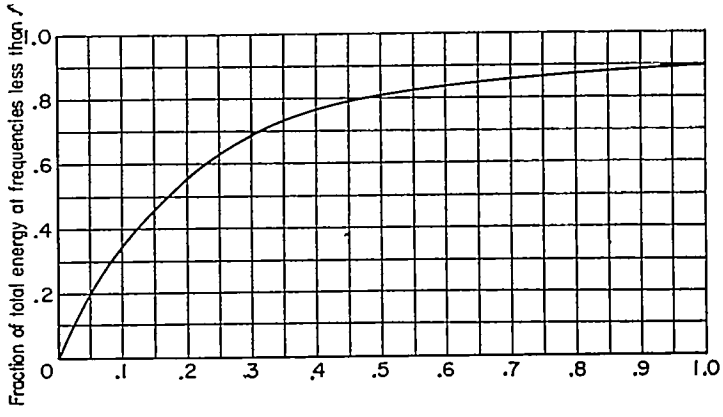


FIGURE 40.—Turbulence energy distribution for exponential correlation coefficient (ref. 38).

The scale of isotropic turbulence that would put the largest percentage of energy in the frequency range $(2/3)(U/2h_1)<f<4U/2h_1$ can be found from the extreme of the quantity (ref. 36)

$$\tan^{-1}\left(2\pi\frac{4U}{2h_1}\frac{L}{U}\right)-\tan^{-1}\left(2\pi\frac{2}{3}\frac{U}{2h_1}\frac{L}{U}\right)$$

or

$$L=\frac{1}{10}2h_1$$

In this case the amount of energy within the frequency range is 55 percent of the total as compared with 50 percent for $L=(1/6)2h_1$, 40 percent for $L=(1/3)2h_1$, and 45 percent for $L=(1/20)2h_1$.

**7. Can the results concerning frequency be applied to multiple flameholders?**—If $n$ flameholders are arranged so that the flow field can be divided into $n$ identical segments, Scurlock's results hold for each segment. The results in the theoretical sections of this report for the stability of the flow field apply to each segment and rely on the condition that $v'$ vanishes at the boundary of each segment. Although one of several modes of instability may satisfy this condition, it is obvious that the foregoing results do not give any information about the other modes.

To illustrate the occurrence of multiple modes, consider a profile examined by Lin (ref. 22, pp. 219–220) where

$$U=A+B\sin\frac{2\pi}{\lambda_y}y$$

Lin shows that the wave numbers for neutral stability of the different modes available depend on the number of inflection points in the flow and can be given by

$$(\alpha l)^2=\left(\frac{2\pi l}{\lambda_y}\right)^2-(n\pi)^2$$

The choice of $l=\lambda_y$ yields the following profile, which is similar to the one studied earlier in this report for a single flameholder:

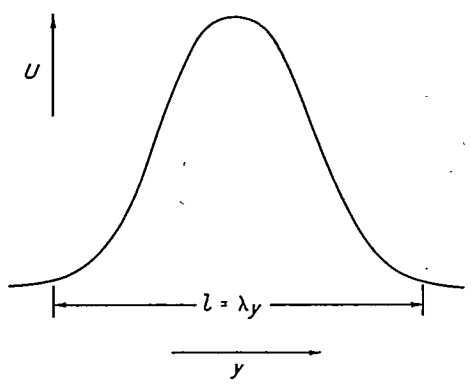


Sketch (l)

For this case neutral stability occurs at $\alpha\lambda_y=\alpha l=\pi\sqrt{3}$, 0.

If two flameholders are present, the following profile may be approximated by setting $l=2\lambda_y$:

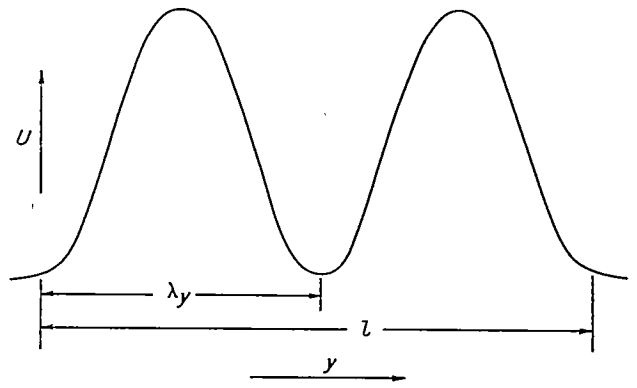


Sketch (m)

For this case the wave numbers for neutral stability of the four modes obtained are

$$\alpha\lambda_y=\alpha\frac{l}{2}=\pi\frac{\sqrt{15}}{2},\ \pi\sqrt{3},\ \pi\frac{\sqrt{7}}{2},\ 0$$

Two new modes appear in addition to the two for the single profile.

Similarly, for three flameholders,

$$\alpha\lambda_y=\alpha\frac{l}{3}=\pi\frac{\sqrt{35}}{3},\ \pi\frac{\sqrt{32}}{3},\ \pi\sqrt{3},\ \pi\frac{\sqrt{20}}{3},\ \pi\frac{\sqrt{\pi}}{3},\ 0$$

that is, there appear four roots in addition to the two for $l=\lambda_y$.

In short, the single mode investigated in this report is applicable to multiple flameholders, but only as one of several modes that combine to give the entire instability.

**8. Can the excitation at the flameholder permit increased combustion rates without destroying the burner walls?**—Yes. In these tests the sound level at the exhaust plane was only 93 decibels with the flame excited. When the flame is excited by the destructive duct resonance, the sound level is of the order of 200 decibels (ref. 17).

In order to apply this type of excitation to an engine, the control exerted herein (a speaker system) would not be needed. Instead, the disturbance can be introduced by suitably placed whistles, mounted on the flameholder and driven by the flowing stream. The whistle ideally should have a number of strong overtones and a fundamental equal to the most sensitive frequency $U_o/2h$. The overtones would serve to increase the heat-release rate near the flameholder, while the fundamental would increase the heat-release rate far from the flameholder.

**9. What would be the sacrifice in stability and pressure drop for such an excitation?**—Both these penalties require further investigation, but from work that has been done the sacrifice does not seem great. For example, when the flameholder was placed ⅝ inch from the nozzle entrance and a 6-inch-long test section was installed, lean blowout at 50 feet per second occurred at a fuel-air ratio of 0.042. At a fuel-ar ratio of 0.0453, the disturbance amplitudes required to cause blowout were found for several frequencies. The results are shown in figure 41. Minimum disturbance velocity was required at 780 cps. At this condition the

flameholder without flame had an eddy-shedding frequency of 420 cps. The Strouhal number is thus 0.206, agreeing well with the results of Roshko (ref. 34). The cold-duct resonance fundamental was 1000 cps. The reason for this result is not known. The main point here, however, is to show the effect of disturbances to be used for promoting flame propagation upon flameholder stability. At a fuel-air ratio of 0.047, it was impossible to induce blowout with speaker inputs as much as 10 times those used in the earlier tests. The imposed disturbances will probably narrow the stability range slightly but not prohibitively, the amount of narrowing depending on the frequencies imposed.

An interesting observation was made in the study of lean blowout. As the lean-blowout fuel-air ratio was approached, the flame emitted a low-frequency noise at 87 cps. The average heat-release rate dropped abruptly. A survey with the photomultiplier probe showed the flame to be intermittently extinguished for all positions greater than ⅞ inch downstream of the flameholder. Typical wave forms observed at several stations downstream of the flameholder are shown in the following sketch:

| Distance downstream of flameholder, in. | Wave form of photomultiplier signal |
|---|---|
| $\frac{7}{8}$ | |
| $1\frac{1}{8}$ | |
| 2 | |
| 4 | 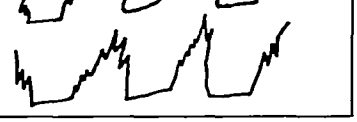 |

Sketch (n)

Random photographs taken at this condition show intervals during which no flame was present in part of the combustor (fig. 42).

It is curious that the flame surface facing upstream at the break in the flame is strong and well-defined both in the photomultiplier and the shadowgraph observations. The flame surface facing downstream is conversely ill-defined in both methods of observation. Near the point of rupture the photomultiplier signal is approximately symmetric. No explanation for this is apparent. The most significant feature of these data is that this form of resonance accompanied by intermittent blowoff downstream of the sheltered zone was the only form of excitation that reduced the heat-release rate in the combustor. On this basis it is tempting to generalize that all oscillations that do not cause flame parting must increase the heat-release rate in the combustor.

For the frequency of maximum amplification (570 cps), an increase of as much as 30 percent in heat release or about 0.2 percent of the kinetic energy of the flowing stream was obtained in the 6-inch-long combustor for an energy flux

$$\frac{\text{Sound energy}}{\text{Kinetic energy of stream}} \approx \frac{6}{2500}$$

In this case the noise level at the exhaust was 93 decibels.

Another way of increasing the heat-release rate that is indirectly suggested is to accelerate the flow locally or alter the profile to a more unstable one by use of a convergent-divergent combustion chamber. One way these can be combined with the introduction of a $v'$ at the desired frequency is to construct a combustor with a wavy wall. Using this method of excitation would require a new experimental determination of the desired wavelength and amplitude of the waves in the wall, but would eliminate any effect on flame anchoring.

**10. Can the behavior of axisymmetric flames in cylindrical ducts be predicted?**—First, the steady-state problem, solved by Scurlock, of the cylindrical flame in a cylindrical duct yielded a ⌒ profile as opposed to the ⋀ profile for plane flow. If the arc part of the curved profile is assumed parabolic, the cylindrically symmetric disturbance equation can be solved by elementary functions for symmetric disturbances. This, however, accomplishes nothing, because the profile is neutrally stable to symmetric disturbances. The same result is obtained for the ⋀ profile in the plane case. For antisymmetric disturbances, the problem is more complicated, and no simple solution is apparent.

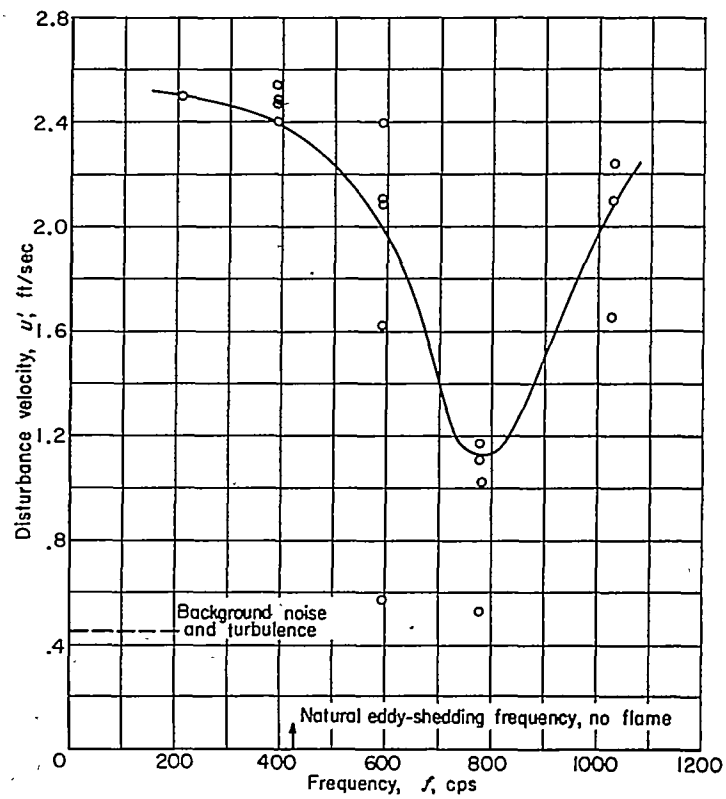


FIGURE 41.—Distribution with frequency of disturbance velocities required to produce blowout at fixed velocity and fuel-air ratio with 0.306-inch flameholder placed ⅝ inch from nozzle. Flow velocity at plane of flameholder, 50 feet per second; duct length, 5.7 inches; antisymmetric disturbances.

If the profile is affected by a flameholder in such a way that it may more nearly be approximated by a ⎽⎺⎺⎽ profile composed of three straight-line segments and two parabolic arcs, a range of instability for symmetric disturbances is obtained. This profile can be compared with the corresponding profile in plane flow ⎽/⎺⎺\⎽. Such an analysis is given in the appendix. A few calculations are given to permit comparison with the data of figure 11, for conditions that $h_1$ approaches infinity and $\rho$ is constant throughout. The results are compared in the following table:

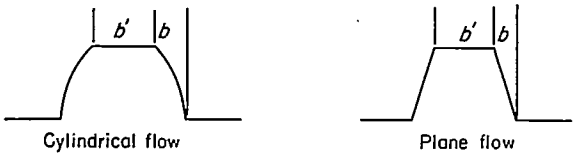


Sketch (o)

| $\frac{b'}{2b}$ | $2ab$ | |
|---|---|---|
| | Plane flow | Cylindrical flow |
| 0.1 | 2.26 | 2.08 |
| .2 | 2.55 | 2.42 |
| 1.0 | 2.55 | 2.54 |

The critical wave numbers agree quite closely. At first glance, the results for plane flow seem to be a fair approximation for cylindrical flow. In order to obtain a rough experimental verification of this supposition, a 1½-inch-inside-diameter glass tube and its accommodating nozzle were installed in place of the rectangular test section. The ½- by 0.306-inch antisymmetric flameholder was retained. At 50 feet per second and a fuel-air ratio of 0.047, resonance-free operation was obtained at a combustor length of 4½ inches or less. With the flameholder set to give this length, the disturbance inputs were calibrated as before to give a disturbance velocity of 1.8 feet per second. Then the burning run was made with the settings indicated by calibration. The flame speeds were measured by the photomultiplier probe plus a measurement of an average local flame diameter. The results are shown in the following table:

| Frequency, $f$, cps | $V_T/V_L$ | | |
|---|---|---|---|
| | 1″ From flameholder | 2″ From flameholder | 4″ From flameholder |
| 0 | 2.27 | 3.31 | 3.58 |
| 200 | ------ | 3.56 | 3.77 |
| 385 | 2.59 | 3.56 | 3.95 |
| 580 | 2.68 | 3.56 | 3.95 |
| 770 | 2.82 | 3.65 | 4.25 |
| 980 | 2.89 | 3.70 | 3.80 |
| 1170 | 2.89 | 3.70 | 3.73 |
| 1360 | 2.96 | 3.65 | 3.73 |
| 1740 | 3.09 | 3.65 | 3.99 |

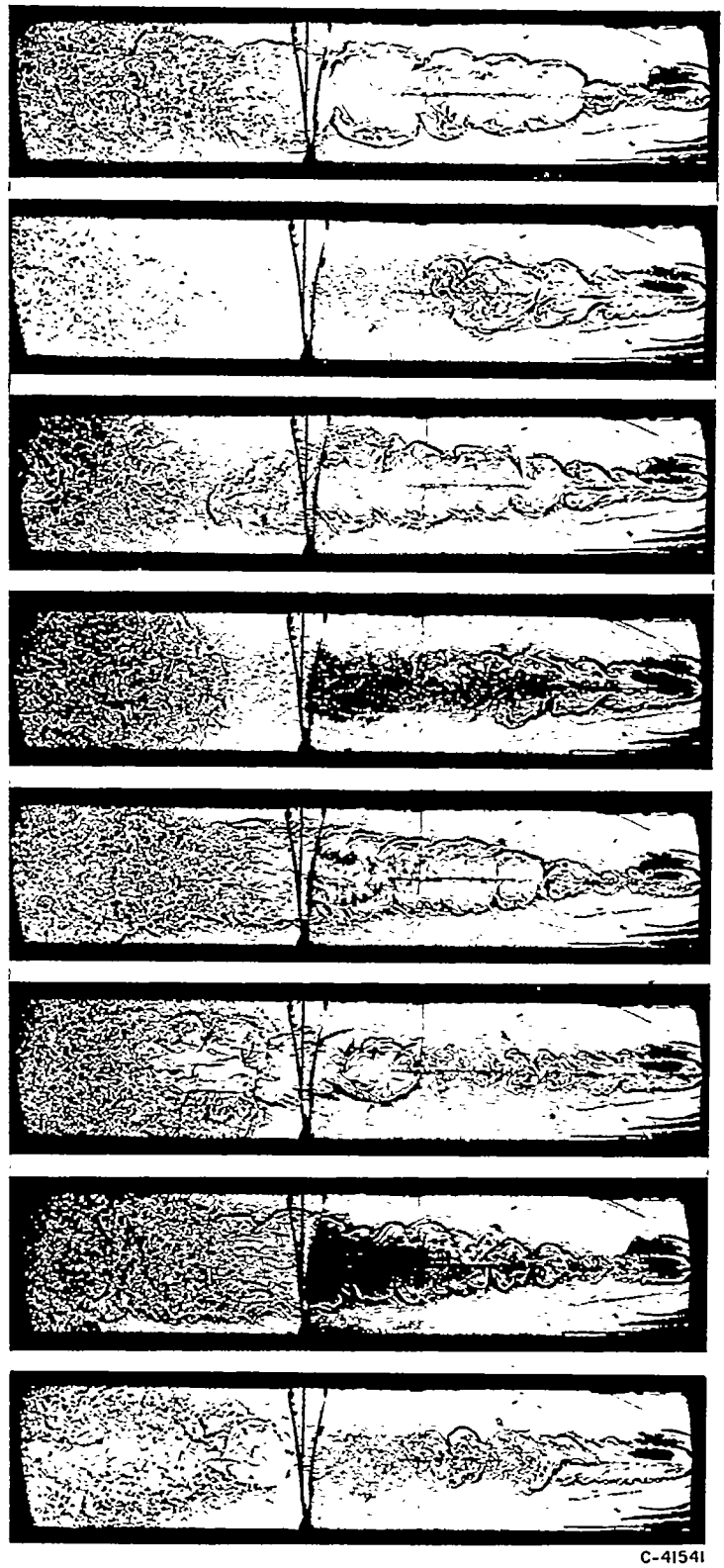

C-41541

FIGURE 42.—Spontaneous oscillations showing intermittent flame interruption. Flow velocity, 50 feet per second; frequency, 85 cps; fuel-air ratio, 0.0444.

The flame speed with this arrangement is almost twice as high as with the plane burner. Part of this increase is undoubtedly due to the disturbances introduced by the corners of the flameholder. The fraction burned is 20 percent at the position 4 inches from the flameholder, corresponding to $h_2/h_1=0.7$. Therefore, the frequencies in 4 inches of this duct may be compared with those obtained in 6 inches or more of the rectangular duct. The values of $2\alpha_o h_1$ giving the greatest increase in flame speed at the termini of the respective ducts are, for $U_o$ of 50 feet per second,

| Geometry | Frequency, $f$, cps | $2h_1$, in. | $2\alpha_o h_1$ for $(V_T/V_L)_{max}$ |
|---|---|---|---|
| Plane | 570 | 2 | 11.95 |
| Cylindrical | 770 | 1.5 | 12.10 |

Of course, these data were obtained in a single test, performed to satisfy curiosity. The agreement does make it seem likely that a carryover of about 1:1 would be feasible in going from plane to cylindrically symmetric flow.

## SUMMARY OF RESULTS

### THEORY

The flow field of a flame in a duct is unstable to transverse disturbances having wavelengths 2.5 times the local flame width.

The amount a given frequency disturbance will grow varies directly as the frequency and inversely as the rate of flame spreading $dh/dx$ and is independent of velocity and density ratio across the flame front. The frequency $f$ where maximum velocity-disturbance growth obtains is $f=(2.8/\pi)(U_o/2h_1)$, where $U_o$ is approach velocity and $2h_1$ is duct width. This maximum growth occurs by the time the flame fills 64 percent of the duct and implies an amplification $v'/v_o=(1.108)^{1/K_2}$, where $K_2=dh_2/dx$. Frequencies higher or lower than this are amplified less. Higher frequencies achieve their terminal amplification at smaller values of $h_2/h_1$. For example, a frequency of $(1.5/\pi)(U_o/2h_1)$ has an amplification of $v'/v_o=(1.07)^{1/K_2}$ by the time the flame fills 28 percent of the duct.

By using a crude model of flame propagation, it is possible to predict the qualitative effect that amplified disturbances of discrete frequencies will have upon turbulent flame speed.

### EXPERIMENT

The effects of disturbances imposed at the flameholder are in substantial agreement with those predicted by theory. In addition, the results show:

1. Eddies shed from the flameholder with flame when suitably excited.
2. The ratio of turbulent to laminar flame speed varies inversely as flameholder size and directly as the ratio of flow velocity to flame speed or the ratio of disturbance velocity to flame speed.
3. Potentially, the most useful theory of turbulent flame propagation would be based on an incident and locally shifting spectrum of turbulence.
4. Gains in local heat-release rates can be obtained without damage to walls or excessive energy expenditure by using acoustic disturbances at a flameholder.

## CONCLUDING REMARKS

In formulating a theory of turbulent flame propagation, the form of instability that is discussed in this paper must be taken into account, as must plane-combustion-wave instability and flameholder boundary-layer instability. At present it is not known whether the latter two forms of instability can be encouraged to influence turbulent flame propagation more than they encourage it spontaneously; from the little evidence that is available, it appears that they cannot.

The type of instability discussed herein is of additional significance because its effect on the ratio of turbulent to laminar flame speed can be increased in some important applications. Several methods of increasing this ratio are as follows:

(1) Increase the disturbance velocity at the frequency that the flame zone can amplify.

(2) Increase the amplification rate by locally raising the mean velocity in the combustor.

(3) Increase the amplification rate by locally varying the velocity profile.

A method of employing all three of these improving factors would be to build a combustor having a wavy wall. Although the second and third methods listed will clearly cause an increase in pressure drop, the first method substantially increases the heat-release rate at the cost of a very small fraction of the kinetic energy in the approach-stream flow and a slight reduction in the operating range of the flameholder.

Lewis Flight Propulsion Laboratory
National Advisory Committee for Aeronautics
Cleveland, Ohio, *October 14, 1957*

# APPENDIX

## AXISYMMETRIC DISTURBANCES IN AXISYMMETRIC FLOW WITH DENSITY JUMPS

This appendix examines the stability of the flow field arising from a flame in a duct for axial symmetry. The results are used in the body of the text to compare wave numbers for neutral stability of comparable plane and axisymmetric flow fields. The symbols are defined where used.

### DISTURBANCE EQUATION

Pillow (ref. 23) defines the quantity $\psi$ as

$$\psi=\varphi(r)e^{i\alpha(z-ct)} \tag{A1}$$

The velocity in the $z$-direction is

$$u=U+u'$$

and in the $r$-direction,

$$v=v'$$

where

$$v'=-\frac{\partial\psi}{\partial z},\ u'=\frac{1}{r}\frac{\partial(r\psi)}{\partial r} \tag{A2}$$

and the continuity equation is satisfied identically. Pillow shows that the disturbance equation then becomes

$$\left[(U-c)-\frac{1}{i\alpha Re}(M-\alpha^2)\right](M-\alpha^2)\varphi-\varphi\left(U''-\frac{1}{r}U'\right)=0 \tag{A3}$$

where

$$M\equiv\frac{d^2}{dr^2}+\frac{1}{r}\frac{d}{dr}-\frac{1}{r^2} \tag{A4}$$

If the study is restricted to cases where $Re\rightarrow\infty$ and $U''=\frac{1}{r}U'$ (i. e., parabolic profiles or flat profiles), then equation (A3) becomes

$$(M-\alpha^2)\varphi=0$$

or

$$\frac{d^2\varphi}{dr^2}+\frac{1}{r}\frac{d\varphi}{dr}-\frac{1}{r^2}+\alpha^2=0 \tag{A5}$$

with solutions

$$\varphi=A_1I_1(\alpha r)+A_2K_1(\alpha r) \tag{A6}$$

where $I_1$ and $K_1$ are modified Bessel functions of the first and second kind. Therefore,

$$\begin{aligned}v'&=\frac{\partial\psi}{\partial z}=-i\alpha\varphi(r)e^{i\alpha(z-ct)}\\&=-i\alpha e^{i\alpha(z-ct)}[A_1I_1(\alpha r)+A_2K_1(\alpha r)]\end{aligned} \tag{A7}$$

and

$$\begin{aligned}u'&=\frac{1}{r}\frac{\partial(r\psi)}{\partial r}\\&=\frac{\partial\psi}{\partial r}+\frac{1}{r}\psi\\&=\varphi'+\frac{1}{r}\varphi e^{i\alpha(z-ct)}\\&=e^{i\alpha(z-ct)}\left\{A_1\left[\alpha I_1(\alpha r)+\frac{1}{r}I_1(\alpha r)\right]+\right.\\&\qquad\left.A_2\left[\alpha K_1(\alpha r)+\frac{1}{r}K_1(\alpha r)\right]\right\}\end{aligned} \tag{A8}$$

where the prime denotes differentiation with respect to the argument.

### BOUNDARY CONDITIONS

Consider the following profile and density distribution:

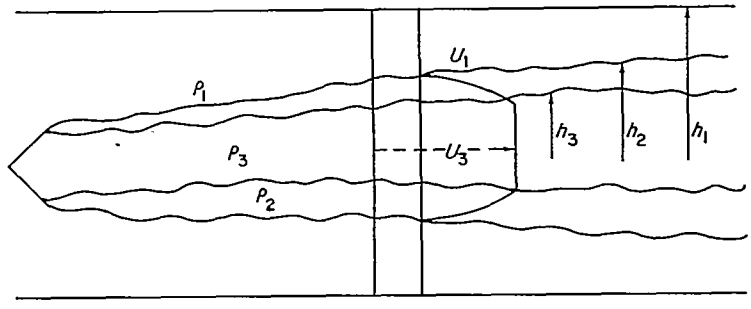


Sketch (p)

Let solutions to equation (A5) be denoted by $\varphi_1$, $\varphi_2$, $\varphi_3$ for regions 1, 2, and 3 with densities $\rho_1$, $\rho_2$, and $\rho_3$, respectively.

As in the plane case, the requirements are

$$\left.\begin{aligned}&\varphi_1=0 \text{ at } h_1\\&\varphi_1=\varphi_2 \text{ at } h_2\\&\varphi_2=\varphi_3 \text{ at } h_3\\&\text{and, because of symmetry,}\\&\varphi_3=0 \text{ at } r=0\end{aligned}\right\} \tag{A9}$$

Similarly,

$$\left.\begin{aligned}&\left(\frac{dp}{dz}\right)_1=\left(\frac{dp}{dz}\right)_2 \text{ at } h_2\\&\left(\frac{dp}{dz}\right)_2=\left(\frac{dp}{dz}\right)_3 \text{ at } h_3\end{aligned}\right\} \tag{A10}$$

Since, at $r=h_1$,

$$\varphi_1=A_1I_1(\alpha h_1)+A_2K_1(\alpha h_1)=0$$

then

$$A_1=-A_1\frac{I_1(\alpha h_1)}{K_1(\alpha h_1)} \tag{A11}$$

At $r=h_2$, $\varphi_1=\varphi_2$ or, with equation (A11),

$$\left.\begin{aligned}\varphi_1&=\alpha_1\left[I_1(\alpha h_2)-\frac{I_1(\alpha h_1)}{K_1(\alpha h_1)}K_1(\alpha h_2)\right]\\&=\varphi_2=B_1I_1(\alpha h_2)+B_2K_1(\alpha h_2)\end{aligned}\right\} \tag{A12}$$

At $r=h_3$, $\varphi_2=\varphi_3$ or

$$\left.\begin{aligned}\varphi_2&=B_1I_1(\alpha h_3)+B_2K_1(\alpha h_3)\\&=\varphi_3=C_1I_1(\alpha h_3)+C_2K_1(\alpha h_3)\end{aligned}\right\} \tag{A13}$$

Since $K_1(\alpha r)\to\infty$ as $\alpha r\to 0$, $I_1(\alpha r)\to 0$ as $\alpha r\to 0$, and at $r=0$, $\varphi_3=0$,

$$C_2=0 \tag{A14}$$

Since

$$\frac{\partial p}{\partial z}=-\rho\left(\frac{\partial u'}{\partial t}+U\frac{\partial u'}{\partial z}+v'\frac{dU}{dr}\right)$$

the pressure conditions yield at $h_2$ (from eqs. (A7) and (A8))

$$\begin{aligned}&-\rho_1\left[(-\alpha c+i\alpha U_1)\left(\alpha\varphi_1'+\frac{1}{h_2}\varphi_1\right)\right]\\&\quad=-\rho_2\left[(-i\alpha c+\alpha U_1)\left(\alpha\varphi_2'+\frac{1}{h_2}\varphi_2\right)-i\alpha\varphi_2\frac{dU}{dr}\right]\end{aligned} \tag{A15}$$

and at $h_3$

$$\begin{aligned}&\rho_3\left\{[-i(\alpha c)+i(\alpha U_3)]\left(\varphi_3'+\frac{1}{h_3}\varphi_3\right)\right\}\\&\quad=\rho_2\left\{[-i(\alpha c)+i(\alpha U_3)]\left(\varphi_2'+\frac{1}{h_3}\varphi_2\right)-i(\alpha)\varphi_2\frac{dU}{dr}\right\}\end{aligned} \tag{A16}$$

## BOUNDARY-VALUE PROBLEM

The following notation is used:

$$\left.\begin{aligned}
&\alpha_1=I_1(\alpha h_2)-\frac{I_1(\alpha h_1)}{K_1(\alpha h_1)}K_1(\alpha h_2)\\
&\alpha_2=\frac{\rho_1}{\rho_2}\left\{\alpha I_1'(\alpha h_2)+\frac{1}{h_2}I_1(\alpha h_2)-\frac{I_1(\alpha h_1)}{K_1(\alpha h_1)}\left[\alpha K_1'(\alpha h_2)+\frac{1}{h_2}K_1(\alpha h_2)\right]\right\}\\
&\beta_1=I_1(\alpha h_2)\\
&\beta_2=K_1(\alpha h_2)\\
&\beta_3=I_1(\alpha h_3)\\
&\beta_4=K_1(\alpha h_3)\\
&\beta_5=\alpha I_1'(\alpha h_2)+\frac{1}{h_2}I_1(\alpha h_2)\\
&\beta_6=I_1(\alpha h_2)\left(\frac{dU}{dr}\right)_{h_2}\\
&\beta_7=\alpha K_1'(\alpha h_2)+\frac{1}{h_2}K_1(\alpha h_2)\\
&\beta_8=K_1(\alpha h_2)\left(\frac{dU}{dr}\right)_{h_2}\\
&\beta_9=\frac{\rho_2}{\rho_3}(\alpha I_1')(\alpha h_3)+\frac{1}{h_3}I_1(\alpha h_3)\\
&\beta_{10}=\frac{\rho_2}{\rho_3}(\alpha K_1')(\alpha h_3)+\frac{1}{h_3}K_1(\alpha h_3)\\
&\beta_{11}=\frac{\rho_2}{\rho_3}I_1(\alpha h_3)\left(\frac{dU}{dr}\right)_{h_2}\\
&\beta_{12}=\frac{\rho_2}{\rho_3}K_1(\alpha h_3)\left(\frac{dU}{dr}\right)_{h_3}
\end{aligned}\right\} \tag{A17}$$

and

$$\gamma_1=I_1(\alpha h_3)=\beta_3$$

$$\gamma_2=\alpha I_1'(\alpha h_3)+\frac{1}{h_3}I_1(\alpha h_3)$$

Setting $U_1=0$ (this merely alters the real part of $c$ by $U_1$), the determinantal equation for $A_1$, $B_1$, $B_2$, and $C_1$ is

$$\begin{vmatrix}\alpha_1 & -\beta_1 & -\beta_2 & 0\\ 0 & \beta_3 & \beta_4 & -\gamma_1\\ -c\alpha_2 & c\beta_5+\beta_6 & c\beta_7+\beta_8 & 0\\ 0 & (U_3-c)\beta_9-\beta_{11} & (U_3-c)\beta_{10}-\beta_{11} & -(U_3-c)\gamma_2\end{vmatrix}=0 \tag{A18}$$

One immediate result of equation (A18) is to show that, if $dU/dr$ vanished at either $h_2$ or $h_3$ in region 2, $c$ is real for all $\alpha_s'$. This can be seen by setting

$$\beta_6=\beta_8=\left(\frac{dU}{dr}\right)_{h_2}=0$$

and factoring $c$ from the third row of equation (A18), or setting

$$\beta_{11}=\beta_{12}=\left(\frac{dU}{dr}\right)_{h_3}=0$$

and factoring $U_3=c$ from the fourth row of equation (A18). Either operation leaves a determinantal equation in which $c$ is wholly real.

If

$$\left.\begin{aligned}\left(\frac{dU}{dr}\right)_{h_2}&=g_2\\ \left(\frac{dU}{dr}\right)_{h_3}&=g_3\end{aligned}\right\} \tag{A19}$$

and

$$\left.\begin{aligned}g_2\beta_1&=\beta_6\\ g_2\beta_2&=\beta_8\\ \frac{\rho_2}{\rho_3}g_3\beta_3&=\beta_{11}\\ \frac{\rho_2}{\rho_3}g_3\beta_4&=\beta_{12}\end{aligned}\right\} \tag{A20}$$

then equation (A18) can be reduced to

$$\begin{bmatrix} -\frac{c\alpha_2-g_2\alpha_1}{\alpha_1}\beta_1+c\beta_5 & -\frac{c\alpha_2-g_2\alpha_1}{\alpha_1}\beta_2+c\beta_7 \\ \frac{(U_3-c)\gamma_2+\frac{\rho_2}{\rho_3}g_3\gamma_1}{\gamma_1}\beta_3+(U_3-c(\beta_9- & \frac{(U_3-c)\gamma_2+\frac{\rho_2}{\rho_3}g_3\gamma_1}{\gamma_1}\beta_4+(U_3-c)\beta_{10} \end{bmatrix}=0 \quad \text{(A21)}$$

This is in the form

$$\begin{vmatrix} jc+k & mc+n \\ oc+q & sc+w \end{vmatrix}=0$$

or

$$jsc^2-moc^2+c(jw+ks-mq-on)+kw-nq=0$$

and the discriminant of $c$ is

$$D\equiv j^2w^2+k^2s^2+m^2q^2+o^2n^2+-2jwks-2mqon-2jwmq-2jwon-2ksmq-2kson+4mokw+4jsnq \quad \text{(A22)}$$

If $D<0$, then $c$ is complex and an unstable mode exists. The symbols of equation (A22) are defined

$$\left.\begin{aligned} j&=\beta_5-\beta_1\frac{\alpha_2}{\alpha_1} \\ k&=\beta_1 g_2 \\ m&=\beta_7-\beta_2\frac{\alpha_2}{\alpha_1} \\ n&=\beta_2 g_2 \\ o&=\beta_3\frac{\gamma_2}{\gamma_1}-\beta_9 \\ q&=U_3\beta_9-\frac{\rho_2}{\rho_3}g_3\beta_3-U_3\frac{\gamma_2}{\gamma_1}\beta_3 \\ s&=\beta_4\frac{\gamma_2}{\gamma_1}-\beta_{10} \\ w&=U_3\beta_{10}-\frac{\rho_2}{\rho_3}g_3\beta_4-U_3\frac{\gamma_2}{\gamma_1}\beta_4 \end{aligned}\right\} \quad \text{A(23)}$$

## REFERENCES


1. Scurlock, A. C.: Flame Stabilization and Propagation in High-Velocity Gas Streams. Meteor Rep. 19, Fuels Res. Lab., M. I. T., May 1948. (Contract NOrd 9661.)
2. Haddock, Gordon W.: Flame-Blowoff Studies of Cylindrical Flameholders in Channeled Flow. Prog. Rep. 3–24, Jet Prop. Lab., C. I. T., May 14, 1951.
3. Zukoski, Edward E., and Marble, Frank E.: The Role of Wake Transition in the Process of Flame Stabilization on Bluff Bodies. Combustion Res. and Rev., Butterworths Sci. Pub., 1955, pp. 167–180.
4. Karlovitz, Béla: A Turbulent Flame Theory Derived from Experiments. AGARD Selected Combustion Problems, Butterworths Sci. Pub. (London), 1954, pp. 248–262. (Discussion by K. Wohl, pp. 268–274, and by G. H. Markstein, pp. 263–265.)
5. Berl, W. G., Rice, J. L., and Rosen, P.: Flames in Turbulent Streams. Jet Prop., vol. 25, no. 7, July 1955, pp. 341–346.
6. Damköhler, Gerhard: The effect of Turbulence on the Flame Velocity in Gas Mixtures. NACA TM 1112, 1947.
7. Shelkin, K. I.: On Combustion in a Turbulent Flow. NACA TM 1110, 1947.
8. Scurlock, Arch C., and Grover, John H.: Experimental Studies on Turbulent Flames. AGARD Selected Combustion Problems, Butterworths Sci. Pub. (London), 1954, pp. 215–247.
9. Leason, D. B.: Turbulence and Flame Propagation in Premixed Gases. Fuel, vol. XXX, no. 10, Oct. 1951, pp. 233–238; discussion, pp. 238–239.
10. Mickelsen, William R.: The Propagation of a Free Flame Through a Turbulent Gas Stream. M. S. Thesis, Case Inst. Tech., 1953.
11. Bolz, Ray E., and Burlage, Henry, Jr.: The Influence of Turbulence on Flame Propagation Rates. Jet Prop., vol. 25, no. 6, June 1955, pp. 265–275: con. p. 283.
12. Mickelsen, William R., and Ernstein, Norman E.: Propagation of a Free Flame in a Turbulent Gas Stream. NACA Rep. 1286, 1956. (Supersedes NACA TN 3456.)
13. Tucker, Maurice: Interaction of a Free Flame Front with a Turbulence Field. NACA Rep. 1277, 1956. (Supersedes NACA TN 3407.)
14. Summerfield, Martin, Reiter, Sydney H., Kebely, Victor, and Mascolo, Richard W.: The Structure and Propagation Mechanism of Turbulent Flames in High Speed Flow. Jet Prop., vol. 25, no. 8, Aug. 1955, pp. 377–384.
15. Rayleigh: The Theory of Sound. Vol. II. Dover Pub., 1945.
16. Fenn, J. B., Forney, H. B., and Garmon, R. C.: Burners for Supersonic Ram-Jets. Ind. and Eng. Chem., vol. 43, no. 7, July 1951, pp. 1663–1671.
17. Blackshear, Perry L., Rayle, Warren D., and Tower, Leonard K.: Study of Screeching Combustion in a 6-Inch Simulated Afterburner. NACA TN 3567, 1955.
18. Truman, John C., and Newton, Roger T.: Why Do High-Thrust Engines Screech? Aviation Age, vol. 23, no. 5, May 1955, pp. 136–143.
19. Kaskan, W. E., and Noreen, A. E.: High-Frequency Oscillations of a Flame Held by a Bluff Body. Trans. ASME, vol. 77, no. 6, Aug. 1955, pp. 885–891; discussion, pp. 891–895.
20. Tsien, H. S.: Influence of Flame Front on the Flow Field. Jour. Appl. Mech., vol. 18, no. 2, June 1951, pp. 188–194.
21. Fabri, J., Siestrunck, R., and Fouré, C.: On the Aerodynamic Field of Stabilized Flames. Fourth Symposium (International) on Combustion, The Williams & Wilkins Co. (Baltimore), 1953, pp. 443–450.
22. Lin, C. C.: On the Stability of Two-Dimensional Parallel Flows, pt. I. Quarterly Appl. Math., vol. III, no. 2, July 1945, pp. 117–142; pt. II, vol. III, no. 3, Oct. 1945, pp. 218–234; pt. III, vol. III, no. 4, Jan. 1946, pp. 277–301.
23. Pillow, A. F.: A Review of Hydrodynamic Stability and Its Bearing on Transition to Turbulent Flow in the Boundary Layer. Rep. A.35, Div. Aero., Council Sci. & Ind. Res. (Australia), May 1945.
24. Schubauer, G. B., and Skramstad, H. K.: Laminar-Boundary-Layer Oscillations and Transition on a Flat Plate. NACA Rep. 909, 1948. (Supersedes NACA WR W-8.)
25. Pretsch, J.: The Stability of Two-Dimensional Laminar Flow with Pressure Drop and Pressure Rise. Joint Intelligence Objectives Agency (Wash., D. C.), July 23, 1946.
26. Lessen, Martin: On Stability of Free Laminar Boundary Layer Between Parallel Streams. NACA Rep. 979, 1950. (Supersedes NACA TN 1929.)
27. Heisenberg, Werner: On Stability and Turbulence of Fluid Flows. NACA TM 1291, 1951.
28. Savic, P.: On Acoustically Effective Vortex Motion in Gaseous Jets. Phil. Mag., ser. 7, vol. 32, Sept. 1941, pp. 245–252.

29. Goldstein, S.: On The Stability of Superposed Streams of Fluids of Different Densities. Proc. Roy. Soc. (London), ser. A, vol. 132, Aug. 1, 1931, pp. 524–548.

30. Goldstein, Sydney, ed.: Modern Developments in Fluid Dynamics. Vols. I and II. Clarendon Press (Oxford), 1938.

31. Mestre, André: Étude des Limites de Stabilite en Relation avec la Résistance des Obstacles à l'Écoulement. Combustion Res. and Rev., Butterworths Sci. Pub., 1955, pp. 72–86.

32. Clark, Thomas P., and Bittker, David A.: A study of the Radiation from Laminar and Turbulent Open Propane-Air Flames as a Function of Flame Area, Equivalence Ratio, and Fuel Flow Rate. NACA RM E54F29, 1954.

33. Mickelser, William R., and Laurence, James C.: Measurement and Analysis of Turbulent Flow Containing Periodic Flow Fluctuations. NACA RM E53F19, 1953.

34. Roshko, Anatol: On the Development of Turbulent Wakes from Vortex Streets. NACA Rep. 1191, 1954. (Supersedes NACA TN 2913.)

35. Blackshear, Perry L., Jr.: Driving Standing Waves by Heat Addition. NACA TN 2772, 1952. (See also Fourth Symposium (International) on Combustion, The Williams & Wilkins Co., 1953, pp. 553–566.)

36. Kaskan, W. E.: An Investigation of Vibrating Flames. Fourth Symposium (International) on Combustion, The Williams & Wilkins Co., 1953, pp, 575–591.

37. Dugger, Gordon L.: Effect of Initial Mixture Temperature on Flame Speed of Methane-Air, Propane-Air, and Ethylene-Air Mixtures. NACA Rep. 1061, 1952. (Supersedes NACA TN's 2170 and 2374.)

38. Dryden, Hugh L.: A Review of the Statistical Theory of Turbulence. Quarterly Appl. Math., vol. I, no. 1, Apr. 1943, pp. 7–42.